

CRACK ANALYSIS OF REINFORCED CONCRETE
TWO-WAY SLABS

MOHAMED A.A. HOSSIN





Library and Archives
Canada

Published Heritage
Branch

395 Wellington Street
Ottawa ON K1A 0N4
Canada

Bibliothèque et
Archives Canada

Direction du
Patrimoine de l'édition

395, rue Wellington
Ottawa ON K1A 0N4
Canada

Your file *Votre référence*
ISBN: 978-0-494-57479-9
Our file *Notre référence*
ISBN: 978-0-494-57479-9

NOTICE:

The author has granted a non-exclusive license allowing Library and Archives Canada to reproduce, publish, archive, preserve, conserve, communicate to the public by telecommunication or on the Internet, loan, distribute and sell theses worldwide, for commercial or non-commercial purposes, in microform, paper, electronic and/or any other formats.

The author retains copyright ownership and moral rights in this thesis. Neither the thesis nor substantial extracts from it may be printed or otherwise reproduced without the author's permission.

AVIS:

L'auteur a accordé une licence non exclusive permettant à la Bibliothèque et Archives Canada de reproduire, publier, archiver, sauvegarder, conserver, transmettre au public par télécommunication ou par l'Internet, prêter, distribuer et vendre des thèses partout dans le monde, à des fins commerciales ou autres, sur support microforme, papier, électronique et/ou autres formats.

L'auteur conserve la propriété du droit d'auteur et des droits moraux qui protègent cette thèse. Ni la thèse ni des extraits substantiels de celle-ci ne doivent être imprimés ou autrement reproduits sans son autorisation.

In compliance with the Canadian Privacy Act some supporting forms may have been removed from this thesis.

While these forms may be included in the document page count, their removal does not represent any loss of content from the thesis.

Conformément à la loi canadienne sur la protection de la vie privée, quelques formulaires secondaires ont été enlevés de cette thèse.

Bien que ces formulaires aient inclus dans la pagination, il n'y aura aucun contenu manquant.


Canada

Crack Analysis of Reinforced Concrete Two-Way Slabs

by

©Mohamed A.A. Hossin, B.Sc. (Eng.)

A thesis submitted to the School of Graduate
Studies in partial fulfillment of the
requirements for the Degree of
Master of Engineering

Faculty of Engineering and Applied Science

Memorial University of Newfoundland

January 2007

St. John's Newfoundland Canada

Abstract

Offshore structures are exposed to harsh environmental conditions, including the structure's existence in the splash zone as well as exposure to seawater and sea spray. The design of offshore structures is controlled by mandatory design codes to ensure structural safety and integrity. The main objective of this study is to investigate the cracking criteria for offshore structures and develop a rational numerical model in order to predict crack width and spacing of high strength concrete under flexural sustained service loads.

An experimental investigation is designed to study the cracking behaviour of high strength concrete plates. Eight two-way reinforced concrete specimens with different thick concrete cover and bar spacing were tested in the structural laboratory at Memorial University of Newfoundland under flexural loading. The tests specimens are divided into three groups. The first two groups are heavily reinforced and designed to fail under punching shear mode. The first group (Series I) is designed to investigate the effect of concrete cover on the crack width and crack spacing. The second group (Series II) is designed to investigate the effect of bar spacing on the crack width and crack spacing. The third group (Series III) is designed to investigate the effect of different modes of failure on the crack width

and crack spacing for two-way reinforced concrete slabs. The structural behaviour of the test slabs with regards to deformations, strains, crack patterns, crack width and mode of failure was examined.

It has been found that the effect of increasing concrete cover from 30 mm to 60 mm of (Series I) increases the crack spacing by 38%. The crack spacing of (Series II) was increased by 28%, when the bar spacing increased from 150 to 250 mm. The test results revealed that the relation of the crack width versus steel strain can be represented by a straight line up to a limiting steel strain of 0.001 to 0.0015 for most of the test slabs. This strain value corresponds to a reinforcement stress equal to 200 MPa to 250 MPa ($0.50-0.63f_y$).

The theoretical investigation includes two phases. The first phase is evaluating the suitability of the existing crack width and crack spacing expressions for structures with large concrete covers. The experimental test results of all test slabs confirmed the recommendation of an existing equation. The second phase includes the development of a numerical crack analysis model based on tension chord method. The developed proposed expression to calculate the crack width is based on the modified assumption of the tension chord method. A second model was recommended based on the fracture energy principles to estimate the crack width. The modified assumptions deal with estimating the tensile strength, bond strength

and the active tension concrete area. The newly developed expressions provided good results for high strength thick concrete cross sections with large concrete cover.

Acknowledgments

Praise to be to Allah Almighty and Peace be upon His Prophet Muhammad.

Many thanks to my parents for their love, prayer and support. Without them, this work would never have come into existence.

I am greatly indebted to Dr. H. Marzouk, Professor of Civil Engineering, for his support, guidance, and patience during the course of the program. I appreciate his commitment to help doing this work since the first day I arrived to Newfoundland.

I had the pleasure of work with Mr. Matthew A. Curtis and Mr. Shawn Organ, Structures and Concrete laboratories technicians. Their assistance made the research possible.

Many thanks to my colleges Ehab El-Tom, Emad Rizk, Nabil Dawood and Tamer Sabrah for their help and friendship.

I appreciate and thank the School of Graduate Studies at Memorial University of Newfoundland for the financial support of this study.

St.John's, Newfoundland

Mohamed Hossin

January, 2007

Contents

Abstract	ii
Acknowledgments	v
Contents	vi
List of Figures	x
List of Tables	xiii
Notation and List of Abbreviations	xv
1 Introduction.....	1
1.1 General.....	1
1.2 Objective.....	4
1.3 Scope.....	5
1.4 Thesis Format.....	7

2	Literature Review.....	9
2.1	General.....	9
2.2	Introduction.....	10
2.3	Fracture Energy and Tension Stiffening.....	11
2.4	Crack control in reinforced concrete members.....	14
2.5	Tension Cord Cracking Model.....	16
2.5.1	Flexural Cracking Cord Model.....	16
2.5.2	Direct Tension Cracking Cord Model.....	19
2.6	Statistical Cracking Models.....	20
2.7	ACI Approach.....	34
2.8	Canadian Offshore Code.....	36
2.9	Norwegian Code.....	38
2.10	CEB-FIP (MC-90) Recommendation.....	40
2.11	Eurocode EC2 Provisions.....	41
3	Experimental Investigation.....	44
3.1	General.....	44
3.2	Properties of Material.....	45
3.2.1	Concrete.....	45
3.2.1.1	Normal Strength Concrete Mixture.....	45
3.2.1.2	High Strength Concrete Mix design.....	46
3.2.1.2.1	Materials.....	46
3.2.1.2.2	Mixing Procedure.....	47
3.2.1.2.3	Curing.....	49
3.3	Compressive Strength of the Test Slabs.....	49

3.4	Test Slabs.....	51
3.5	Slab Formwork and Fabrication.....	52
3.6	Test Set-up.....	54
3.7	Instrumentation and Measurements.....	56
3.7.1	Deflections.....	56
3.7.2	Steel Strains.....	57
3.7.3	Concrete Strains.....	58
3.7.4	Crack Measurements.....	59
3.7.5	Data Acquisition System.....	60
3.8	Procedure.....	60
4	Test Results and Discussion.....	62
4.1	Introduction.....	62
4.2	Load-Deflection Relations.....	63
4.3	Deflection Profiles.....	69
4.4	Ductility and Energy Absorption.....	74
4.5	Steel Reinforcement Strain.....	76
4.6	Concrete Strains.....	79
4.7	Cracking Characteristics.....	80
4.7.1	Crack Spacing.....	80
4.7.2	Crack Width Measurements.....	93
5	Proposed Crack Analysis.....	99
5.1	Introduction.....	99
5.2	Cracking of reinforced concrete structures.....	100
5.3	Crack Spacing.....	102

5.4	Crack Width Calculations Based on Fracture Energy.....	109
5.4.1	Comparison of Crack Width Test Results with the Predictions of Other International Codes.....	115
5.5	Calculating Crack Width Using Modified Tension Chord Assumptions (MTCA).....	118
5.5.1	Average Concrete Tensile Strain (ϵ_{cm}) in Tension Chord.....	119
5.5.2	Bond Shear Stress (τ_b).....	123
5.5.3	Average Steel Tensile Strain (ϵ_{sm}) in Tension Chord.....	125
5.6	Numerical Example.....	126
5.6.1	Cracked Width Calculations Using the Modified Tension Chord Assumptions.....	127
5.6.2	Cracked Width Calculations Based on Fracture Energy....	127
5.7	Comparison of Test Results with the Developed an Analytical Model and Different Code Predictions.....	128
6	Conclusion1 and Recommendation.....	132
6.1	Summary.....	132
6.1.1	Experimental Investigation.....	133
6.1.2	Theoretical Investigation.....	137
6.2	Conclusions.....	141
6.3	Recommendations for Future Research.....	145
	References.....	146
	Appendix A1.....	152
	Appendix A2.....	155

List of Figures

2.1	Principal of fictitious crack model (Gustafsson and Hillerborg, 1986).....	15
2.2	Cracked reinforced concrete slab tension chord model (Gilbert, 2005).....	18
2.3	First cracking in a restrained tension member (Gilbert, 2005).....	21
2.4	Broms' mechanism of tension cracking with a single reinforcing bar.....	24
2.5	Broms' mechanism of tension cracking (flexural members).....	25
2.6	Effective embedment thickness of concrete.....	29
2.7	Effective embedment thickness of concrete.....	43
3.1	The concrete compression test machine.....	50
3.2	Details of a test specimen NSC1.....	51
3.3	A reinforcement cage in the formwork for a typical slab.....	53
3.4	The test set-up.....	55
3.5	A typical arrangement of LPDT's.....	56
3.6	A typical arrangement of the steel strain gauges.....	57
3.7	Concrete Strain gauge locations (The strain gauges were located at 150 mm apart).....	58
3.8	(KG-A) Crack Displacement Transducer.....	59
3.9	Marking the cracks on a typical slab.....	61
4.1	Typical load-deflection characteristics at center span of test slabs.....	67

4.2	Deflection profile for NSC1.....	70
4.3	Deflection profile for HSC1.....	71
4.4	Deflection profile for HSC3.....	71
4.5	Deflection profile for HSC4.....	72
4.6	Deflection profile for HSC5.....	72
4.7	Deflection profile for NSC2.....	73
4.8	Deflection profile for NSC3.....	73
4.9	Typical load-tension steel strain behavior at the column periphery for Series I.....	77
4.10	Typical load-tension steel strain behavior at the column periphery for Series II.....	78
4.11	Typical load-tension steel strain behavior at the column periphery for Series III.....	78
4.12	Load versus concrete strain for NSC1.....	81
4.13	Load versus concrete strain for HSC1.....	82
4.14	Load versus concrete strain for HSC3.....	82
4.15	Load versus concrete strain for HSC4.....	83
4.16	Load versus concrete strain for HSC5.....	83
4.17	Load versus concrete strain for NSC2.....	84
4.18	Load versus concrete strain for NSC3.....	84
4.19	Crack patterns of Series I.....	89
4.20	Crack patterns of Series II.....	90
4.21	Crack patterns of Series III.....	91
4.22	Crack width expansion versus steel strain for NSC1.....	96
4.23	Crack width expansion versus steel strain for HSC1.....	96

4.24	Crack width expansion versus steel strain HSC3.....	97
4.25	Crack width expansion versus steel strain for HSC4.....	97
4.26	Crack width expansion versus steel strain for NSC2.....	98
5.1	Flexural cracking in a singly reinforced concrete member.....	101
5.2	Effective embedment thickness.....	103
5.3	Comparison of average crack spacing for Series I.....	107
5.4	Comparison average crack spacing for Series II.....	107
5.5	Comparison average crack spacing for Series III.....	108
5.6	Comparison average crack spacing for Series III.....	108
5.7	Complete tension stiffening model for high strength concrete.....	114
5.8	Comparison of maximum crack width for Series I.....	117
5.9	Comparison of maximum crack width for Series II.....	117
5.10	Elongations of the steel and concrete between two consecutive cracks.....	119
5.11	Elongations Bond shear stress, concrete and steel stress.....	120
5.12	Tension Chord in a singly reinforced concrete member.....	120
5.13	Free body diagram in a tension Chord.....	121
5.14	Analytical model for flexural cracking in a singly reinforced flexural member.....	125
5.15	Comparison of crack width for Series I.....	130
5.16	Comparison of crack width for Series II.....	131

List of Tables

2.1	Guide to reasonable crack widths in reinforced concrete under service load.....	36
3.1	Mix proportions for one batch of the normal strength concrete.....	46
3.2	Mix proportions for one batch of the high strength concrete.....	48
3.3	Slab specimen details.....	52
4.1	Group specimens' details.....	64
4.2	Deflection characteristics of test slabs.....	67
4.3	Ductility and energy absorption of test slabs.....	75
4.4	Comparison of the concrete cover effect on crack spacing.....	87
4.5	Comparison of the bar spacing effect on crack spacing.....	88
4.6	Comparison of the bar spacing effect on crack spacing of Series III.....	88
4.7	Maximum crack width measurements of Series I at 250 MPa steel stress.....	94
4.8	Maximum crack width measurements of Series II at 250 MPa steel stress.....	95
4.9	Maximum crack width measurements of Series III at 250 MPa steel Stress.....	95

5.1	Comparison of crack spacing test results with the predictions of other codes.....	106
5.2	Comparison of the test results with the predictions of other international codes.....	116
5.3	Comparison the test results of crack width with the modified tension chord assumptions and fracture energy.....	129
A1.1	Reinforced concrete cracked section properties.....	151
A1.2	Crack properties calculation using (CSA S474, 2004).....	151
A1.3	Crack properties calculation using (NS 3473E, 1992).....	152
A1.4	Crack properties calculation using (EC2, 1991).....	152
A1.5	Crack properties calculation using (CEB-FIP,1990).....	153
A2.1	HSC1 properties.....	154

Notation and List of Abbreviations

The following notations were used in the thesis

- A : Area of concrete symmetric with reinforcing steel divided by number of bars
- A_{cef} : The effective tension area
- A_e : Average effective concrete area around a reinforcing bar
- A_s : Area of reinforcement within the effective embedment thickness (mm^2)
- A_{st} : Area of tensile reinforcement
- a_1 : Clear distance to the first steel layers plus bar diameter
- a_2 : Clear distance to the second steel layers plus bar diameter
- b : Width of the section
- c : Depth in under compression
- c : Concrete cover (mm)
- C_c : Clear cover at tension side
- d : Effective depth
- d_b : The bar diameter
- d_{be} : Bar diameter of outer layer
- d_{b1} : Diameter of the reinforcement in Direction 1 closest to the concrete outer fibers;

d_c	:	Bottom cover measured from center of lowest bar
E	:	Modulus of elasticity
E_c	:	Concrete modulus of elasticity
E_{sk}	:	Characteristics modulus of elasticity of steel (MPa)
E_S	:	Steel modulus of elasticity
f_c	:	The average tensile stress
f_{cr}	:	Cracking strength of concrete
f_{ct}	:	The direct tensile strength of concrete
f_{ctm}	:	Nominal concrete tensile strength
f_s	:	Steel stress calculated by elastic cracked section theory, Actual average service-load stress level or 40% of the specified yield strength f_y ;
f_{sy}	:	Steel yield stress
f_t	:	Material tensile strength
G_F	:	The area under the entire softening stress elongation curve
h	:	Section height
h_{ef}	:	Effective embedment thickness
h_l	:	Distance from the neutral axis to the center of the reinforcing bar
k	:	Constants depends on concrete mix properties, Fracture coefficient with a value $k = 2.8 \times 10^{-5}$ for uniformly loaded restrained

two-way action square slabs and plates. For concentrated loads or reactions or when the ratio of short to long span is less than 0.75 but larger than 0.5, a value of $k = 2.1 \times 10^{-5}$ is applicable. For span aspect ratios less than 0.5, $k = 1.6 \times 10^{-5}$

- k_1 : A dimensionless coefficient depending upon bond properties of the reinforcing bars
- k_2 : Coefficient to account for strain gradient
- L : Member length
- l_{ch} : Characteristic length
- $l_{s,max}$: The length over which slip between steel and concrete occurs; steel and concrete strains, which occur within this length, contribute to the width of the crack
- m : Number of tensile reinforcing bar
- M_{cr} : Cracking bending moment
- M_s : Service bending moment
- n : Modular ratio of the section
- s : Maximum permissible bar spacing
- s_o : The distance which stresses vary on each side of the crack
- s_1 : Spacing of the reinforcement in Direction 1;
- s_2 : Spacing of the reinforcement in perpendicular Direction 2;
- S : Bar spacing of outer layer

S^*	:	Final crack spacing
S_m	:	The average crack spacing
S_{rm}	:	Mean crack spacing, average stabilized crack spacing
S_{r0}	:	Represents the distance between the first crack and the cross-section at which concrete stress reaches f_{ct}
t_b	:	Bottom cover measured from the center of the lowest bar
t_s	:	Side cover measured from the center of outer bar
T	:	Axial tensile force
w	:	Material Elongation
w^*	:	Final crack width
w_b	:	Maximum (measured or calculated) bottom crack width at level of steel centroid in constant moment region
w_c	:	The critical crack separation displacement, limiting crack width
w_k	:	Characteristic maximum crack width, design crack width
w_{lim}	:	The nominal limit value of crack width which is specified for cases of expected functional consequences of cracking, or some particular cases related to durability
w_m	:	Average crack width
w_s	:	Maximum (measured or calculated) side crack width at level of steel centroid in constant moment region
σ	:	Material stress
σ_{ct}	:	A uniform tensile stress
σ_s	:	Stress in the reinforcement in the crack (MPa)

σ_{sr}	:	Stress in the reinforcement at calculated crack (MPa)
σ_{st}	:	Steel stress
$\sigma(w)$:	Softening stress separation curve
ρ_{tl}	:	Active steel ratio, that is, the area of steel A_s per ft width / $[12d_{bl} + 2c_1]$, where c_1 is clear concrete cover measured from the tensile face of concrete to the nearest edge of the reinforcing bar in Direction 1, and
ϵ	:	Material strain
$\epsilon_1 = \epsilon_I$:	The largest tensile strains in the effective area, the principal tensile strain at level of tensile reinforcement
$\epsilon_2 = \epsilon_{II}$:	The smallest tensile strains in the effective area
ϵ_{cm}	:	The average concrete strain within
ϵ_{cs}	:	The strain of concrete due to shrinkage; it has introduced
ϵ_{sh}	:	Shrinkage strain
ϵ_{sm}	:	The average steel strain, mean strain under relevant combination of loads and allowing for the effect such as tension stiffening or shrinkage
ϵ_t	:	Concrete tensile strain
ϵ_{to}	:	Concrete cracking strain
α_1	:	Factor depends on the steel stress at crack
α_2	:	Factor accounts for short or long term calculations

β	:	Ratio of distances to neutral axis from extreme tension fiber to center of reinforcement; ratio of distance between neutral axis and tension face to distance between neutral axis and reinforcing steel; a coefficient account for type of action; coefficient relating the average cracks width to the design value and equals to 1.7 and 1.3, respectively, for section whose minimum dimension exceed 800 mm or is smaller than 300 mm, 1.25 (chosen to simplify calculations, although it varies between 1.20 and 1.35)
Δe_c	:	Concrete elongation
Δe_s	:	Steel elongation
Δ_{slip}	:	Slip in two adjacent half segments
Δu	:	Supports movement
τ_b	:	Bond stress between the steel and the surrounding tensile concrete
λ	:	Constants depends on concrete mix properties
ϕ	:	Bar diameter
ξ	:	A dimensionless coefficient between 0 and 1, representing the effect of the participation of concrete in the tension zone to stiffness the member
ACI	:	American Concrete Institute
CEB	:	<i>Comité Euro-Internationale de Beton</i>
CSA	:	Canadian Standard Associations
EC2	:	<i>Euro-code</i>
FIP	:	Federation Internationale de la Procontrainte
MTCA	:	Modified Tension Chord Assumptions

NS : Norwegian Council for Building Standardization

Chapter 1

Introduction

1.1 General

Plate elements such as a two-way slab system, is a unique and efficient structural system. It is economical, and widely used in different structural applications, such as floors and roofs of buildings, walls of tanks, and offshore structures. Plate element system such as two-way slab system is used to build offshore concrete platforms successfully. Offshore concrete structures proved to present a competitive alternative for substructures in the North Sea and in other places where large

offshore structures are required for production of oil and gas. Furthermore, offshore concrete structures have proved to be highly durable and to have good resistance against corrosion. The low tensile strength of concrete directly contributes to cracking of concrete in offshore structure. While the specific causes of cracking are numerous, cracks are normally caused by stresses that develop in concrete due to restraint of volumetric change or due to external loads applied to the structure.

Cracks in structural concrete, in most cases, are not structurally significant but it can be beneficial when serving as an indicator for those cases where there may be more serious structural performance problems. However, nominal cracking that accompanies flexural behavior can affect the appearance of monolithic construction and raise concerns about resistance and durability

The issue of corrosion control and structural durability is generally believed to be the real basis for the crack control provisions in offshore structural design codes. It seems entirely intuitive that limiting crack widths limits the possibility for the entry of moisture and salts to the surface of the reinforcing steel that, together with oxygen, can set the stage for corrosion.

Cracking usually starts as microcracks in the cement paste. Microcracks extend and join into visible cracks whose widths are measurable. Where reinforcement is used to control cracking, the gradual development of shrinkage

strains with time increases the extent and width of cracks, regardless of whether the initial cause was extreme loads or restrained deformation. Crack width depends on the quantities, orientation, and distribution of reinforcing steel across the crack and on the characteristics of the bond between the concrete and reinforcement bars in and near the crack. The maximum crack width considered acceptable depends on the type of structure, the location within the structure, the environment, and the consequences of excessive cracking.

Offshore structures are exposed to harsh environmental conditions, including exposure to seawater and sea spray or the structure's existence in the splash zone. The design of offshore structures is controlled by mandatory design codes to ensure structural safety and integrity. Most of the available expressions for crack width were developed for building structures using normal strength concrete and relatively small concrete cover. However, offshore structures are built using thick high strength concrete cross sections with thick concrete cover.

The current Canadian Offshore Code, CSA Standard S474-04, indirectly specifies a crack width limit of 0.25 mm in the splash zone and 0.5 mm in other zones. A lack of available research data on the prediction of crack properties results in unnecessary overdesign of steel reinforcement to satisfy conservative offshore

crack code requirements. The engineer must be aware that also controlling crack width is directly related to the public perception of engineering competence.

1.2 Objective

The main objective of this study is to investigate the cracking criteria for offshore structures. The specific objectives can be summarized as follows:

- To establish experimental data for the cracking behaviour of high strength concrete sections up to 200 mm thick with 30 mm to 60 mm concrete cover under tensile and flexure loading.
- To develop a rational numerical model suitable for predicting the cracking criteria of high strength concrete that affect crack width and spacing of flexural cracks under sustained service loads.
- To investigate the suitability of the current crack width control equation recommended by the CSA Standard S474-04 against other existing crack models.
- To check the validity of the developed cracking criteria against experimental data.

Assessment of the proposed model will be achieved through comparing the prediction of maximum crack width given by each model against collected test

results. Eight two-way reinforcing concrete specimens with different thick concrete cover and bar spacing will be tested under flexural loading.

1.3 Scope

There is a lack of available research data on the prediction of crack properties. Most of the published research related to crack width predictions is addressed for one-way slabs and beams. However, offshore structures are built using two-way slabs made of high strength concrete with thick concrete cover.

The current research is focused on enriching the literature with a comprehensive study on crack properties prediction of two-way slabs. The scope of this work includes investigating experimentally and numerically the effectiveness of concrete cover and bar spacing.

The proposed experimental research program is designed to investigate the behavior of high strength thick concrete panels reinforced up to 200 mm thick with a 30 mm to 60 mm concrete cover. The experimental investigation shall be conducted on the two-way slab test set up at the Structural Lab of Memorial University. The existing test setup was modified to handle thicker specimens under higher flexural loads. Based on the results of this investigation, the parameters for the developed cracking model will be calibrated and verified. The main test variables will include the concrete compressive strength, bar spacing and bar diameter.

The proposed theoretical investigation includes the development of a numerical crack analysis model that will be based on the tension chord method (Marti et al, 1998), equilibrium and compatibility equations. The second model is based on equilibrium and fracture energy principles. Fracture energy is a material property, and by definition it is the energy needed to create a crack of unit length and unit width. Tension softening of plain concrete is defined by Hillerborg *et al.* (1976) as the integration of the tensile stress-displacement relation as the "fracture energy". The contribution of reinforcement through bond is known as tension stiffening. Tension stiffening affects the total energy release of the reinforced concrete member in the post cracking range. The tension stiffening contribution also enhances the serviceability requirements, and it plays a major role in the non-linear analysis of reinforced concrete. The idealization of the post cracking range was developed using several approaches. Among these approaches is the use of fracture energy principles. This idealization was adapted earlier by many researchers to overcome the size effects on the response of reinforced concrete members (Gustafsson and Hillerborg 1998; Marzouk and Chen 1995). The second proposed model will utilize the fracture energy principal for the calculation of crack width.

1.4 Thesis Format

This thesis consists of six chapters. Chapter 1, contains a brief introduction on crack phenomena in two-way reinforced concrete slab followed by the scope of the current research as well as the significant of the research study. Chapter 2, contains a literature review of research that has led to some of the existing equations in European and North American codes such as ACI 318, Canadian offshore code, Norwegian Code, CEB-FIP and Euro code EC2. The chapter also provides the background for present day studies related to predicting cracking behavior in reinforced concrete. Chapter 3, describes the experimental investigation, test program, test set up, instrumentation and preparation of high strength concrete specimens. The cracking behavior of high reinforced concrete two-way slab is examined experimentally, with emphasis on the effect of concrete cover, bar spacing and slab thickness. Chapter 4, reports the observed test results in terms of load-deflection relationship, the strains in the concrete and the steel bars, the crack width, and the crack patterns. Chapter 5, evaluates the cracking criteria and some proposed empirical expressions using current experimental results. The effect of different variables on crack properties of high reinforced concrete two-way slabs are also examined. A novel empirical analysis for design purpose is proposed. The

conclusions of this study along with recommendations for further research are presented in Chapter 6.

Chapter 2

Literature Review

2.1 General

Reinforced concrete two-way slab is a popular structural system. This system has contributed to the development of reinforced concrete as a construction material since the construction of the first two-way slab in 1906 in the USA by Turner, as reported by Sozen and Seiss (1963). In the same year, Maillart of Switzerland built a two-way slab system in Europe. A considerable amount of research has been

conducted to investigate the behavior of reinforced concrete two-way slabs since that time.

Cracking problem in reinforced concrete members has been investigated by many researchers since at least the turn of the 20th century. Many theoretical models have been proposed by several researches to predict cracking in both radial and tangential directions.

In this chapter, a short review is presented for the most relevant literature on cracking and bond effect of reinforced concrete flexural members. It starts with an introduction that gives an idea about the crack phenomena and the main reasons for it followed by an explanation of the behavior of plain concrete under direct tension at different stages of loading. Current methods used for controlling the crack width are detailed and the crack spacing in reinforced concrete structures are examined. Moreover, this chapter presents the different European and North American approaches that deal with the prediction of cracking properties.

2.2 Introduction

Flexural members such as beams and slabs represent the majority of structural elements. In general, concrete can handle compressive forces very effectively. However, concrete cracks under tension forces can cause several problems. Cracks play an important role in concrete's response to load in both compression and

tension. Moreover, there are extra internal forces and stresses that develop due to temperature and long term effects. If such cracks are too wide, it will destroy the aesthetics of the structure and will cause a significant reduction in flexure stiffness of the structure member.

Cracks may expose bars to the environment causing corrosion of steel. In order to protect the structure members from these effects, cracks should be minimized to acceptable limits under normal service loads. With adequate design and good reinforcement details, cracks can be limited to a small value in width, such that the appearance or performance of the structure is not harmed. Many methods have been suggested to control cracking; however, most of such methods are merely empirical rules resulting from observations or testing. Furthermore, there is no agreement on what crack width should be permitted for different types of structures. Besides, the accurate prediction of crack width is not possible yet.

2.3 Fracture Energy and Tension Stiffening

The cracking process starts at a low tensile stress level. This cracking phenomenon is governed by concrete tensile properties which is an important feature of concrete and has a significant effect on the behavior of concrete structural member. The stress-strain response of concrete is closely associated with formation of micro cracks at the coarse-aggregate boundaries and propagates through the surrounding

mortar. The nonlinearity of concrete behaviour is highly dependent upon the response of these two materials, namely; the cement paste and the aggregate. Cracking is less dependent upon bond and mortar micro cracking. A fracture mechanics model called the fictitious crack model was developed by Hillerborg, (1976) and Crisfield, (1986) to explain the plain concrete behavior, as shown in Figure 2.1.a, b and c. This model is a method for description of stress versus deformation properties of material section. Before peak stress, the deformation of the specimen under uniform tension is assumed to be uniform along the length of the specimen. At peak stress, a localized fracture zone, or a concentrated damage zone is assumed to develop. As the total elongation of the specimen increases further, the stress within the specimen decreases gradually and the strain outside the concentrated fracture zone decreases (unloading) while additional deformation or elongation w within the fracture zone increases (softening). The properties of the material are described in Figure 2.1.c, by a stress-strain ($\sigma - \epsilon$) diagram, valid for the additional deformation of the material within the fracture. Both ($\sigma - \epsilon$) and ($\sigma - w$) are simplified to straight lines as shown in Figure 2.1.c. Also the straight lines in ($\sigma - \epsilon$) diagram corresponds to purely elastic conditions that indicates that the cracks developed at this stage can be closed when the load is released. For defined or assumed linear or nonlinear normalized shapes of ($\sigma - \epsilon$) and ($\sigma - w$)

curves, there are three parameters f_t tensile strength, E modulus of elasticity and G_F fracture energy. G_F is defined as the area under the entire softening stress elongation curve $\sigma - w$, which is given by

$$G_F = \int_0^{w_c} \sigma(w) dw \quad (2.3.1)$$

where:

G_F = The area under the entire softening stress elongation curve,

$\sigma(w)$ = Softening stress separation curve,

w_c = The critical crack separation displacement.

In another way G_F , which can also be defined as the energy absorbed per unit area of crack, is regarded as the fracture parameter. In order to relate f_t to G_F a characteristic length is introduced that represents the ratio between the two straight lines curves ($\sigma - \epsilon, \sigma - w$)

$$l_{ch} = \frac{EG_F}{f_t^2} \quad (2.3.2)$$

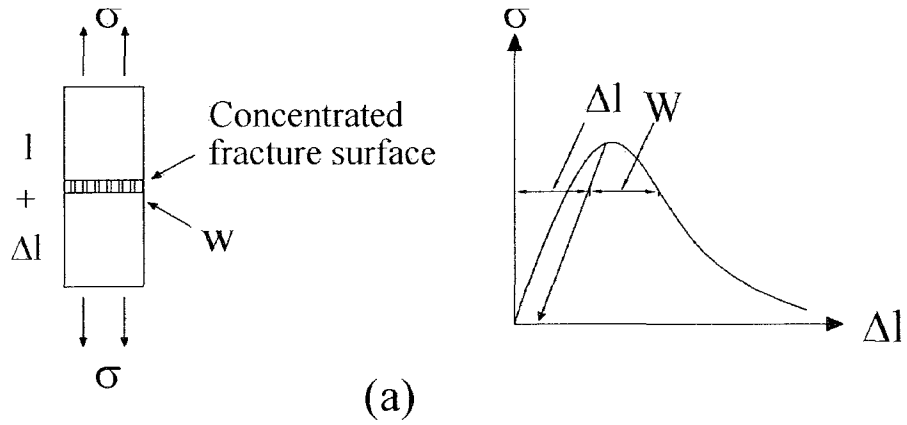
where:

l_{ch} = Characteristic length,

For different mixes of concrete, l_{ch} values are in the range of 180 mm to 1300 mm (Gustafsson and Hillerborg, 1988) and (Phillips and Binsheng, 1993). Marzouk and Chen (1995) reported that characteristic length strongly decreases as concrete strength increases, and high strength concrete characteristic length is about 2-3 times smaller than normal-strength concrete prepared with the same aggregate

2.4 Crack Control in Reinforced Concrete Members

The control of cracking in reinforced concrete structures is usually achieved by limiting the stress increments in the bonded steel bars to an appropriate low value and ensuring that the bonded reinforcement is suitably distributed. The width of crack also depends on the quantity, orientation and distribution of reinforcing steel crossing the crack. It also depends on the deformation characteristic of the concrete and the bond between the concrete and the reinforcement bars. The bonded reinforcement in every reinforced concrete structures provides restraint to shrinkage. As concrete shrinks under compressive force, the steel reinforcement imposes an equal and opposite tensile force on the concrete at the level of the bonded steel. These internal restraining forces are often significant enough to cause time-dependent cracking.



Before Peak stress $\Delta l = \epsilon l$
 After peak stress $\Delta l = \epsilon l + w$

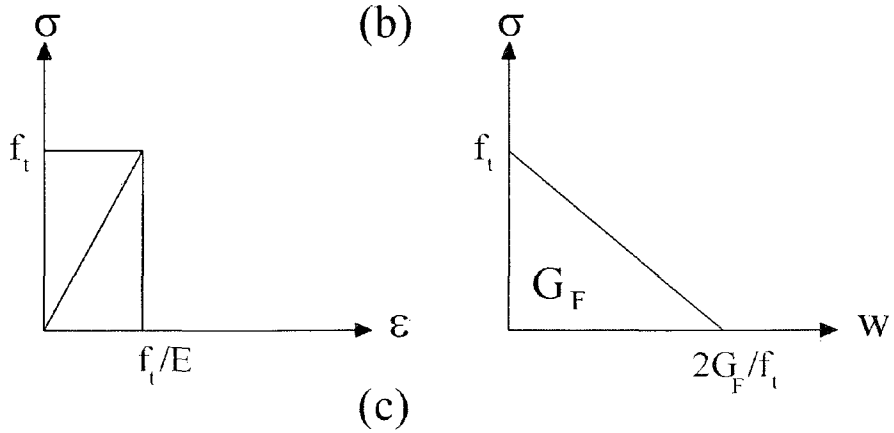
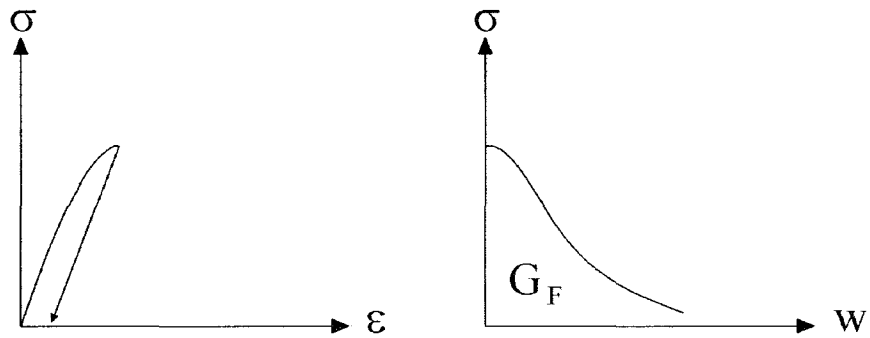


Figure 2.1: Principal of fictitious crack model (Gustafsson and Hillerborg, 1986)

2.5 Tension Cracking Model Chord

There are two analytical models that have been developed to predict the crack width based on equilibrium and the tension chord assumptions as summarized by Gilbert (2005). The first model is to explain flexure cracking and the second model to explain direct tension model.

2.5.1 Flexural Cracking Chord Model

Consider a segment of a reinforced concrete rectangular section, as shown in Figure 2.2, subjected to a service bending moment M_s which is greater than M_{cr} . The spacing between concrete cracks is S . Away from the crack the area of concrete in tension is assumed to carry a uniform tensile stress σ_{ct} which will develop due to the bond stress τ_b that exists between the tensile steel and the surrounding concrete. As the distance x from the crack increases, the stress in steel reduces due to the bond stress τ_b between the steel and the surrounding tensile concrete as shown in Figure 2.2. For reinforced concrete under service loads, where σ_{st} is less than the yield stress f_{sy} , Martie, Alvarez, Kaufmann and Sigrist, (1998) assumed a rigid plastic bond stress slip relationship at all values of slip which is about twice the direct tensile strength of concrete f_{ct} . In reality τ_b is affected by steel stress, concrete cover, bar spacing, stirrups, lateral pressure, degree of compaction, and

size of bar deformations and it is likely to be reduced by shrinkage. Experimental observation indicates that τ_b reduces as the stress in the reinforcement increase (Gilbert, 2005).

$$\tau_b = \alpha_1 \alpha_2 f_{ct} \quad (2.5.1.1)$$

where:

α_1 = Depends on the steel stress at crack,

α_2 = For short or long term calculations,

f_{ct} = Direct tensile strength of concrete.

Under sustained load, additional cracks occur between widely spaced cracks due to the combined effect of tensile creep rupture and shrinkage. The final crack width can be defined as the difference between the elongation of the steel over the distance between cracks and the extension of the concrete caused by σ_{cx} plus the shortening of the concrete between cracks due to long term deformation.

$$w^* = \frac{S^*}{E_s} \left[\frac{T}{A_{st}} - \frac{\tau_b S^*}{\phi} (1 + n\rho) - \epsilon_{sh} E_s \right] \quad (2.5.1.2)$$

where:

w^* = Final crack width,

S^* = Final crack spacing,

E_s = Steel modulus of elasticity,

T = Axial tensile force,

ϕ = Bar diameter,

A_{st} = Area of tensile reinforcement,

τ_b = Bond stress (between existing steel and surrounding concrete)

n = Modular ratio of the section,

ρ = Reinforcement ratio (A_{st} / A_{ct}).

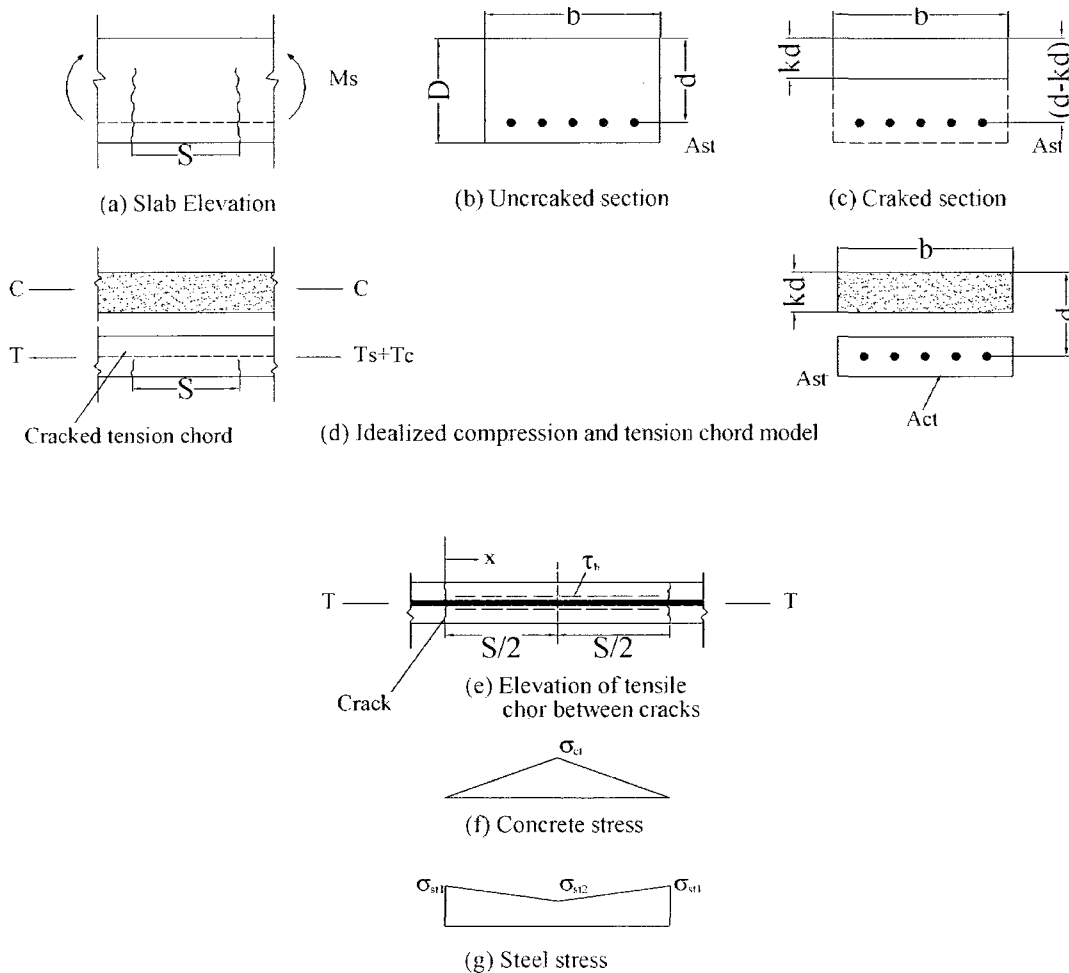


Figure 2.2: Cracked reinforced concrete slab tension chord model (Gilbert, 2005).

2.5.2 Direct Tension Cracking Chord Model

When the first crack occurs as shown in Figure 2.3, the restraining forces reduce to N_{cr} and the concrete stress away from the crack is less than the tensile strength of the concrete f_{ct} . At the crack, the steel carries the entire force N_{cr} and the stress in the concrete is zero. At some distance s_o on each side of the crack, the concrete and steel stresses are no longer influenced by the presence of the crack (See Figure 2.3).

$$s_o = \frac{\phi}{10\rho} \quad (2.5.2.1)$$

where:

s_o = The distance over which stresses vary on each side of the crack,

ϕ = Bar diameter,

ρ = Reinforcement ratio.

The following expression was earlier used by Faver, 1983 for members containing deformed bars or welded wire mesh.

$$S_{ro} = k_1 \frac{d_b}{4\rho} \quad (2.5.2.2)$$

where:

S_{ro} = Represents the distance between the first crack and the cross-section at which concrete stress reaches f_{ct} ,

k_1 = A dimensionless coefficient depending upon bond properties of the reinforcing bars,

d_b = The bar diameter.

The final crack width can be calculated as the shortening of the concrete between the cracks due to shrinkage minus the elongation of the concrete due to tensile stress between the cracks plus the final elongation of the member over the distance between cracks due to support movement

$$w^* = \frac{S^*}{E_s} \left[\frac{\Delta u E_s}{L} - \frac{\tau_b S^* n \rho}{\phi} - \epsilon_{sh} E_s \right] \quad (2.5.2.3)$$

where:

Δu = Supports movement,

L = member length,

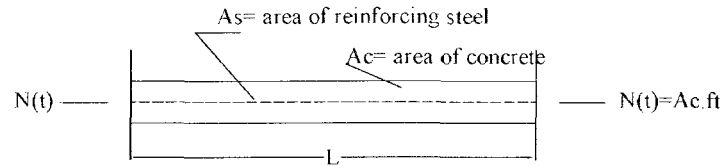
ϵ_{sh} = Shrinkage strain.

$$S^* = 0.5S_{max} \quad (2.5.2.4)$$

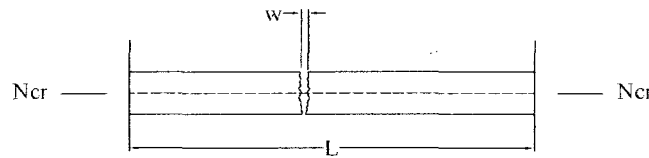
2.6 Statistical Models for Crack Predictions

Many theoretical models have been proposed to predict cracking in either direct or flexural tension. The earliest approach, which is still being applied in present day research, may be termed the semi-empirical approach (statistical approach) whereby experimental data are analyzed and a predictive equation for

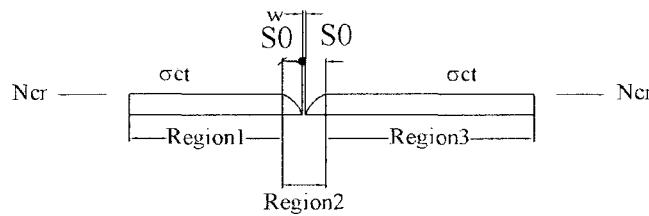
crack width is developed which minimizes the variation between model and experiment. A German paper published in 1904, as referenced by Nawy (1968), is the earliest



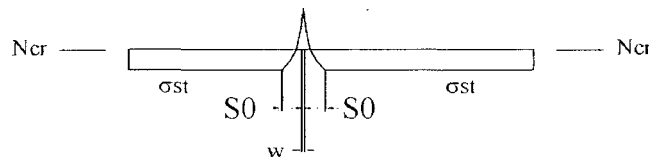
(a) Just prior to first cracking



(b) Just after first cracking



(c) Average concrete stress just after cracking



(d) steel stress just after first cracking

Figure 2.3: First cracking in a restrained tension member (Gilbert, 2005)

record of research found relating to the cracking behavior of reinforced concrete. Since that time, extensive research studies have resulted in a number of predictive equations which, typically, predict the probable maximum crack width.

Investigations prior to 1940 concerning cracks in symmetrically reinforced concrete members were summarized by Watstein and Parsons (1943). The researchers concluded that for a given type of steel at a constant stress level, the most prominent factor affecting crack width and spacing was the ratio D/ρ , where D is the diameter of the reinforcing bar (in) and ρ is the reinforcement ratio of longitudinal reinforcement. In addition, crack width was almost completely independent of the concrete strength.

In 1956, Clark modified the Watstein and Parsons, (1943) equation that was originally derived for symmetrically reinforced and axially loaded cylindrical specimens, to apply to reinforced concrete flexural members. The modification was based on data gathered in the first large-scale test program to investigate the influence of various beam parameters on crack widths on the flexural tension face of beams. A total of 70 beams with different widths, depths, spans, bar sizes and reinforcement ratios were tested which led to the addition of the term $(h-d)/d$ into the crack width equation and the observation causing initial cracking.

$$W_{avg} = C_1 \frac{D}{\rho} \left[f_s - C_2 \left(\frac{1}{\rho} + n \right) \right] \cdot \frac{(h-d)}{d} \quad (2.6.1)$$

$$W_{max} = 1.64 W_{avg} \quad (2.6.2)$$

where:

W_{avg} = Average crack width,

W_{max} = Maximum crack width,

$C_1 = 0.0227$,

$C_2 = 0.0566$,

h = The beam height in (in),

d = The effective depth of longitudinal reinforcement.

Chi and Kirstein (1958) continued Clark's research of by testing an additional 16 beams from which a new expression was developed assuming the bond stress between concrete and steel varies linearly from zero at a crack face to maximum midway between cracks.

$$w = 5 \phi D \left(\frac{f_s - \frac{2500}{\phi \cdot D}}{E_s} \right) \quad (2.6.3)$$

where:

w_{ave} = The average crack width in (in),

ϕ = A semi-empirical dimensionless parameter depending on the general arrangement and diameter of reinforcement,

E_s = Modulus of elasticity of steel (ksi).

At about the same time in 1963, Broms working with reinforced concrete tensile and flexural specimens introduced the concept of primary cracks, secondary crack and the zero axial stress circles as shown in Figure 2.4.

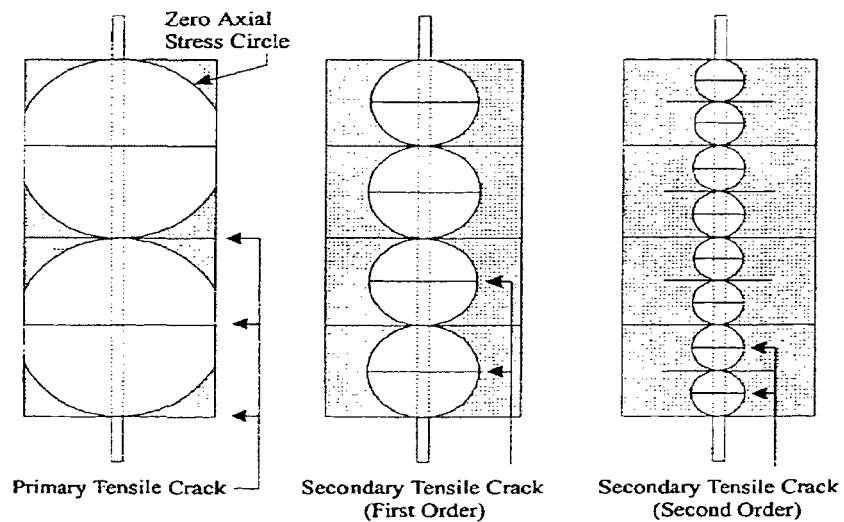


Figure 2.4: Broms' mechanism of tension cracking with a single reinforcing bar

(Brom, 1963)

In flexural specimens, primary cracks develop across a cross-section when the axial load exceeds concrete tensile strength while secondary cracks develop

midway between primary cracks at higher steel stresses. The length of the secondary cracks is approximately equal to the distance between two adjacent primary cracks, making them equal in length to the diameter of the zero stress circle. Using this model, the minimum theoretical primary crack spacing, for cracks to be observable on the surface of the specimen, is equivalent to the thickness of the concrete cover, where cover thickness is measured from the centre of the reinforcing bar as shown in Figure 2.5. However, the theoretical primary crack spacing will vary between a value equal to the thickness of the concrete cover and just less than twice the thickness of cover. An average crack spacing of 1.5 times the thickness of cover is then expected. This expected spacing is reduced as the ability of the reinforcement to develop high bond stress increases

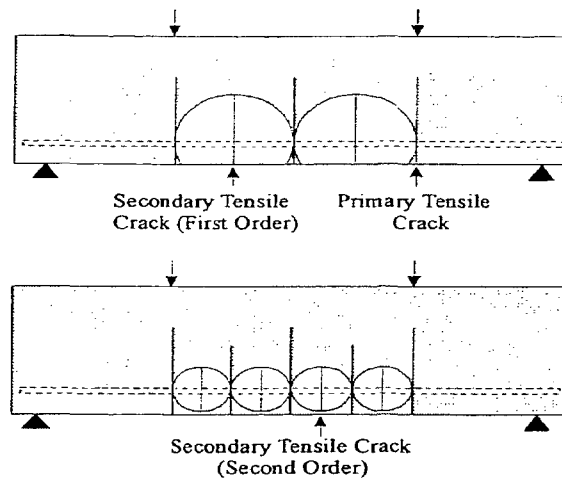


Figure 2.5: Broms' mechanism of tension cracking (flexural members)

In 1965, Broms tested a total of 37 tension members and 10 flexural members reinforced with a single high strength bar. Using the test data, it was concluded that

measured average crack spacing was closer to twice the cover thickness rather than the theoretical value of 1.5 times cover thickness. The average crack width was then calculated assuming the elongation of the concrete between cracks is small as compared to the elongation of the reinforcement and can be neglected. Later Broms and Lutz (1965) extended the Hongestad and Kaar-Mattock (1965) equation to include members with multiple bars.

$$S_{avg} = 2t \quad (2.6.4)$$

$$W_{avg} = S_{avg} \epsilon_s \quad (2.6.5)$$

where:

S_{avg} = Average crack spacing,

t = The distance from the center of the reinforcing bar to the nearest surface,

ϵ_s = The average steel strain.

Gergely and Lutz (1968) performed a statistical evaluation of experimental cracking data using a multiple regression analysis computer program resulted in the well known equation for the calculation of crack widths. The data used in the study included test results from Hongestad (1962), Kaar and Mattock (1963), Kaar and Hongestad (1965) and Clark (1956). Crack widths were recorded at two primary locations; the bottom tension surface as shown in Figure 2.6 and the side face at the level of the reinforcement and the crack width was measured at certain stress levels

which were considered statistically as an observation. The following general conclusions were reached:

- The reinforcing steel stress is the most important variable;
- The thickness of the concrete cover is an important variable since the concrete strain is proportional to it;
- The area of concrete surrounding each reinforcing bar is also an important geometric variable;
- The ratio of crack width at the surface to that at the reinforcement level is proportional to the ratio of the nominal strain at the surface and the reinforcement strain.

The equation that was considered to best predict the maximum bottom and side crack widths are

$$w_b = 0.091\sqrt[3]{t_b A} \beta (f_s - 5) \times 10^{-3} \quad (2.6.6)$$

$$w_s = \frac{0.091\sqrt[3]{t_b A}}{1 + \frac{t_s}{h_1}} (f_s - 5) \times 10^{-3} \quad (2.6.7)$$

where:

w_s = Maximum (measured or calculated) side crack width at level of steel in constant moment region,

w_b = Maximum (measured or calculated) bottom crack width at level of steel in constant moment region,

t_b = Bottom cover measured from the center of the lowest bar,

t_s = Side cover measured from the center of outer bar,

f_s = Steel stress calculated by elastic cracked section theory,

$A = A_c / m$ = average effective concrete area around a reinforcing bar,

m = Number of tensile reinforcing bar,

h_1 = Distance from the neutral axis to the center of the reinforcing bar,

β = Ratio of distances to neutral axis from extreme tension fiber to center of reinforcement.

Simplification of bottom crack width equation yielded the following equation

$$w_b = 0.076\beta f_s \sqrt[3]{d_c A} \quad (2.6.8)$$

where:

d_c = bottom cover measured from center of lowest bar.

Another equation developed by Kaar and Mattock (1963) using a curve fit of limited data primarily from Hongstad and Kaar-Mattock (1965) is:

$$w_b = 0.115\beta f_s \sqrt{A} \quad (2.6.9)$$

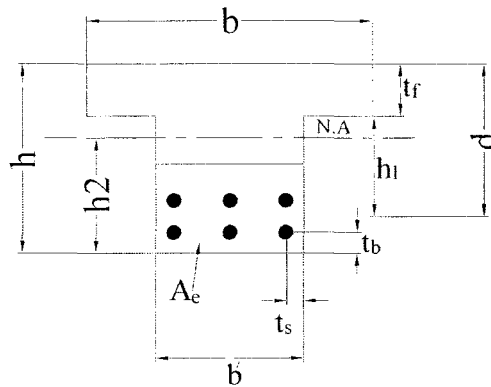


Figure 2.6: Dimensional notation

Other researchers like Goto (1971) found that the initial internal cracks occur behind the ribs of the deformed steel bars. After initial cracking, the axial tensile forces will be carried by the concrete surrounding the steel bar. The contribution of the bond slip to the crack width was illustrated by Leonhardt (1977) whose investigation proved that a sudden jump in steel stress is a result of the concrete cracking and that a combination of bond slippage and internal cracking determine the crack width size. Finally, the average crack spacing equation was modified by Rizkalla et al. (1983) as follows:

$$S_m = 5(d + 7.2) + 1.33c + 0.08d/\rho \quad (2.6.10)$$

where:

S_m = average crack spacing (mm),

d = diameter of reinforcing bar (mm),

c = concrete cover to the surface of bar (mm),

ρ = steel ratio.

The final cited research which used the semi-empirical approach to study the cracking behavior of concrete was done by Oh and Kang (1987). The background of their study was based on fracture mechanics principles. However, the proposed equations for predicting crack width and spacing in flexural members were derived using the data of past researchers Clark (1956), Chi and Kirstein (1958), Watstein and Mathey (1959), Hognestad (1962), and Kaar and Mattock (1963). Both Equations 2.6.8 and 2.6.9 gave reasonable results for crack width up to 2.5 in (63.5 mm) and since the test data for thicker covers are not available; it is not possible to determine which, if either, equation is correct. Therefore, an alternative approach for the calculation of crack widths is proposed for thicker concrete cover ($d_c \geq 2.5$ in) by Frosch (1999). In his approach, a flexural cracking model is considered and the crack width is assumed as a function of the bar spacing and the distance between the reinforcing steel. Therefore, crack control can be achieved by

limiting the spacing of the reinforcing steel. The equation for the maximum crack width of uncoated reinforcement is

$$w_c = 2 \frac{f_s}{E_s} \beta \sqrt{d_c^2 + \left(\frac{s}{2}\right)^2} \quad (2.6.11)$$

where:

w_c = Limiting crack width,

s = Maximum permissible bar spacing,

d_c = Bottom cover measured from the center of the bar,

$f_s = 0.6 f_y$,

$\beta = 1.0 + 0.08 d_c$.

Since the width of the crack at the surface of the tension side concrete is going to be wider than the width of the crack at the center of reinforcement level, β is used as an amplification factor to account for the change of the strain over the beam section. Makhoulf and Malhas (1996) evaluated the effect of concrete cover on crack width equation used by the American and British design code provisions and recommended that additional research be directed toward modifying the effect of concrete cover on the computed value of maximum crack width.

$$\beta = \frac{\epsilon_2}{\epsilon_1} = \frac{h - c}{d - c} \quad (2.6.12)$$

where;

ϵ_s = Strain at the level of steel reinforcement,

ϵ_c = Strain at the tension surface of the concrete section,

c = Compression depth,

d = Effective depth,

h = Section height,

d_c = bottom cover measured from the center of the lowest bar.

Nawy and Blair (1971) found that crack-control equations for beams underestimate the crack widths developed in two-way slabs and do not indicate the optimum spacing of reinforcement. The crack width in two-way plate is controlled primarily by the steel stress level and the spacing of the reinforcement in the two perpendicular directions. In addition, the clear concrete cover in two-way slabs and plates is nearly constant (20 mm for most interior structural slabs), whereas it is a major variable in the crack-control equations for beams.

Analysis of data on cracking in two-way slabs and plates conducted by Nawy and Blair (1971) has provided the following equation for predicting the maximum crack width

$$w = k\beta f_s \sqrt{I} \quad (2.6.13)$$

Where the terms inside the radical are collectively termed the grid index:

$$I = \frac{d_{b1}s_2}{\rho_{t1}} \left[\frac{s_1s_2d_c}{d_{b1}} \frac{8}{\pi} \right] \quad (2.6.14)$$

where;

k = Fracture coefficient with a value $k = 2.8 \times 10^{-5}$ for uniformly loaded restrained two-way action square slabs and plates. For concentrated loads or reactions or when the ratio of short to long span is less than 0.75 but larger than 0.5, a value of $k = 2.1 \times 10^{-5}$ is applicable. For span aspect ratios less than 0.5, $k = 1.6 \times 10^{-5}$;

$\beta = 1.25$ (chosen to simplify calculations, although it varies between 1.20 and 1.35);

f_s = Actual average service-load stress level or 40% of the specified yield strength f_y ;

d_{b1} = Diameter of the reinforcement in Direction 1 closest to the concrete outer fibers;

s_1 = Spacing of the reinforcement in direction 1;

s_2 = Spacing of the reinforcement in perpendicular direction 2;

ρ_{t1} = Active steel ratio, that is, the area of steel A_s per ft width $/[12d_{b1} + 2c_1]$,

where c_1 is clear concrete cover measured from the tensile face of concrete to

the nearest edge of the reinforcing bar in direction 1, and

w = Crack width at face of concrete caused by flexure,

Direction 1 refers to the direction of reinforcement closest to the outer concrete fibers; this is the direction for which crack-control check should be made.

2.7 ACI Approach (ACI 318-05)

Flexural crack control in beams and one way slabs (span-depth ration in the range of 15 to 20) are based on the statistical analysis (Geregy and Lutz, 1968) of maximum crack width data from a number of sources. Equations that ACI considered best to predict the maximum bottom and side crack width are

$$w_b = 0.091\sqrt[3]{t_b A} \beta (f_s - 5) 10^{-3} \quad (2.7.1)$$

$$w_s = \frac{0.091\sqrt[3]{t_b A}}{1 + \frac{t_s}{h_1}} (f_s - 5) 10^{-3} \quad (2.7.2)$$

where:

w_b, w_s = Most probable crack widths at the bottom of the beam and at level of reinforcement respectively,

f_s = Reinforcing steel stress,

A = Area of concrete symmetric with reinforcing steel divided by number of bars,

t_b = The bottom cover to the center of bars,

t_s = The side cover to the center of bars,

β = Ratio of distance between neutral axis and tension face to distance between neutral axis and reinforcing steel,

h_1 = Distance from neutral axis to the reinforcing steel.

As mentioned earlier a study made by (Frosch, 1999) showed that these equations are valid for a relatively narrow range of covers (up to 63 mm). Frosch proposed a new equation based on the physical phenomenon for determination of the flexural crack widths of reinforcing concrete members. ACI 318 (2005) Section-10.6 does not make any distinction between the exterior and interior exposure. It is required for crack control in beams and one way slabs, however, the spacing of reinforcement shall not be exceeded.

$$s(\text{mm}) = [(95000 / 540f_s) - 2.5C_c] \quad (2.7.3)$$

$$\text{Shall not exceed } 300 \left(\frac{252}{f_s} \right) \text{ mm} \quad (2.7.4)$$

where:

f_s = Reinforcing steel stress at service load,

C_c = Clear cover at tension side,

S = Center to center spacing of flexural tension reinforcement.

The maximum crack width that may be considered not to impair the appearance of a structure and will not endanger the corrosion of steel reinforcement is as presented in Table 2.1 ACI 224R (2001). These values depend on the environment surrounding the structure and depend on various factors such as the position, length and the surface texture of the crack as well as the illumination in the surrounding area.

Table 2.1: Guide to reasonable crack widths in reinforced concrete under service load

Exposure condition	w
Dry air or protective membrane	0.41
Humid, moist air or soil	0.30
De-icing chemicals	0.18
Seawater and seawater spray; wetting and drying	0.15
Water-retaining structures	0.10

w = Maximum allowable crack width in (mm)

2.8 Canadian Offshore Code

CSA S474, (2004) provides the following expression for calculating the crack spacing:

$$S_m = 2.0(c + 0.1S) + k_1 k_2 d_{be} h_{ef} b / A_s \quad (2.8.1)$$

where:

S_m = The average crack spacing (mm) ,

c = Concrete cover (mm) ,

S = Bar spacing of outer layer (mm) ,

k_1 = Coefficient that characterizes bond properties of bars,

k_2 = Coefficient to account for strain gradient,

d_{be} = Bar diameter of outer layer (mm),

h_{ef} = Effective embedment thickness as the greater of $(c + d_{be}) + 7.5d_{be}$ not greater than the tension zone or half slab thickness (mm) ,

b = Width of the section (mm) ,

A_s = Area of reinforcement within the effective embedment thickness (mm²) ,

$\epsilon_1 = \epsilon_t$ and $\epsilon_2 = \epsilon_{ll}$ are the largest and the smallest tensile strains in the effective embedment zones.

The crack spacing provided in Equation 2.8.1 can be divided into two terms. Term A is a function of concrete cover and bar spacing [$A = 2.0(c + 0.1S)$]. Term B relates to the type of bar, the diameter and type of stress [$B = k_1 k_2 d_{be} h_{ef} b / A_s$]. The CSA code recommends that the average crack width may be calculated as the average crack spacing Equation 2.8.1 times the product of the total average tensile concrete strain after considering the contribution of the tension stiffening. The tension stiffening effect calculated according to Equation 2.8.2 is going to reduce the crack width.

$$f_c = f_{cr} / (1 + \sqrt{500\epsilon_1}) \quad (2.8.2)$$

$$f_{cr} = 0.33\lambda\sqrt{f'_c} \quad (2.8.3)$$

where:

f_c = The average tensile stress (MPa),

f_{cr} = Cracking strength of concrete (MPa),

ϵ_1 = Principal concrete strain; tensile strain measured with respect to base lengths long enough.

The maximum crack width according to CSA is in the range of 0.25 mm in the splash zone and up to 0.5 mm elsewhere.

2.9 Norwegian Code

Both the Norwegian code (NS 3473E, 1992) and the CSA code provide similar expressions for calculating crack spacing given by Equation 2.8.1. NS provide the following equations for calculating the crack width.

$$w_k = 1.7w_m \quad (2.9.1)$$

$$w_m = r\epsilon_1 S_{rm} \quad (2.9.2)$$

$$r = 1 - \frac{\beta}{2.5k_1} (\sigma_{sr} / \sigma_s)^2 \geq 0.4 \quad (2.9.3)$$

where:

w_k = Characteristic maximum crack width (mm),

w_m = Average crack width (mm) ,

ϵ_l = The principal tensile strain at level of tensile reinforcement,

$\epsilon_l = \epsilon_s = \sigma_s / E_{sk}$,

σ_s = Stress in the reinforcement in the crack (MPa) ,

σ_{sr} = Stress in the reinforcement at calculated crack (MPa) ,

E_{sk} = Characteristics modulus of elasticity of steel (MPa) ,

k_1 = Coefficient that characterizes bond properties of bars,

β = A coefficient account for type of action,

S_{rm} = Mean crack spacing (mm) .

Compared to the CSA code, the NS code calculates the crack width at the level of steel reinforcement. Moreover, NS code provides more detailed regulations for crack width limitation depending on the environmental conditions. Four environment classes were identified in NS; namely, especially aggressive environment, severely aggressive environment, moderately aggressive environment and mildly aggressive environment. The Canadian offshore structures usually exist in a severely aggressive environment that indicates that crack width limits should be in the range of 0.20 mm and 0.10 mm.

2.10 CEB-FIP (MC-90) Recommendation

The (CEB-FIP, 1990) gives the following equation for calculation of the design crack width:

$$w_k = l_{s,max} (\epsilon_{sm} - \epsilon_{cm} - \epsilon_{cs}) \quad (2.10.1)$$

$$\text{And } w_k \leq w_{lim}$$

where:

w_k = The characteristic crack width,

w_{lim} = The nominal limit value of crack width which is specified for cases of expected functional consequences of cracking, or some particular cases related to durability problems. In absence of specific requirements, it may assume that for exposure cases (as specified in Section 1.5 of the CEB-FIP 1990), a (w_{lim}) value equal to 0.30 mm for reinforced concrete members with respect to both appearance and durability,

$l_{s,max}$ = The length over which slip between steel and concrete occurs; steel and concrete strains, which occur within this length, contribute to the width of the crack,

ϵ_{sm} = The average steel strain within $l_{s,max}$,

ϵ_{cm} = The average concrete strain within $l_{s,max}$,

ϵ_{cs} = The strain of concrete due to shrinkage.

The crack spacing expression of the European CEB-FIP model code (MC 1990) is different when compared to other codes (CSA, NS, and EC2). The CEB-FIP expression does not take into account the strain variation in concrete. In the mean time, the bond effect of CEB-FIP is treated in a different manner. The stress in the steel caused by steel strain will be reduced due to the bond stress between the steel and surrounding tensile concrete. Therefore, instead of using a factor to account for bond effect, the CEB-FIP model code uses the bond stress directly in the expression.

2.11 Eurocode EC2 Provisions

The (EC2-91) limits the maximum crack width to 0.30 mm for sustained load under normal environmental conditions which will not impair the proper functioning of the structure. An expression similar to the CSA code for the average crack spacing is recommended by the EC2 (Equation 2.10.2). However, the EC2 uses a constant for Term A (equation 2.8.1) equal to 50 mm, indicating that the effect of concrete cover and bar spacing is not variable in the first part of the crack spacing equation. It seems that this expression is more suitable for building structures rather than offshore thick concrete with large cover.

Compared to the EC2-91 Equation 2.10.2, CSA and NS codes estimate Term A of the crack spacing Equation 2.8.1 to be equal to 150mm for a typical offshore concrete section (400-600mm thickness and 50-60mm concrete cover). This is a very serious error resulting in a 100mm difference between the two equations once analyzed for a thick concrete offshore structure with a large cover. The crack width is estimated by the next expression.

$$w_k = \beta S_{rm} \xi \epsilon_{sm} \quad (2.10.1)$$

where:

w_k = Design crack width;

S_{rm} = Average stabilized crack spacing;

ξ = A dimensionless coefficient between 0 and 1, representing the effect of the participation of concrete in the tension zone to stiffness the member.

ϵ_{sm} = Mean strain under relevant combination of loads and allowing for the effect of shrinkage;

β = Coefficient relating the average crack width to the design value and equals to 1.7 and 1.3, respectively, for section whose minimum dimension exceed 800mm or is smaller than 300mm.

$$S_{rm} = 50 + k_1 k_2 \frac{d_b A_{cef}}{4A_s} \quad (2.10.2)$$

where:

S_m = The average crack spacing (mm),

k_1 = Coefficient that characterizes bond properties of bars,

k_2 = Coefficient to account for strain gradient,

d_b = Bar diameter of outer layer (mm),

A_s = Area of reinforcement within the effective embedment thickness (mm^2),

A_{cef} = The effective tension area (mm^2) as shown in Figure 2.7.

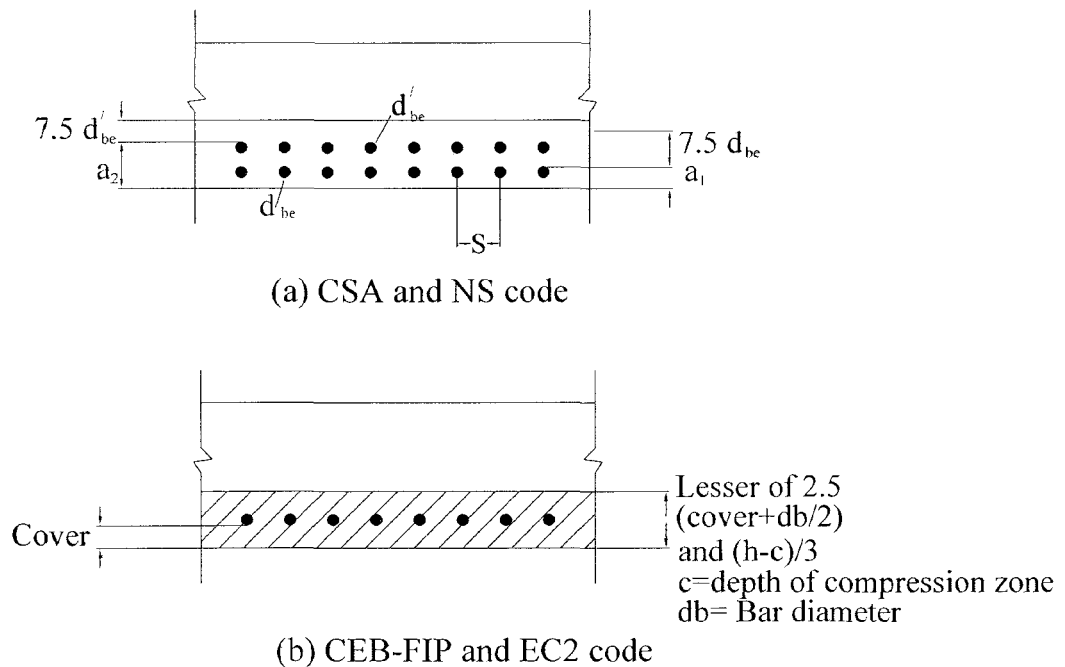


Figure 2.7: Effective embedment thickness of concrete

Chapter 3

Experimental Investigation

3.1 General

This chapter gives a detailed description of the experimental program that was carried out to investigate the cracking behavior of two-way slabs reinforced with steel rebars. It includes sections describing the preparation of the form work, the steel reinforcement and mixing of concrete. The test program consisted of testing and evaluation of the structural performance of five high-strength concrete and three normal-strength concrete slabs. Test setup and different instrumentations are

used to measure the deformations and strains throughout the test program are described in this chapter. The test set-up includes the loading test frame and the hydraulic jack that has been used to apply the loads. In addition, a description of the data acquisition system is also provided in this chapter.

3.2 Properties of Material

3.2.1 Concrete

3.2.1.1 Normal Strength Concrete Mixture

The normal strength concrete (NSC) used in casting the test slab was supplied from a local batch plant. The concrete had a 28 day nominal compressive strength of 35 MPa . The NSC used in casting the column stub was produced in the concrete laboratory at Memorial University of Newfoundland (MUN). The NSC mixture for the column was designed to achieve a target compressive strength of 35 MPa after 28 days. Ordinary Type 10 Portland cement was used in this mix. The maximum aggregate size was 20 mm. The mixture proportions are listed in Table 3.1

Table 3.1: Mix proportions for one batch of the normal strength concrete ($0.1m^3$)

Ingredient	Amount
Cement (kg)	40
Coarse aggregate (kg)	125
Fine aggregate (kg)	83
Water (liter)	18
Obtained compressive strength at 28 days	35 MPa

3.2.1.2 High Strength Concrete Mix design

The high strength concrete (HSC) mix was produced in the concrete laboratory at MUN. The different material used in the mix design are briefly described in this section.

3.2.1.2.1 Materials

CSA Cement Type 10 E-SF cement with blended silica fume was used for all the mixes. The maximum aggregate size was 20mm and the modulus of the fine aggregate was 2.91. Low water cement ratio is required to achieve the high strength. In order to produce the HSC mix, low water to cementitious material ratio (w/c) in range of 0.27 to 0.3 was used in the mixes. To compensate for such low water cement ratio, three chemical admixture systems that include a high- range water reducer, a retarding agent and a water reducing agent had to be used in all mixtures.

The high range water-reducing admixture (superplasticizer) used for the HSC mixtures is commercially known as EUCON 37, it has Naphthalene Sulfonate base and it complies with the requirement of ASTM C-494, Type A & F admixtures.

The water reducing, retarding, and strength increasing liquid admixture used in the HSC mixture is commercially known as EUCON 727. It contains a double metal-organic salt derived from hydroxycarboxylic acids and conforms to ASTM C 494 Type D.

The strength-increasing, water-reducing, liquid admixture for concrete used in the HSC mixture is commercially known as EUCON DX. It is an aqueous solution of hydroxycarboxylic acids and catalyst which provides a better hydration of the cementitious material and it complies with the requirements of ASTM C 494 Type A.

3.2.1.2.2 Mixing Procedure

The concrete mixer in the lab has a limited capacity of 0.12 m^3 . As a result, eight to nine HSC batches were required to cast one slab depending on the size of the specimen. The mix proportions are given in Table 3.2. A total of 3 hours was needed to cast these batches. Therefore, the workability of the concrete was the

major concern during the HSC mix design. The target compressive strength was 70 MPa .

Table 3.2: Mix proportions for one batch of the high strength concrete

Ingredient	Amount
Cement (kg)	40
Coarse aggregate (kg)	107
Fine aggregate (kg)	65
Superplasticizers (ml)	1200
Retarder (ml)	40
Water Reducing Agent (ml)	240
Water (liter)	18
Obtained compressive strength at 28 days	75 MPa

The following mixing procedure was developed for the production of a workable high strength mix using local Newfoundland materials:

- Charge 100% of coarse aggregate;
- Batch 100% of cement;
- Batch 100% of sand;
- Mix for 3-5 minutes after adding 50% of estimated water with superplasticizers;
- Add 25% of estimated water with water reducing agent and mix for 3 minutes;
- Add the last 25% of estimated water with retarder and mix for 3 minutes.

3.2.1.2.3 Curing

Curing the HSC specimens is an essential way to avoid evaporation from the surface of the slab and to achieve the design properties. Without proper curing, significant shrinkage could be found in the specimen. This could lead to a large number of shrinkage cracks on the surface of the slab. It was noted that covering HSC specimen with burlap sheets after casting was an effective way to reduce shrinkage. After 18 hours, the concrete mixture began to consolidate and produced a lot of heat due to the chemical reaction. Watering the HSC specimen at this stage reduced the heat of hydration and did not impair the concrete strength development. By keeping the burlap sheets wet, it kept the surface of the specimen wet and prevented the evaporation of water. The HSC slabs were cured in this way for seven days and then kept in the laboratory until the day of testing.

3.3 Compressive Strength of the Test Slabs

The concrete compressive strength of the test slabs was measured according to the ASTM C39-04. Three standard concrete cylinders (100 mm × 150 mm) were cast from each slab at the same time of casting each slab. The cylinders were cured and kept at the same locations as the slabs in the lab in a temperature around 20 degrees. The control concrete cylinders were capped with melting sulfur and tested at the same time of testing the slab. A compression test machine was used to apply the

load on the specimens up-to-failure under a stress rate of 0.25 MPa /seconds. Figure 3.1 shows a photo of the concrete compression test machine.

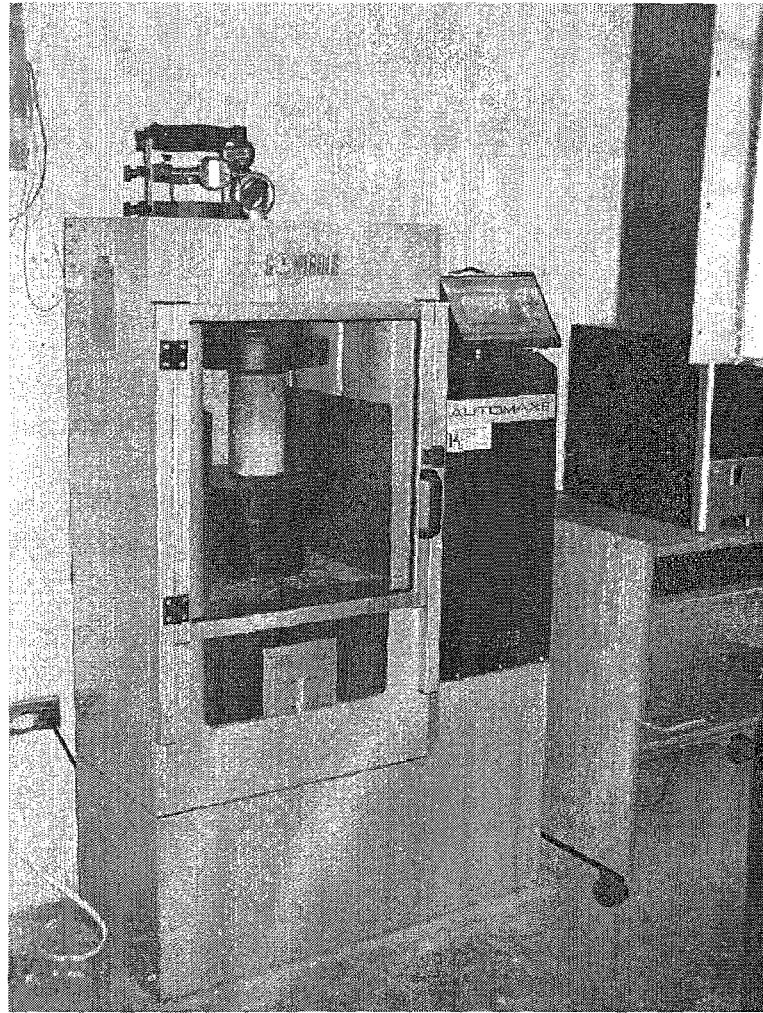


Figure 3.1: Compression test machine.

3.4 Test Slabs

Eight full-scale specimens were cast, instrumented and tested in the current experimental program. The slabs had a side dimension of 1900mm in both directions and were simply supported along all four edges with the corners free to lift. A central load was applied on the slab through a 250mm x 250mm column stub. The dimensions and reinforcement details of a typical test slab are shown in Figure.3.2.

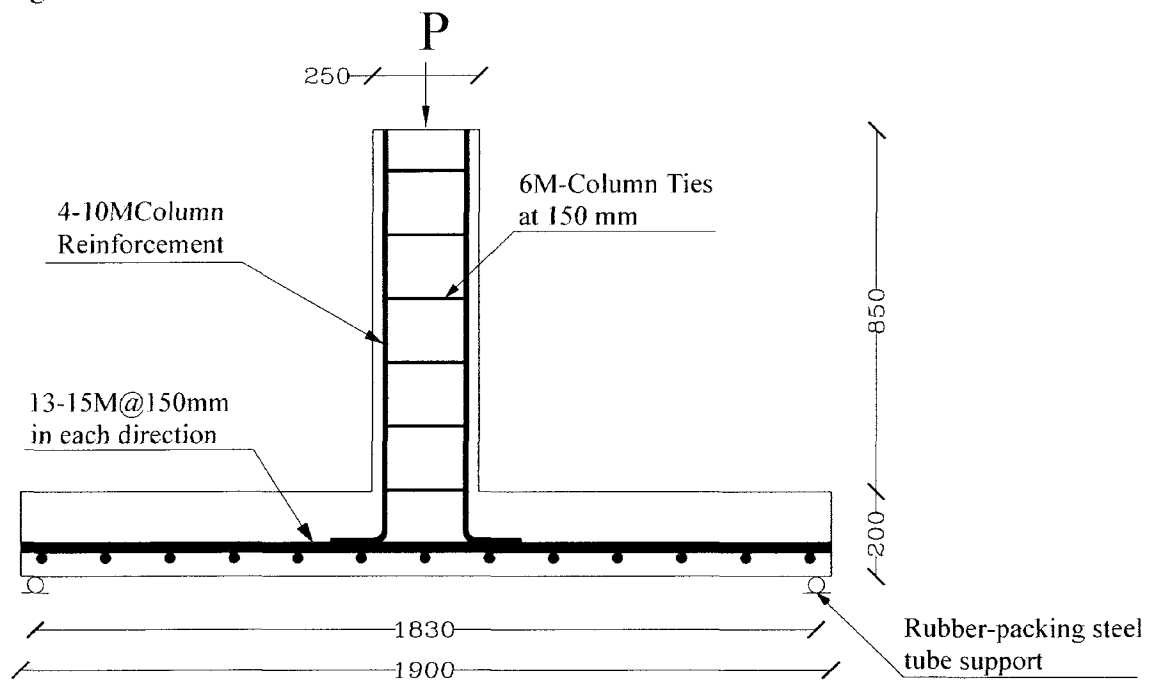


Figure.3.2: Details of a test specimen NSC1

Main variables were concrete cover, bar spacing and slab thickness as shown in Table 3.3.

Table 3.3: Slab specimen details

Series No	Slab No.	h (mm)	Slab Dimensions (mm)	No of Bars	S (mm)	d _{be} (mm)	f' _c (MPa)	f _y (MPa)
Series I	NSC1	200	1900X1900	13	150	25.2	35	400
	HSC1	200	1900X1900	13	150	25.2	68.5	400
	HSC2	200	1900X1900	13	150	25.2	70	400
Series II	HSC3	200	1900X1900	10	200	25.2	66.7	400
	HSC4	200	1900X1900	8	250	25.2	61.2	400
Series III	HSC5	150	1900X1900	20	100	16	70	400
	NSC2	200	1900X1900	8	240	16	33	400
	NSC3	150	1900X1900	8	210	11.3	34	400

d_{be} = Bar diameter

3.5 Slab Formwork and Fabrication

The test slabs were cast in a permanent steel formwork in the concrete lab at MUN. The formwork is supported on steel W-shape columns that are connected with steel I-beams. A square steel 2.0m×2.0m plate with 7 mm thickness is supported on the steel beams. Four removable steel plates with a height of 150 mm are installed at the four edges of the plate as the sides of the formwork. Additional steel plates with a height of 50 mm that could be joined to the side plates were used to construct the 200mm thick slabs as shown in Figure 3.3. Care was taken in order to keep the slab and the column mutually perpendicular while the concrete was being poured. The steel was tied together into a sturdy mat and lifted into the form. The reinforcing mat rested upon chairs made of cement mortar. The

chairs were placed far away from the punching zone in order to eliminate their effect on the observed shear strength. However, during concreting great care was taken to insure that the cover provided was uniform.

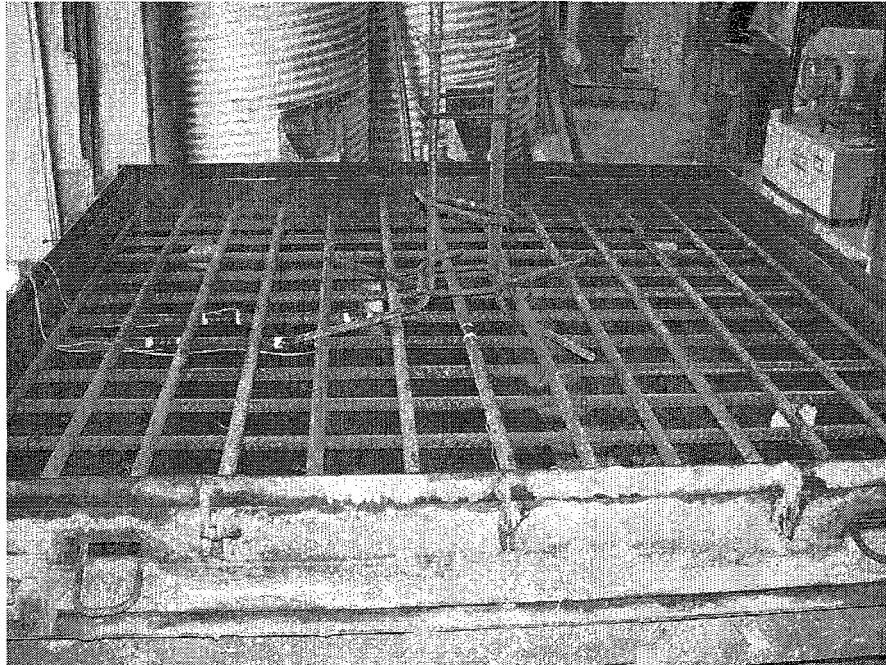


Figure.3.3: A reinforcement cage in the formwork for a typical slab

Steel bars were all cut to the same length of 1840 mm that allowed for a distance of 30 mm from each side of the formwork edges. The strain gauges were mounted at predetermined locations on the steel bars. The steel bars were arranged together to form a reinforcement cage. For the column stub reinforcement, four 900 mm long steel bars bent at right angles were used with horizontal legs. Two 10mm steel hooks were placed on one side of the slab for lifting purposes.

During casting, the concrete was vibrated using a vibrator. When full compaction was attained, the top face of the slab was leveled and finished with a steel trowel. As mentioned earlier, three 100 mm x 150 mm concrete cylinders were also cast to determine the compressive strength. On the next day, a steel mould used for construction of the column stub was placed at the center of the slab. The column stub was cast using a concrete mix that was produced in the lab.

3.6 Test Set-up

All the slabs were tested in a vertical position in order to detect and mark the cracks as it developed. The test frame is a space frame made of steel wide flange and channel sections as shown in Figure. 3.4. The frame is anchored to the concrete floor and is self-reacting. Four 32 mm diameter rods are welded on the vertical W-shape sections to form the four sides of the slab support system. A 3 mm packing rubber was placed on the supports that were made of steel tubes to minimize the friction between the support and the slab.

A hydraulic jack is mounted to the frame and is used to apply a central load on the column stub in a horizontal position. A CLRG-30012 type hydraulic jack cylinder with a maximum capacity of 1335 kN (300 kips) and a maximum displacement of 300 mm (11.81 in) was used. The applied load and the

displacement of the hydraulic jack were measured by its external load cell and a linear voltage displacement transducer (LPDT) attached to it, respectively.

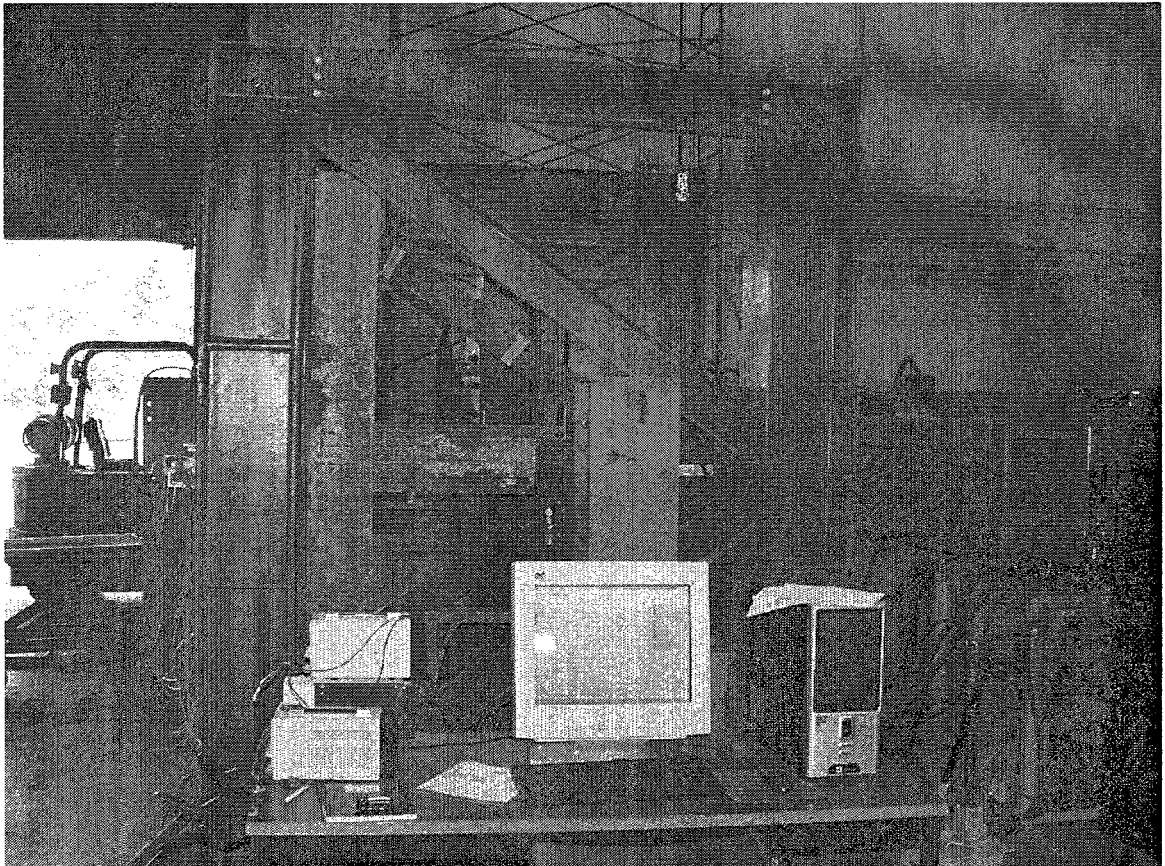


Figure.3.4: The test set-up

3.7 Instrumentation and Measurements

3.7.1 Deflections

The deflection of the slabs was measured during loading by five linear potential differential transducers (LPDTs) at five predetermined locations on the tension

surface as shown in Figure 3.5. The readings from the LPDTs were logged into a data acquisition system. The measured deformation values were readjusted by relating all the deformations to the deformation measured with the LPDT that was placed just above the support.

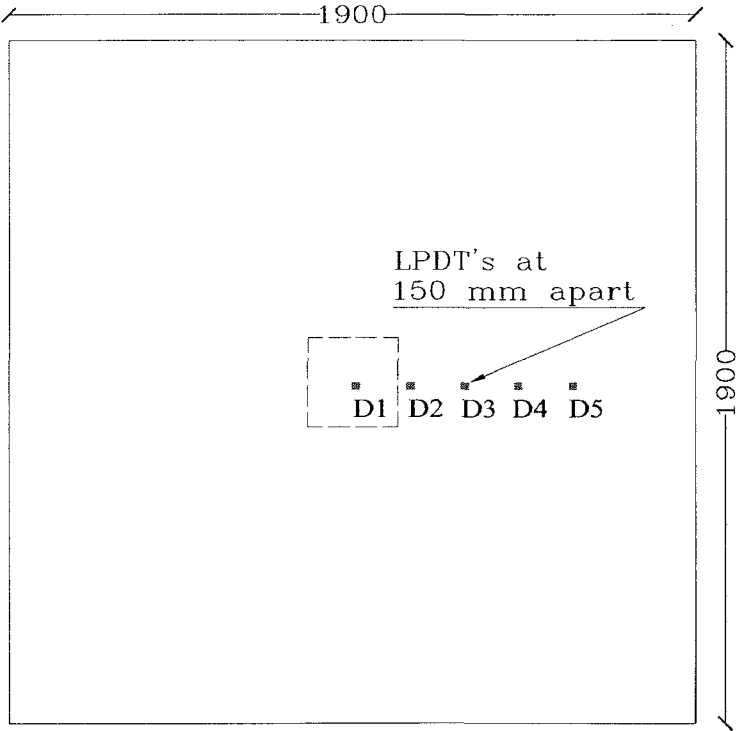


Figure 3.5: A typical arrangement of LVDT's

3.7.2 Steel Strains

The steel strains were measured in each connection at different locations by means of electrical strain gauges. Figure 3.6 shows a typical arrangement of the steel strain gauges. The strain gauges were 6 mm long, with a strain limit

of approximately 5%. The resistance of strain gauge is $120\Omega \pm 0.2\%$ at 24°C and the gauge factor is $2.075 \pm 0.5\%$ at the same temperature. The normal use temperature range for the static strain measurement is 75°C to 175°C . For protection against any possible water damage during casting, the strain gauges were coated with a protective sealant and then covered with a shrink tube sealed with wax at the ends.

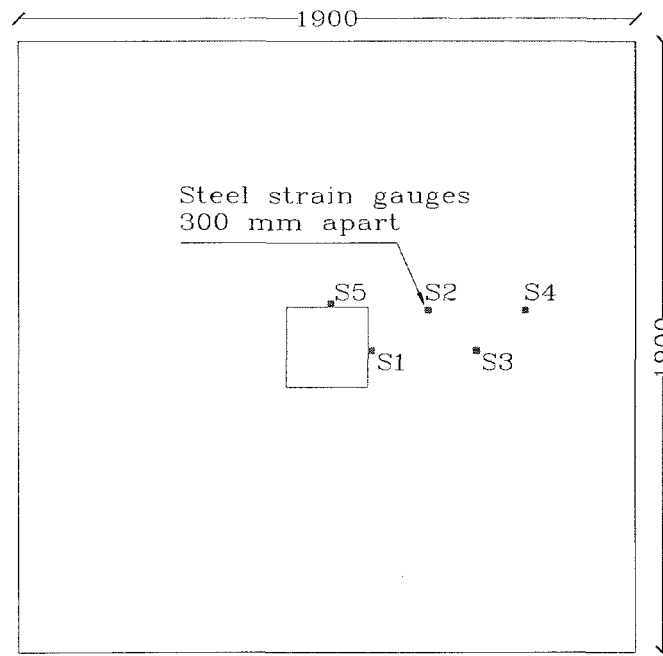


Figure 3.6: A typical arrangement of the steel strain gauges

3.7.3 Concrete Strains

The concrete strains were measured at four locations in the tangential directions on the compression side of the slabs. The gauges were 6 mm long; with a resistance

of $120\ \Omega$. The concrete strains were measured by gluing the strain gauges to the concrete surface at various distances from the column face as shown on Figure 3.7. The locations of the strain gauges were marked on the concrete surface. The concrete surface at the specified locations was ground with a hand grinder, and a very thin film of epoxy resin was placed on the concrete surface in order to make the surface even. Each strain gauge was placed in position and the wire connections were connected to the data acquisition system.

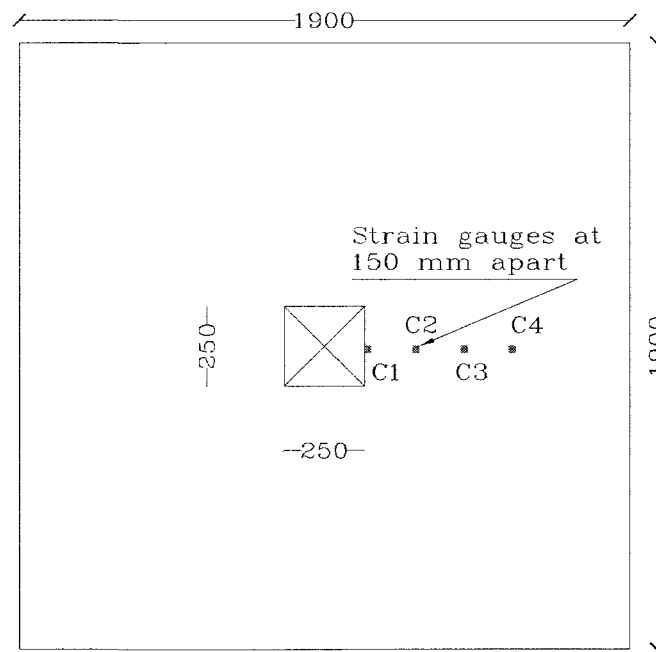


Figure 3.7: Concrete Strain gauge locations

(The strain gauges were located at 150 mm apart)

3.7.4 Crack Measurements

Each slab was carefully inspected at each load step. The cracks were marked and the maximum visible crack width was measured using a crack width measuring gauge. The Crack Displacement Transducer (CDT) was mounted on the concrete surface cracks and joints in order to measure opening displacement as shown in Figure 3.8. The CDT is a waterproof device that enables accurate measurements in range of $\pm 2\text{mm}$. The accuracy of the measurements improved as the cracks started to widen.

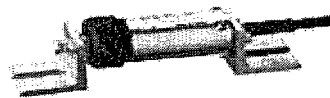
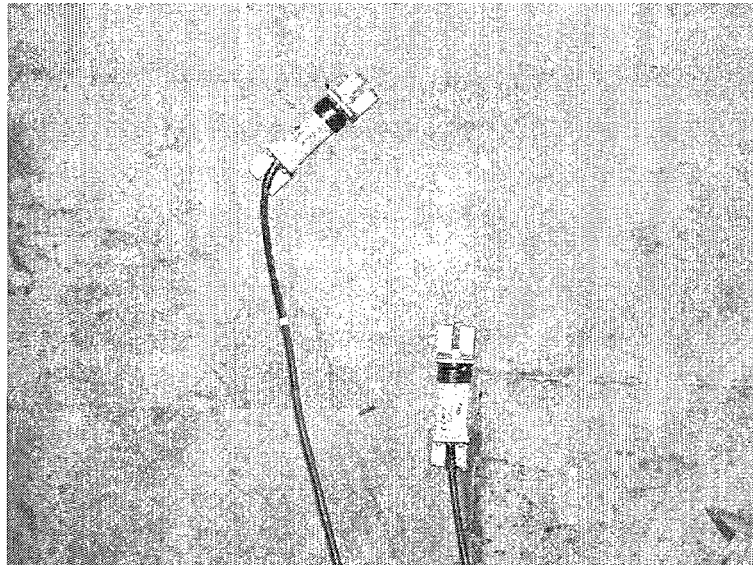


Figure 3.8: (KG-A) Crack Displacement Transducer

3.7.5 Data Acquisition System

The electrical strain gauges, LPDTs and the load readings were logged to a computerized data acquisition system. This system can be divided into two broad categories, analog systems and digital systems. In analog systems, the measurement information is processed and displayed in analog form. In digital systems, the original information may also be acquired in the form of an analog electrical signal, but the signal is then converted to a digital signal for further processing and display. A digital electrical signal has the form of a group of discrete and discontinuous pulses. Typically, the instrument first subjects the analog signal to amplification. Next, the amplified signal is converted into digital form by an analog-to-digital (A/D) conversion circuit. Finally, the digital signal is either displayed on a digital display device or is made available for transmission to other digital instruments such as a computer for further processing and display. All measurements were stored in a computer file. The software (Lab-VIEW, 2005) was used and the data scanning and saving rate was set to record the readings every 3 seconds.

3.8 Procedure

The tested slab was placed in the frame in the vertical position using a 10-ton capacity crane. The test slabs were simply supported along all four edges with the corners free to lift. At the beginning of the test, an initial load equal to 10 % of

the ultimate load was applied until the slab started cracking. Then crack gauges were installed using epoxy glue on the tension surface of the slab where left under load for one hour in order to enable the epoxy to dry. The load was applied at selected load increment of 44.8 kN (10 Kips). The slab was carefully inspected at each load step and the cracks were marked as shown in Figure 3.9.

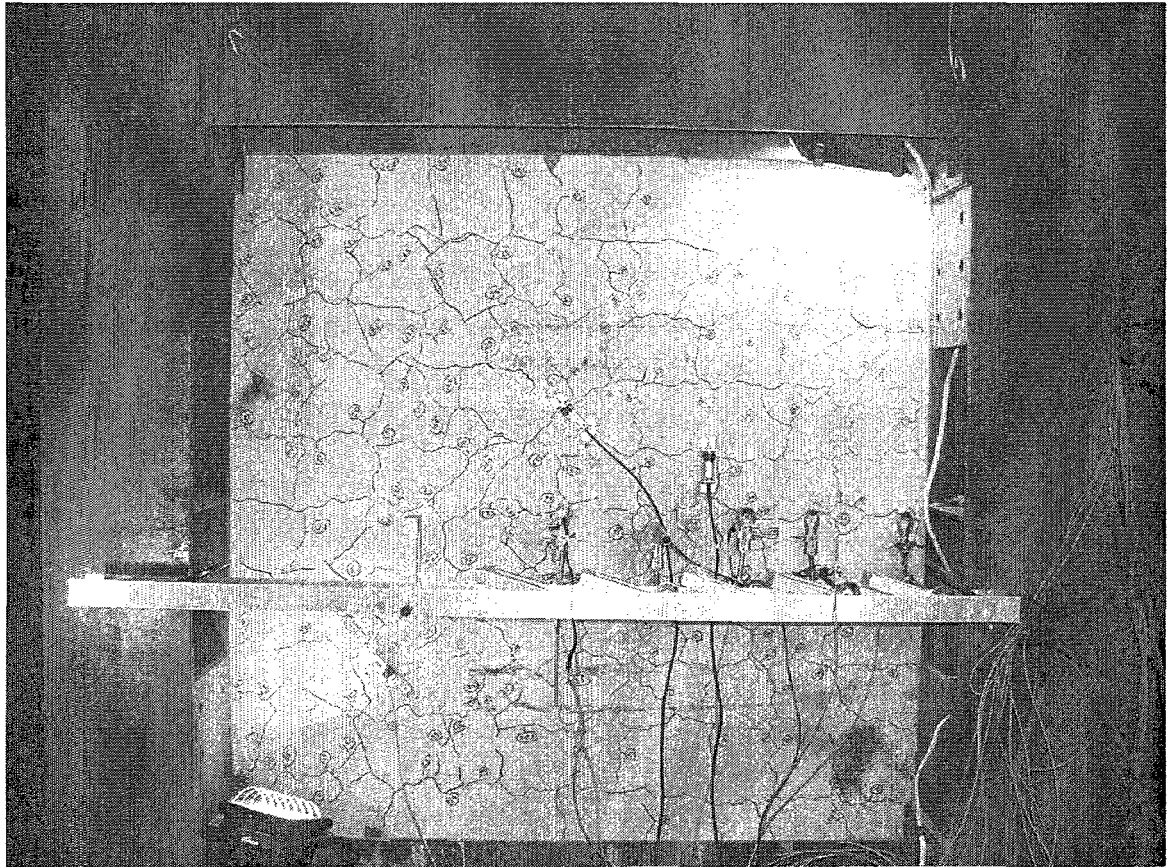


Figure 3.9: Marking the cracks on a typical slab

Chapter 4

Test Results and Discussion

4.1 Introduction

The results and observations obtained from the experimental program are given in this chapter. Eight reinforced concrete slabs were tested at the structural lab of Memorial University. The tests results are divided into three groups. The following parameters were examined in this investigation; concrete cover, bar spacing, bar diameter, and the slab effective depth on the crack properties were examined. A large volume of data was recorded and the related graphs were plotted and

summarized. Few data sets that are important for interpretation of the cracking test results are presented here. The behavior of the slabs presented in terms of the load-deflection relationship at different load stages, service and ultimate load, and crack width-steel strain relationship. Failure modes and crack patterns are reported and also depicted by means of photographs.

The first group (Series I) presented in Table 4.1 is designed to investigate the effect of concrete cover on the crack width. The group is made of three slabs designated as NSC1, HSC1, and HSC2. All the slabs have the same depth of 200 mm, the same bar spacing of 150 mm and the same size of bar 25M with different concrete covers. The second group (Series II) presented in Table 4.1 is designed to investigate the effect of bar spacing on the crack width. The slabs of this group have the same slab depth of 200 mm, the same concrete cover of 30 mm, the same size of bar space 25M and different bar spacing. Specimen NSC1 from the first group (Series I) was considered for the comparison as a part of this series. The third group (Series III) was designed to investigate the effect of pure flexure failure and ductile shear failure. The third group includes HSC5, NSC2, and NSC3.

4.2 Load-Deflection Relations

The deflections measured by the LPDT's gauges located at equal spaced locations placed at the back of the slab. Deflection profiles give a global indication of the

deformational response to the applied load. The deflection values at five equal-spaced locations along the slab width versus the central load as shown in Figure 3.5 were recorded at each load step. The load deflection profile can be used in classifying the type of failure. The two-way slab failure modes can be classified into three categories; pure flexural failure, pure punching failure and ductile shear

Table 4.1: Group specimens' details

Series No	Slab No.	f'_c (MPa)	Bar size (mm)	Bar spacing (mm)	Concrete cover (mm)	Slab thickness (mm)	Steel ratio ($\rho\%$)
Series I	NSC1	35	25M	150	30	200	2.17
	HSC1	68.5	25M	150	50	200	2.48
	HSC2	70	25M	150	60	200	2.68
Series II	HSC3	66.7	25M	200	30	200	1.67
	HSC4	61.2	25M	250	30	200	1.13
Series III	HSC5	70	15M	100	30	150	1.88
	NSC2	33	15M	240	30	200	0.52
	NSC3	34	10M	210	40	150	0.40

failure (Hussein, 1990). Pure flexure failure takes place in the slab when most of the reinforcement yields before punching occur and consequently the slab exhibits large deflections prior to failure. Pure flexure failure is normally associated with low reinforcement ratios. The second mode of failure type is a pure punching failure for over reinforced concrete specimens such as offshore structures. The third type of

failure, ductile-shear failure, is a transition mode between the cases of pure punching and pure flexure failures.

The first crack of each specimen was visually inspected and the corresponding load was recorded as the first crack load. The first yield of the bottom reinforcement is indicated on each load-deflection curve by a circle. The steel yield strain was recorded at a value of $2000\mu\epsilon$ that produce a stress in the steel rebar equal to 400MPa . The yielded strain was measured at location 125 mm from the center of the slab. The value of $2000\mu\epsilon$ was suggested based on experimental observations of the stress-strain curve of a single rebar. Table 4.2 shows the measured deflections at first crack, first yield of tension steel, and ultimate load for all slabs. Based on the result of the specimens of Series I and Series II, the cracking load is largely influenced by the concrete strength f'_c .

All slabs of Series I and Series II failed due to pure shear as indicated by their load deflection curves. In general, the load deflection curve for the slabs failing in punching can be represented by two straight lines with two slopes. High-strength concrete specimens, HSC1, HSC3, and HSC4, have almost the same slope for the first line representing the pre-cracking stage and it is steeper than the slopes of the later stages. The slope of the first line on the load-deflection curve corresponds to the stiffness of the uncracked slab. The second line of the load

deflection curve extends up to the load caused that first yielding in tension reinforcement. The slope of the second line represents the stiffness of the cracked slab. Within a given series such as Series II, the variation of the deflection values against the load was largely dependent on the reinforcement ratio. The deflection of the normal strength concrete was slightly greater than high-strength concrete slab as shown in Figure 4.1 (a).

At any given load, the deflection of normal strength concrete slab NSC1 was slightly greater than HSC3 and HSC4; in spite of the effective depth of slab NSC1 was greater than the effective depth of slabs HSC3 and HSC4. For slabs that failed under flexure such as NSC2 and NSC3 of Series III, it can be concluded that the failure took place after most of the reinforcement reached the yield point and the slab exhibited a large deflection prior failure as shown in Figure 4.1 (c). Moreover, slab NSC3 reached a flat load-deflection response near the ultimate load indicating an excessive increase of deflection without an increase of the applied load. The pure flexure failure is normally accompanied by excessive deflection and free lift of the four slab corners. The mode of failure for HSC5 specimen was a ductile shear, indicating a transition mode between pure flexure failure and pure shear failure.

Table 4.2: Deflection characteristics of test slabs

Slab No.	Steel ratio ($\rho\%$)	f'_c (MPa)	First crack load (kN)	First crack deflection (mm)	Yield load P_y (kN)	Yield load deflection Δ_y (mm)	Ultimate load P_u (kN)	Ultimate load deflection Δ_u (mm)
NSC1	2.17	35	70	1.6	640	16	678	17
HSC1	2.48	68.5	180	5.37	-	-	788	15.9
HSC2	2.68	70	178	-	-	-	800.6	-
HSC3	1.67	66.7	101	0.8	577	7.44	802	11.6
HSC4	1.34	61.5	178	4.5	637	11.5	811	15.6
HSC5	1.13	70	155	5.6	269.3	11.1	480.39	30.26
NSC2	0.52	33	147	4.1	328	7.8	479	14.8
NSC3	0.40	34	88	5.56	127.4	6.68	228	30

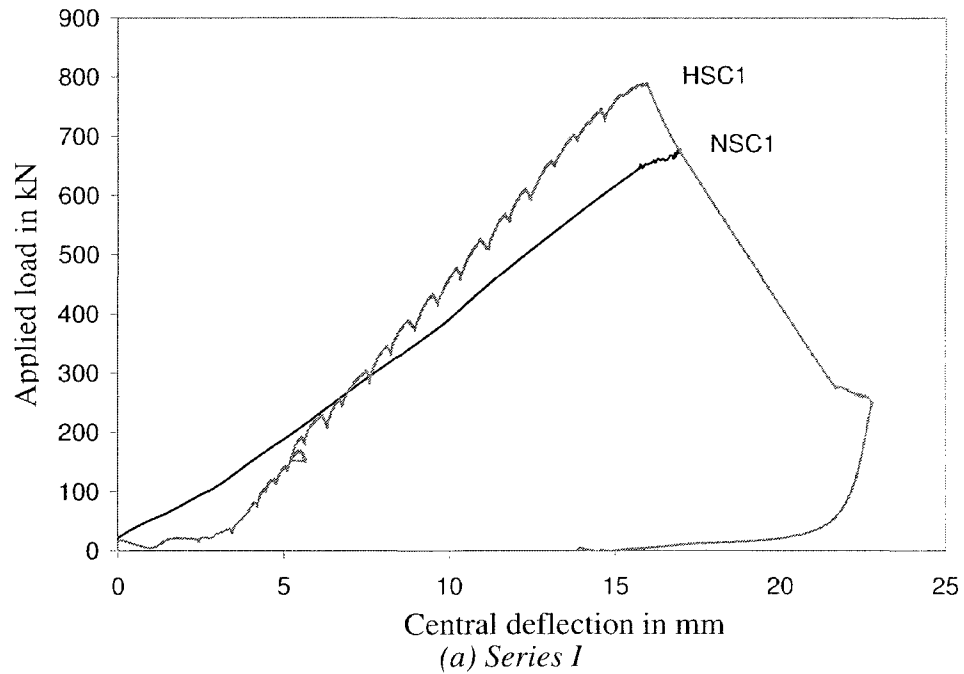
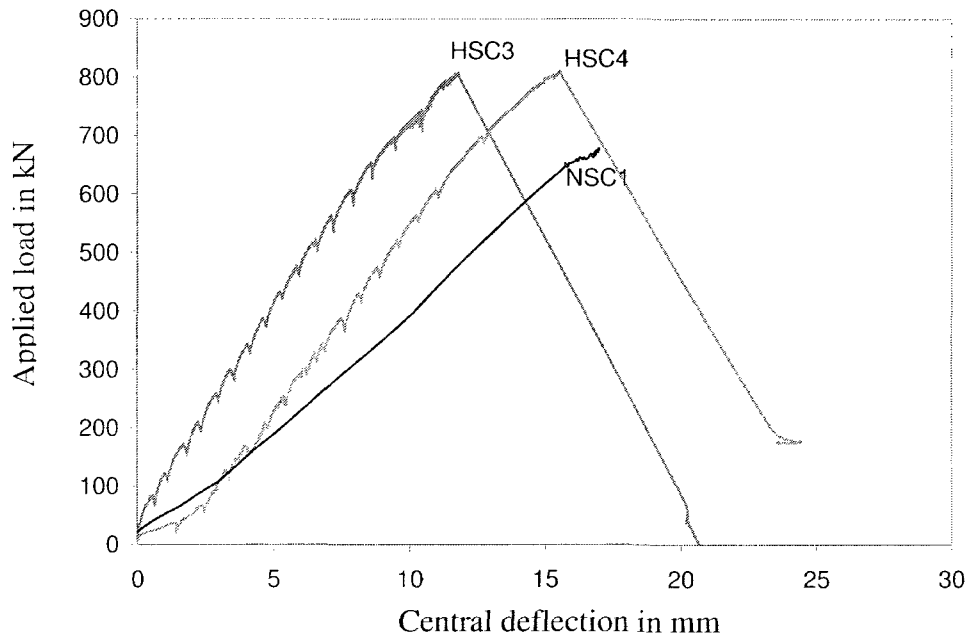
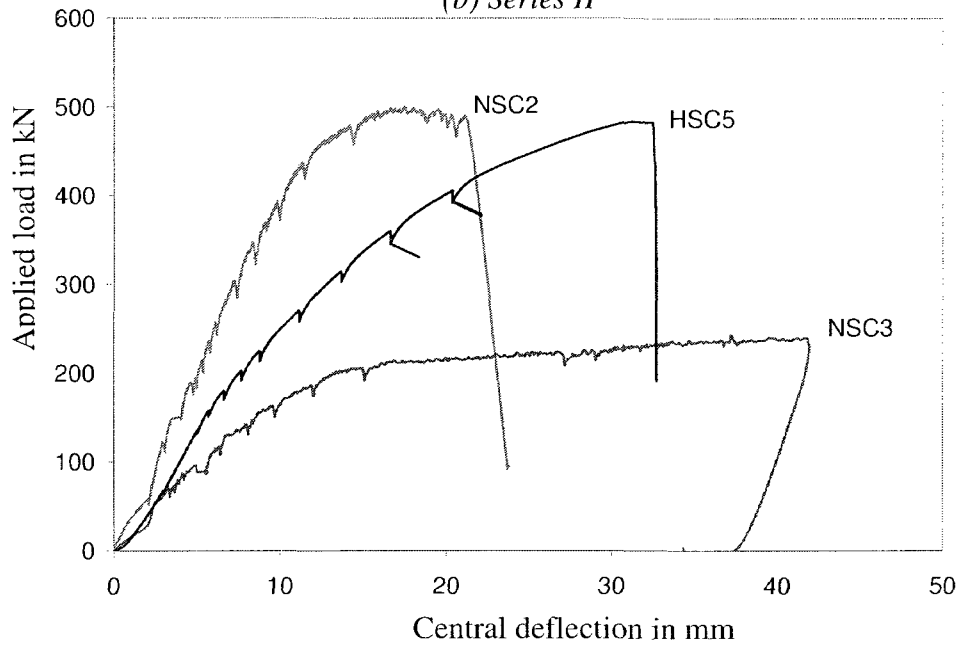


Figure 4.1: Typical load-deflection characteristics at center span of test slabs



(b) Series II



(c) Series III

Figure 4.1: Typical load-deflection characteristics at center span of test slabs (Condt.)

4.3 Deflection Profiles

The deflection measurements at different locations along a specimen width are used to construct the deflection profile for each specimen. Deflection profiles give a global indication of the deformational response to the applied load not just at the location of load application but also along the slab width. The deflection values were measured at five different locations on one side of the symmetrical specimen as show in Figure 3.5. The recorded value of the central deflection at each increment was recorded and used to determine the deflection profile at the increment.

Figures 4.2 and 4.4 indicate that specimen HSC3 requires more load to reach the same level of deformation as that of specimen NSC1. It is also clear that the zone of high deformation of normal concrete specimen NSC1 is extending over a less distance from the center of the slab than that of high strength concrete HSC3. This is a clear indication that specimen NSC1 tends to deform more at the center unlike specimen HSC3. Moreover, the failure load occurred right after the yield of bottom steel reinforcement for specimen NSC1 while for specimen HSC3 it took more load increments of loading before reaching the ultimate failure. This support the idea that specimen NSC1 tends to fail in shear more suddenly than HSC3, indicating the great ductility of high strength concrete. In Figure 4.3, although the

effective depth d of specimen HSC1 is less than NSC1, it requires higher load to reach the same deflection of specimen NSC1. This can be attributed to the concrete strength f'_c .

Figures 4.4 and 4.5 show that for the same loading; the deflection of specimen HSC4 is larger than HSC3. This is due to the fact that the reinforcement ratio of HSC4 is less than the effective depth of HSC3. Figures 4.6 to 4.8 show the deflection profile of some typical slabs of the current test program.

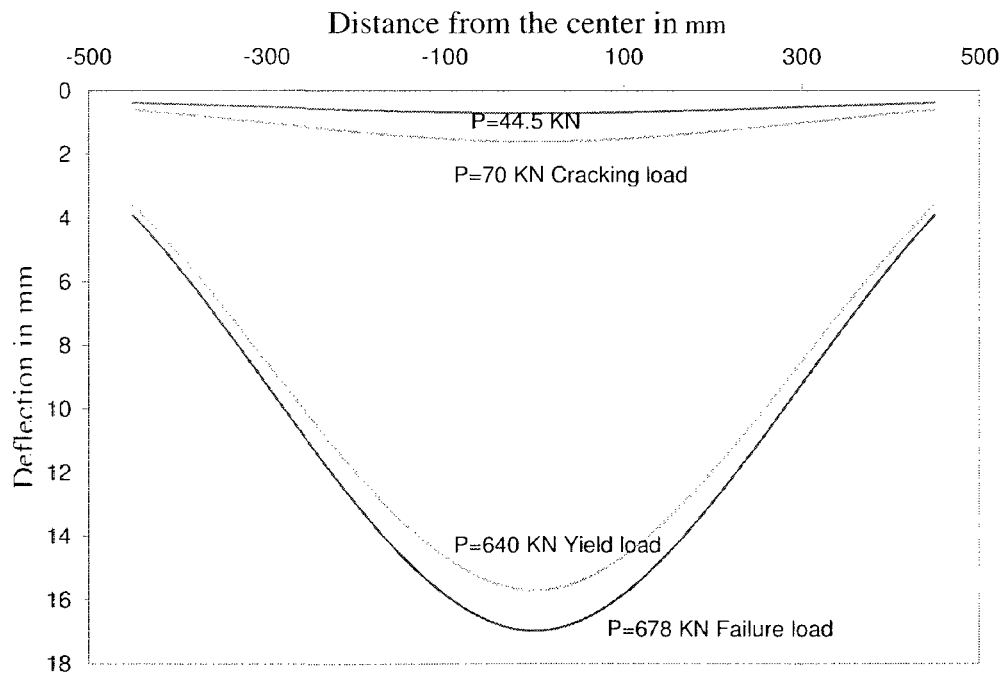


Figure 4.2: Deflection profile for NSC1

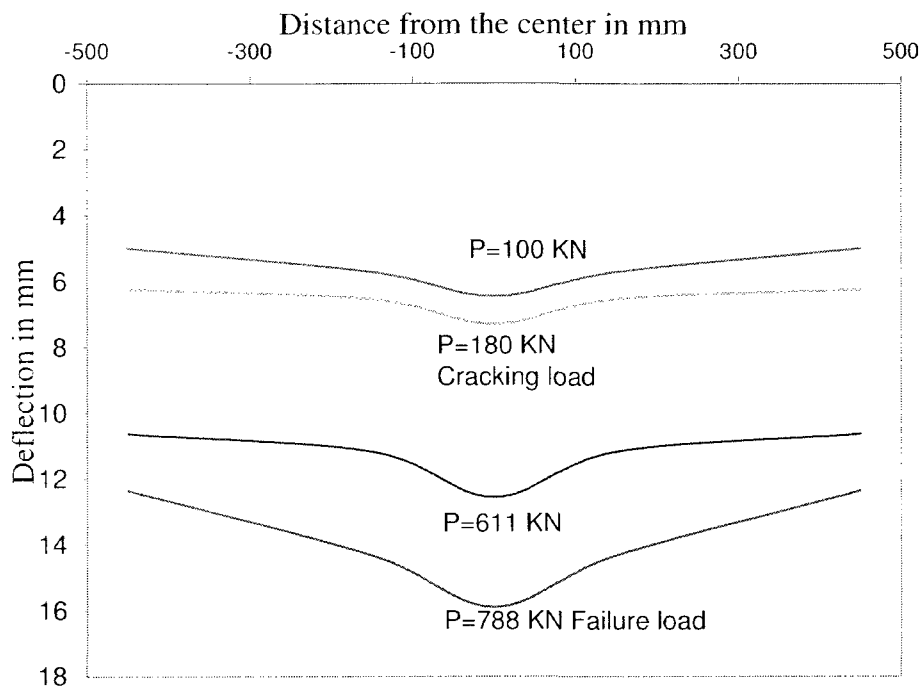


Figure 4.3: Deflection profile for specimen HSC1

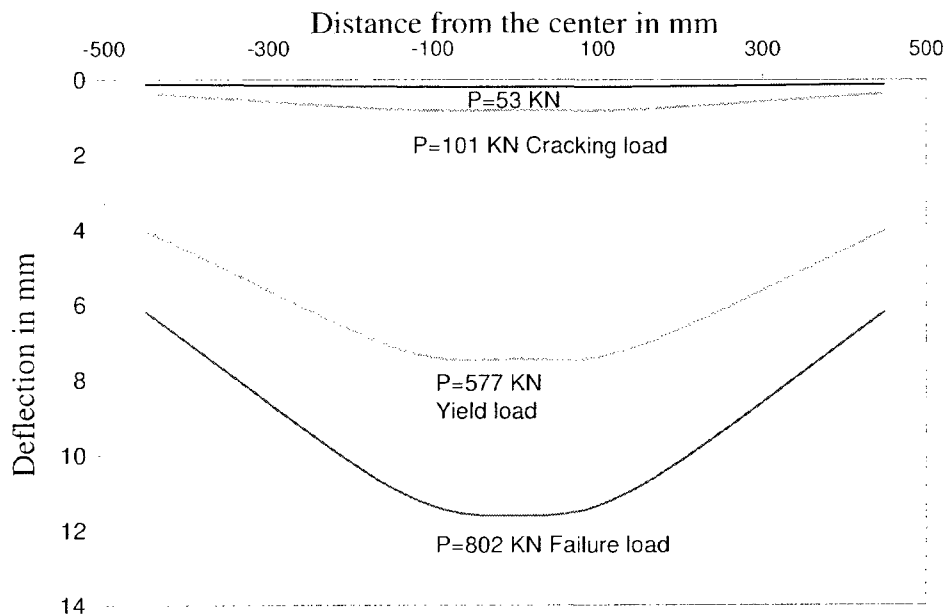


Figure 4.4: Deflection profile for specimen HSC3

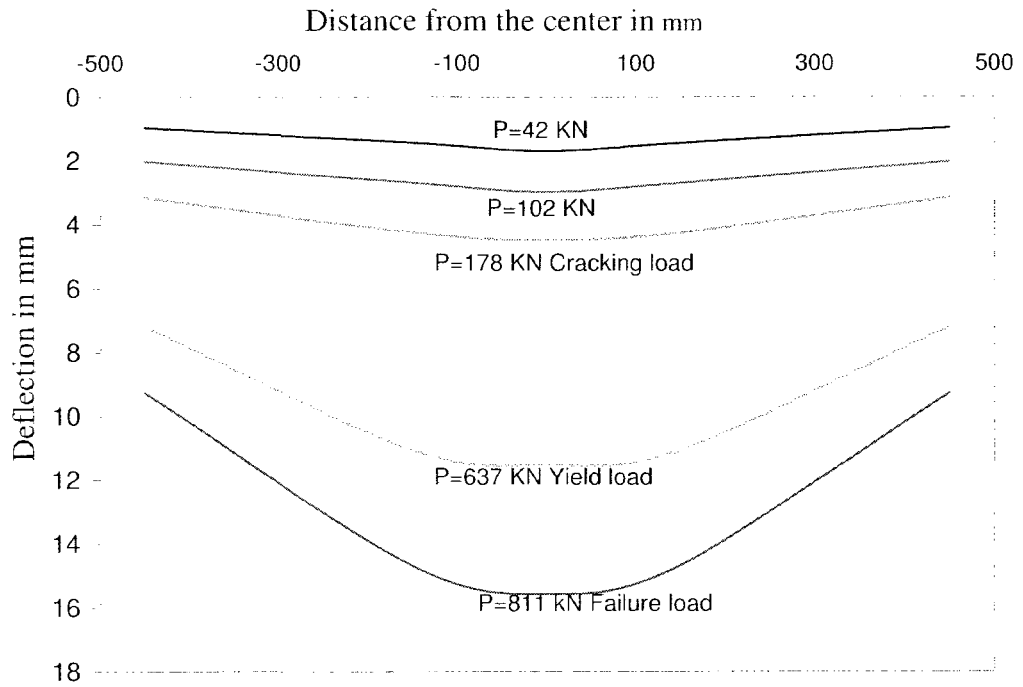


Figure 4.5: Deflection profile for specimen HSC4

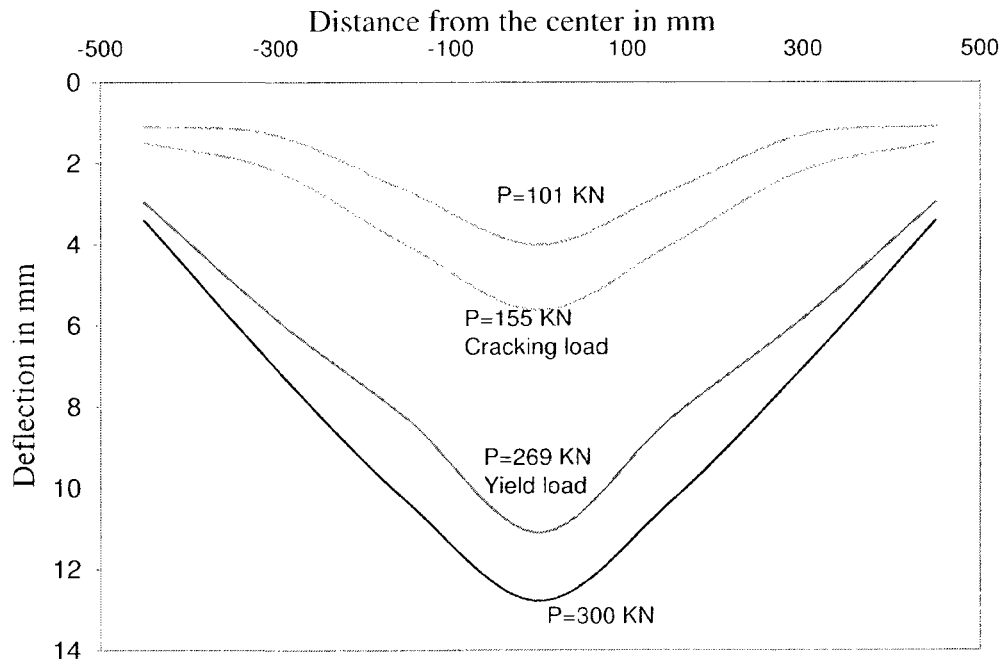


Figure 4.6: Deflection profile for specimen HSC5

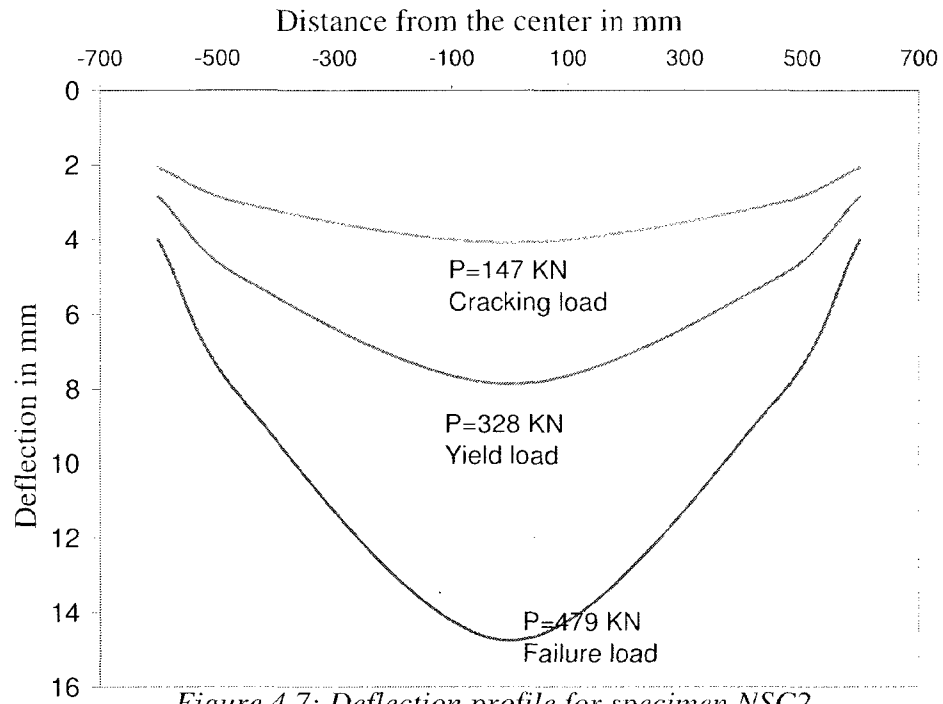


Figure 4.7: Deflection profile for specimen NSC2

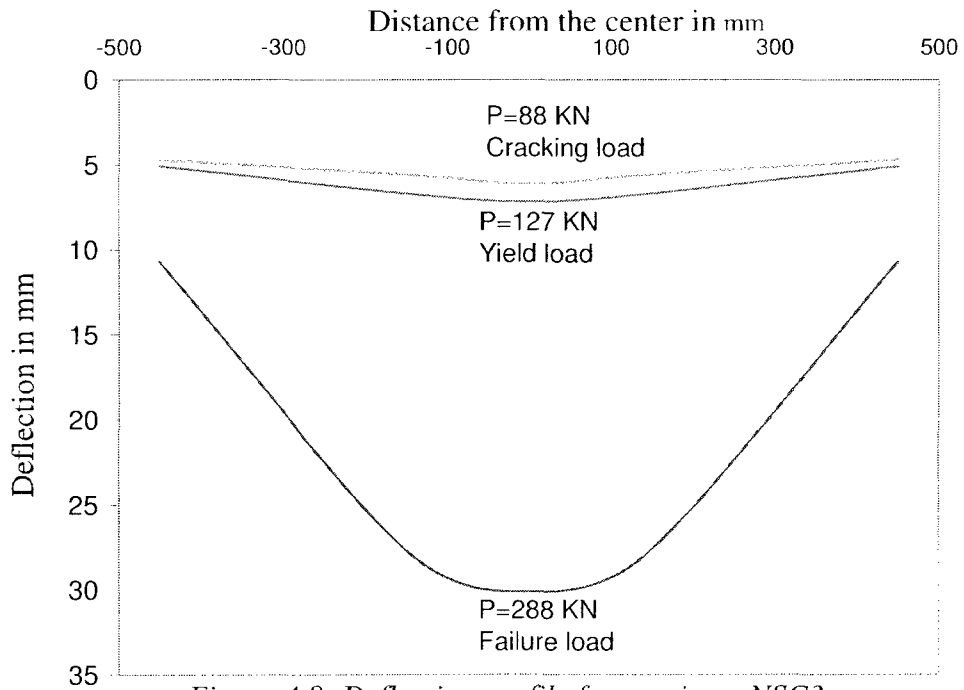


Figure 4.8: Deflection profile for specimen NSC3

The steel reinforcement of specimen HSC1 did not reach the yield strain, the punching-shear failure of HSC1 was localized around the column area and it appeared in the deflection profile as a sudden jump in the curve. The deflection profile for specimen NSC2 and NSC3 indicates that the zone of high deformation is extended over a large distance from the center of the slab and there were more increments of loading between the yield load point and the failure load point. The deformation pattern of specimen NSC2 and NSC3 indicates that the specimens tend to deform due to pure flexure. The deformation pattern of specimens NSC1, HSC1, HSC3 and HSC4 are due to local punching-shear while for specimen HSC5 is due to the ductile shear failure.

4.4 Ductility and Energy Absorption

Ductility as a term reflects the deformation capacity of a structural member before failure. In other words, the ductility of a reinforced concrete slab is quantified in terms of the ratio of the deflection at the ultimate load to the deflection at the first yielding of flexural reinforcement. The energy absorption is defined as the area under the load deflection curve up to failure. The ductility and energy absorption capacity of all slabs are shown in Table 4.3.

The slabs of Series I and II failed under pure punching mode, the ductility decreased as the reinforcement ratio was increased. Specimen NSC1 of Series I

with a reinforcement ratio of 2.17% produced 1.08 ductility compared to NSC2 of Series III with 0.52% reinforcement ratio and 1.88 ductility.

Ductility increases as reinforcement ratio is decreased. For example, decreasing the reinforcement ratio of Series II, from 2.17 to 1.13 increased ductility by 25%. While for Series III, ductility increased by 74% of specimen NSC2, when the reinforcement ratio was decreased from 2.17% to 0.52%. That result demonstrates that slabs fails under pure flexure have a large ductility comparing to slabs fails under pure shear for slabs in Series I and II.

Table 4.3: Ductility and energy absorption of test slabs

Slab No.	Steel ratio ($\rho\%$)	f'_c (MPa)	Ductility $\frac{\Delta_u}{\Delta_y}$	Energy absorption capacity ($\text{kN}\cdot\text{mm}\times 10^3$)
NSC1	2.17	35	1.08	5.997
HSC1	2.48	68.5	-	5.42
HSC2	2.68	70	-	-
HSC3	1.67	66.7	1.65	5.215
HSC4	1.13	61.2	1.35	6.269
HSC5	1.88	70	2.73	9.28
NSC2	0.52	33	1.88	4.35
NSC3	0.40	34	4.51	8.99

The energy absorption of the slab increase as the reinforcement ratio decreased. Slabs failing under flexure mode showed a higher energy absorption

capacity than slabs failing under shear mode, where the slab depth decreased, as in the case of specimen NSC2 and NSC3, the energy absorption increased.

4.5 Steel Strain

The strain gauge locations on the steel reinforcement cage were detailed in Section 3.7.2. The shown locations were selected to measure the maximum strains in the steel reinforcement during the test duration and to obtain the strain profile along the radius. The highest strain of initial yielding occurred below the slab center. In all the test slabs except slab HSC1, the tension reinforcement yielded prior to punching of the slab. For lightly reinforced slabs, yielding initiated at the edge of the columns stub and gradually progressed throughout the whole tension reinforcement. The load versus strain curves are shown in Figure 4.10 to Figure 4.11. The steel strain gauge at the edge of the column slab HSC2 failed to record the steel strain at that location.

In general the slope of load-steel strain curve is very steep for high-strength concrete slabs that failed in shear compared to other slabs. After reaching the ultimate load, the load-steel strain slope gradually decreased. Slabs failed under pure punching for Series I and II, yielding of tension reinforcement occurred at a higher load and was localized at the edge of the column stub. The extent of yielding spread over the reinforcement varied with the reinforcement ratio. It can be noticed

that for Series II as the reinforcement ratio decreased, the yielding load for slabs HSC3 and HSC4 of Series I is decreased.

In Figure 4.11, NSC2 and NSC3, yielding was initiated at the edge of the column stub and gradually progressed through the whole tension reinforcement. Moreover, both specimens NSC2 and NSC3 reached the state of steady steel strain that increased at a constant load which is a normal behaviour for slabs that fail in pure flexure.

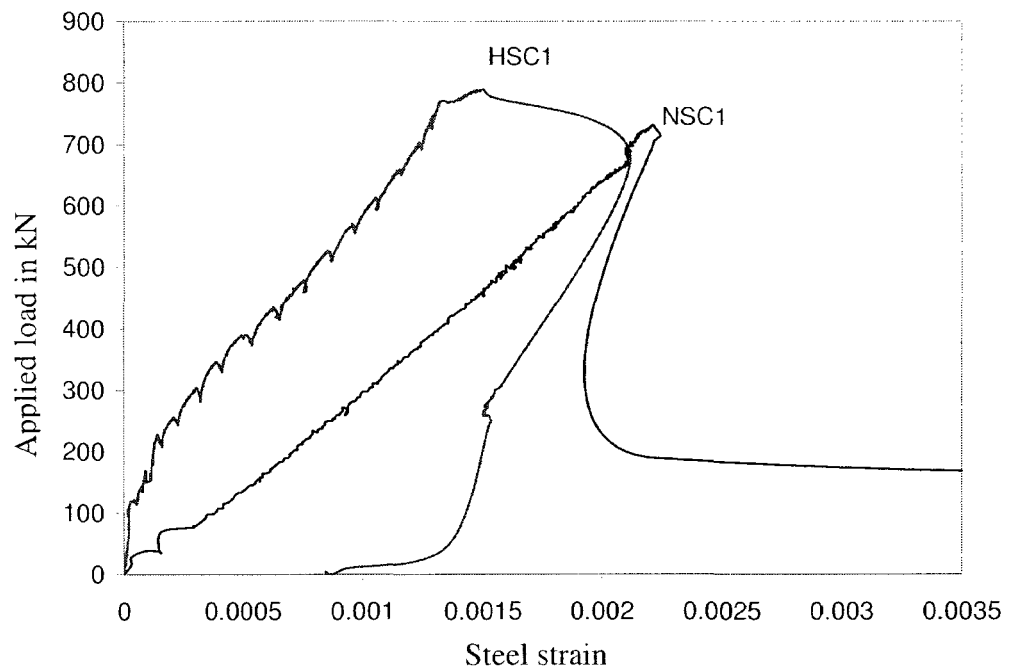


Figure 4.9: Typical load-tension steel strain behavior at the column periphery for Series I

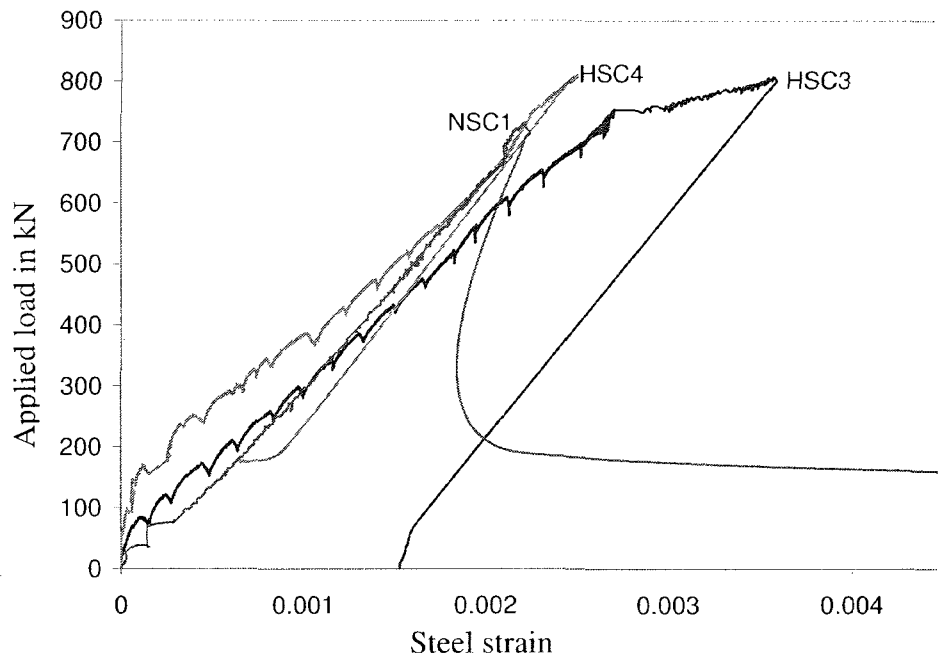


Figure 4.10: Typical load-tension steel strain behavior at the column periphery for Series II

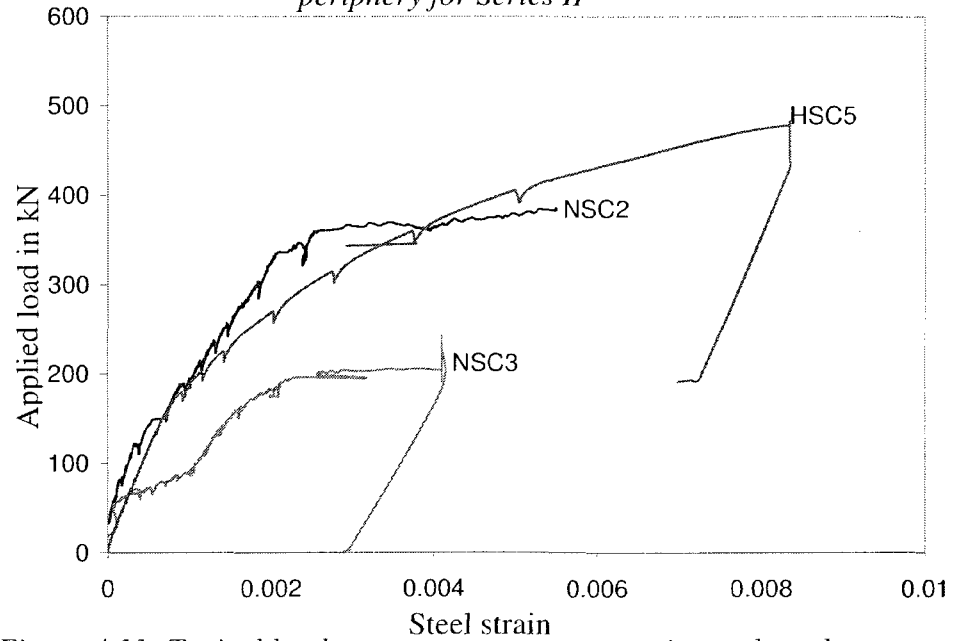


Figure 4.11: Typical load-tension steel strain behavior at the column periphery for Series III.

4.6 Concrete Strains

The concrete strains were measured at various locations as described in Section 3.7.3. These locations were selected to measure the concrete strain along a radius of the slab. Figure 4.12 to 4.18 represent the compressive concrete strains at different points from the face of the column in each tested specimens.

In general, the concrete strain gauges never reached the crushing strain value 0.0035. The concrete strain increased as the load was increased at the initial stages. After a certain load level, which was close to ultimate load, the strain started to decrease in most slabs. This observation of concrete strain is common in literature. (Hallgren, 1996) reported similar behavior for high strength concrete slabs reinforced with steel rebars. It can be attributed to the strain redistribution in the concrete (Rashid, 2004). If two parallel cracks develop on the tension face at certain load level, the crack width and depth will increase gradually. On the other hand, compressive stress concentration could develop at directly opposite points of these tension cracks at the same time. Thus, stress concentration could develop along two parallel lines, on the compression side and the stress concentration could gradually rise. At the same time, the concrete between these two lines may experience gradual stress relaxation. This could explain the reduction of concrete

strain C1 of specimen NSC1 after certain load. The slope of load-concrete strain curve for specimen that failed in shear was sharp as shown in Figure 4.12 to 4.15.

The load-concrete strain curve for NSC2, NSC3 and HSC5 of Series III was linear until the cracking point beyond that with every increase in loading the concrete strain were relatively high.

4.7 Cracking Characteristics

4.7.1 Crack Spacing

Numerous cracks developed on the tension face of the slab at the time of failure. Crack mapping of all specimens is depicted by means of photographs at each stage of loading throughout the experiment as shown in Figures 4.19 to 4.21. By using AutoCad the cracks were traced and the spacing was measured and averaged. The average spacing of the primary cracks that transversed the full width of the specimen was calculated. The distance between these cracks was measured using a computer aided drafting program (AutoCad). It was found that, for all the specimens, the first crack forms along the rebar passes through the slab center or close to the slab center. The second crack forms along the perpendicular rebar in other direction. Crack Displacement Transducers (CDT) were mounted on the concrete surface of the first, second and third visible cracks in order to measure

opening displacement. The corresponding load of each crack was recorded accurately. The cracks that form in

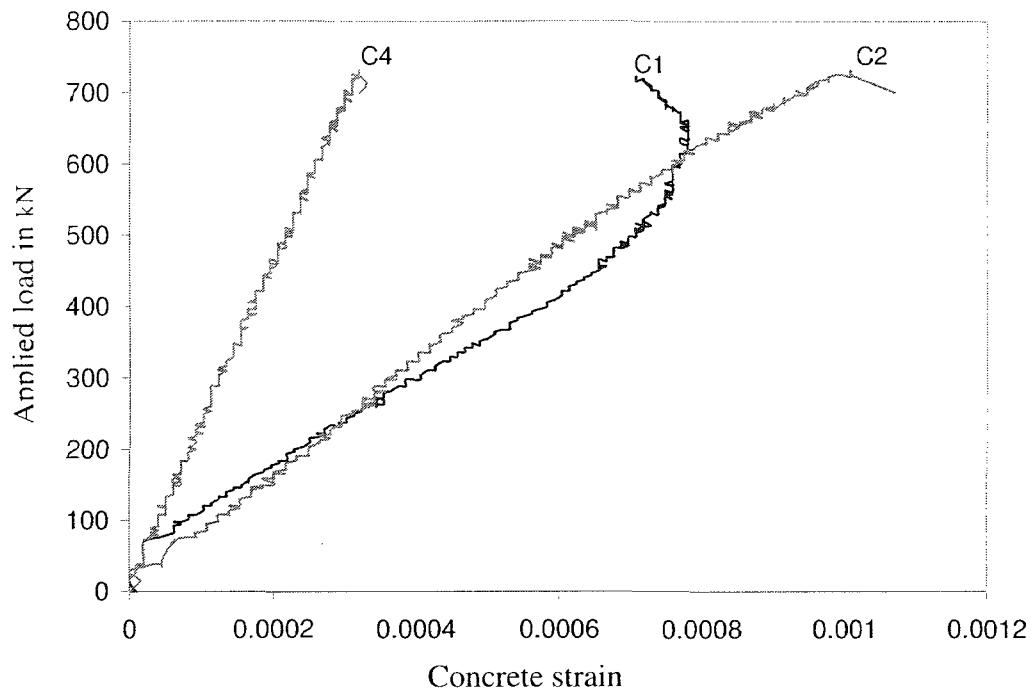


Figure 4.12: Load versus concrete strain for NSC1

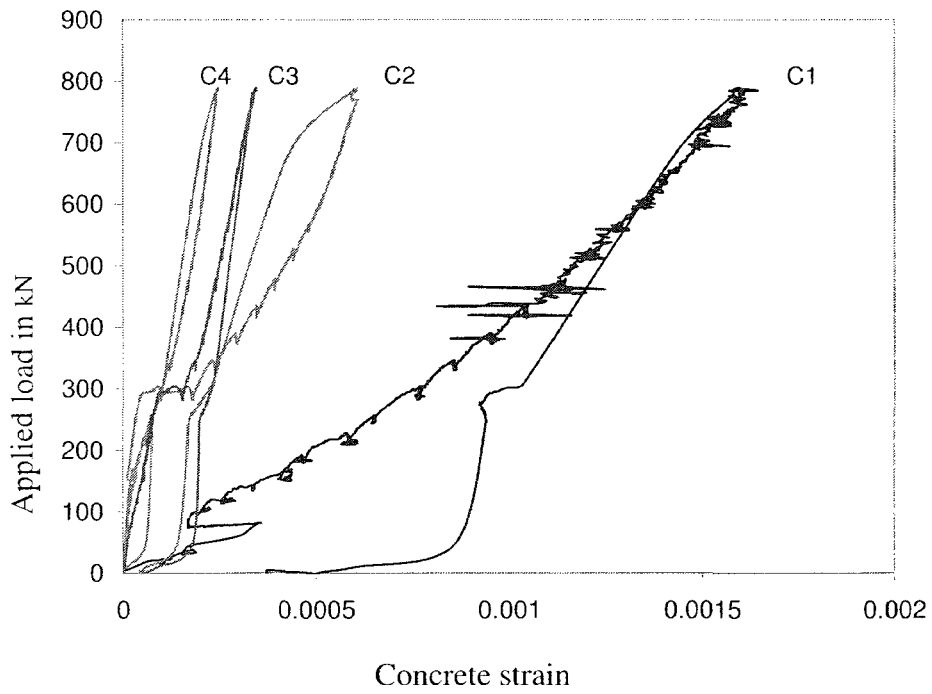


Figure 4.13: Load versus concrete strain for HSC1

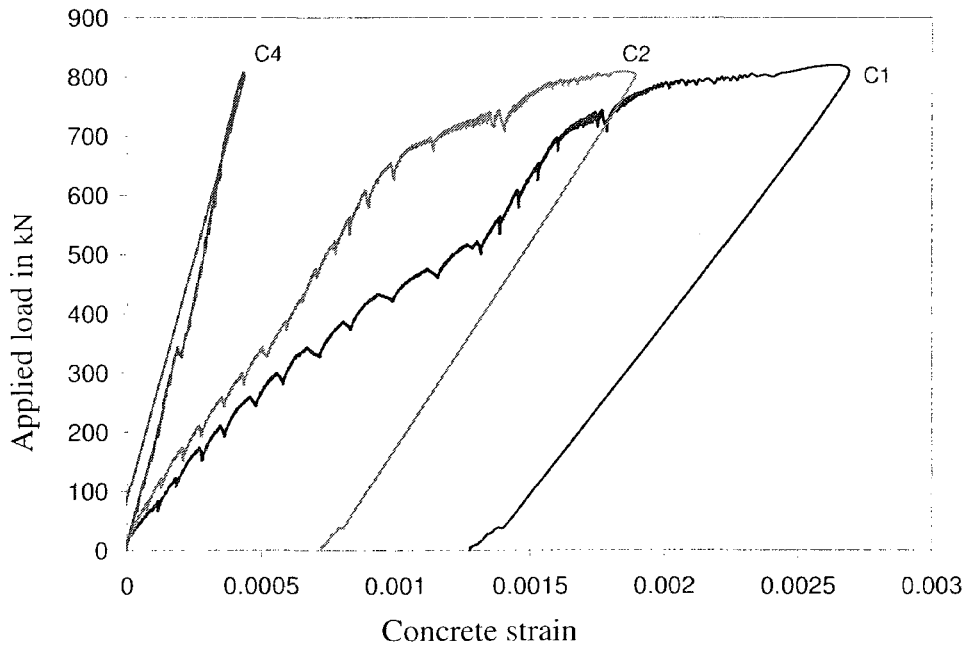


Figure 4.14: Load versus concrete strain for HSC3

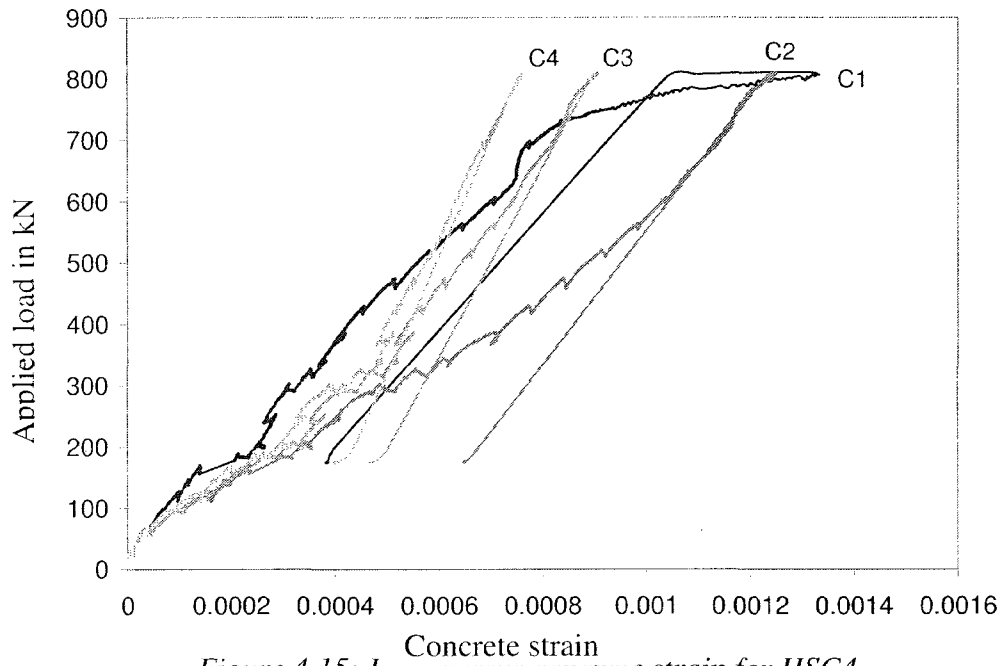


Figure 4.15: Load versus concrete strain for HSC4

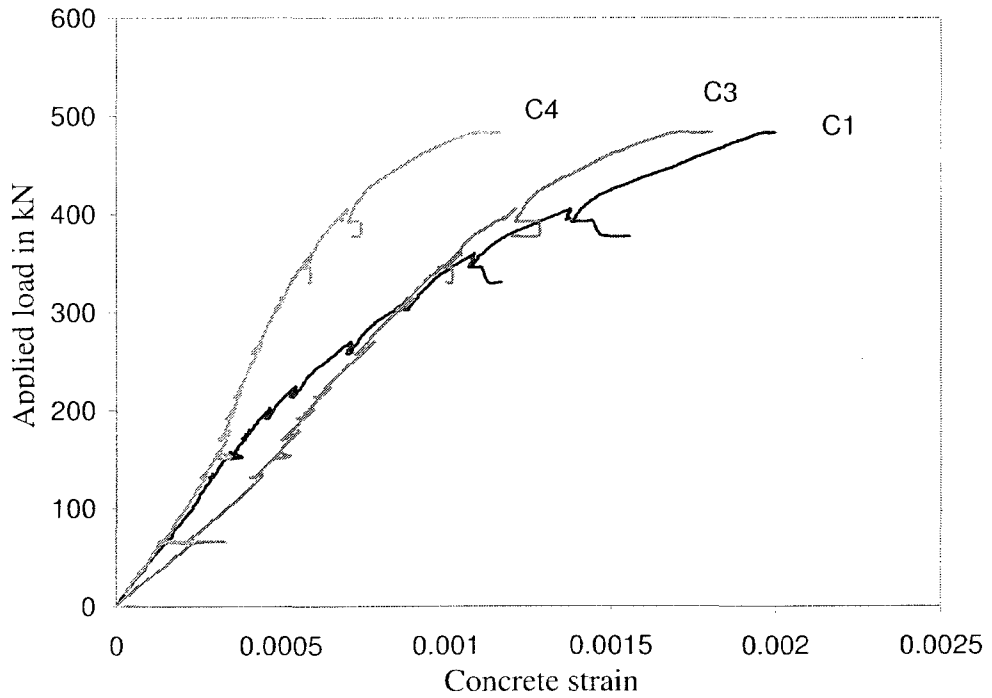


Figure 4.16: Load versus concrete strain for HSC5

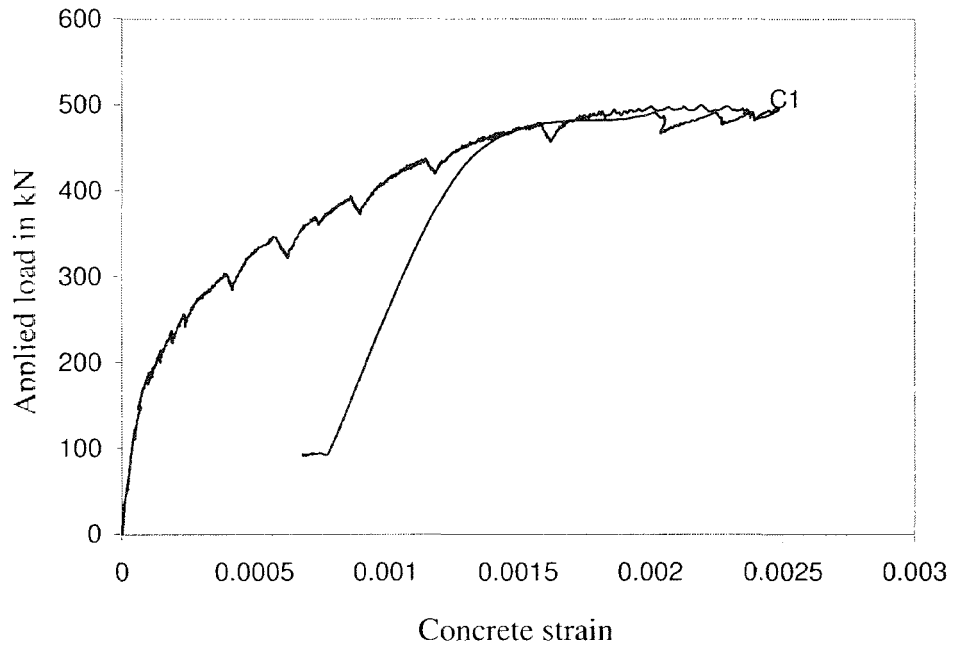


Figure 4.17: Load versus concrete strain for NSC2

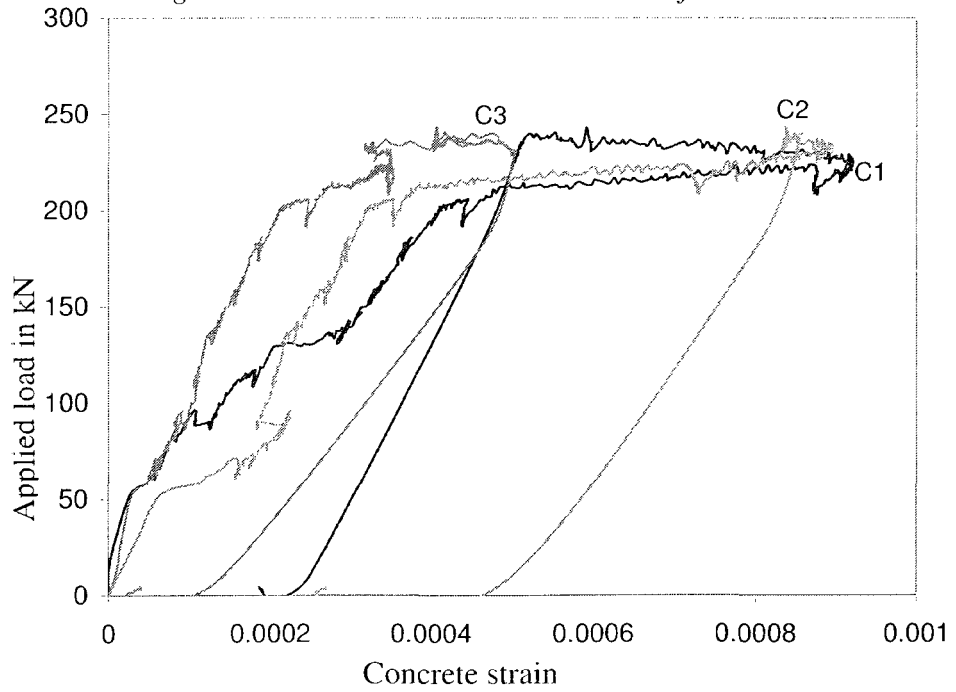


Figure 4.18: Load versus concrete strain for NSC3

The initial stage is preliminary and depends on the concrete strength and has no effect on the characteristics of the crack pattern.

In the current test program, two parameters; namely, the concrete cover and bar spacing were examined separately to investigate their effect on crack spacing and crack width. The crack patterns of the tested concrete slabs are classified into two types of cracks, radial or tangential. In all tested slabs, the initial observed cracks were first formed tangentially under the edge of the column stub, followed by radial cracking extending from the column edge toward the support of the slab. It was noticed that increasing the concrete cover in Series I can affect the crack spacing. The tangential cracks in slab NSC1 were much more pronounced along lines parallel to the reinforcement crossing through the column stub. This pattern changed to radial cracks that extended outside the circumference of the column stub as shown in Figure 4.19.b and c. Interestingly enough, this behavior is similar to slabs that fail under flexure mode such as NSC2 and NSC3 of Series III. Moreover, the average developed crack spacing of both radial and tangential cracks that was measured, as previously described at the beginning of section 4.7.1, increased each time the concrete cover increased for each specimen.

All the reinforced concrete slabs of Series II as shown in Figure 4.20 exhibited a tangential crack pattern which forms along the direction of the

reinforcement. The tangential cracks are function of the bar spacing as it was evident for Series II. Once the bar spacing is increased the average tangential crack spacing is also increased. However, for NSC1, HSC3 and HSC4 the average crack spacing was less than the bar spacing by 79% as shown in table 4.5. For specimen HSC5 in Figure 4.21a, the crack pattern was radial, which is a normal behavior of slab exhibits at large deflections.

To examine the effect of concrete cover on spacing of primary cracks, it is necessary to compare specimens with the same amount of reinforcement, but with varying concrete cover. Table 4.4 presents the crack spacing for each of the specimens of (Series I) compared with theoretical estimations based on CSA standards (Equation 2.8.1). The data suggested that the concrete cover did affect the pattern and the spacing of primary cracks in each specimen. Also as the concrete cover increased, the crack spacing increased. This result was expected but the effect of increasing the concrete cover on cracks pattern was unexpected. The observations showed that as the concrete cover increased by 67%, the average crack spacing became larger by 27% experimentally and 32% theoretically. Once the concrete cover increased by 100%, the average crack spacing increased by 38% experimentally and 47% theoretically. These measurements were taken at 250 MPa steel stresses.

Table 4.4: Comparison of the concrete cover effect on crack spacing for Series I

Slab No.	C (mm)	s (mm)	% C increase	Theoretical		Experiment	
				S_{rm} (mm)	% S_{rm} increase	S_{rm} (mm)	% S_{rm} increase
NSC1	30	150	0	127	0	134	0
HSC1	50	150	67	167	32	171	27
HSC2	60	150	100	187	47	185	38

$\% S_{rm}$ = Ratio of increasing crack spacing with respect to NSC1

To directly investigate the effect of bar spacing of Series II on crack spacing, the average crack spacing for each specimen with the same concrete cover were recorded and presented in Table 4.5. The theoretical predictions for crack spacing using Equation 2.8.1 of CSA are also presented for comparison. Table 4.5 shows that as the spacing of the reinforcement increased, there was a corresponding increase in the spacing of the cracks. The data indicates that once the bar spacing increased by 67%, the crack spacing increased experimentally by 28% and theoretically by 34%. In general, the calculated average crack spacing were lower than test results and as both the concrete cover and bar spacing increased, the crack spacing increased theoretically and experimentally.

Table 4.5: Comparison of the bar spacing effect on crack spacing for Series II

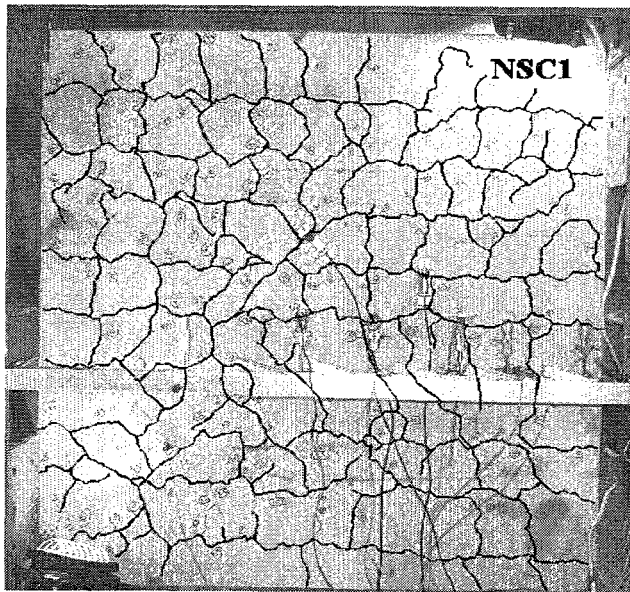
Slab No.	C (mm)	s (mm)	% s increase	Theoretical		Experiment	
				S _{rm} (mm)	% S _{rm} increase	S _{rm} (mm)	% S _{rm} increase
NSC1	30	150	0	127	0	134	0
HSC3	30	200	33	148	16.5	163	22
HSC4	30	250	67	170	34	172	28

As the third group (Series III) was designed to investigate the effect of pure flexure failure and ductile shear failure on crack properties, a comparison of the experimental results of the average crack spacing measurements and theoretical estimations (Equation 2.8.1) were made. The data showed a good agreement between the CSA average crack spacing equation and the experimental results as shown in Table 4.6.

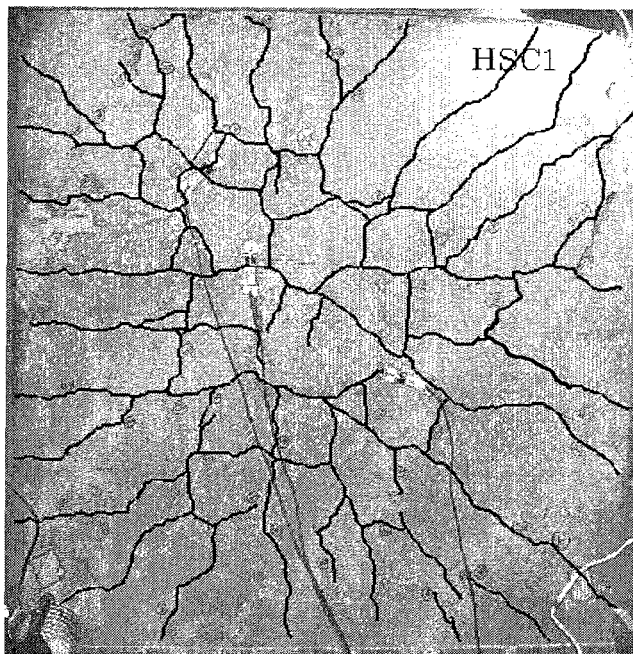
Table 4.6: Comparison of the bar spacing effect on crack spacing of Series III

Slab No.	Theoretical	Experiment	S _{rm(Exp)} / S _{rm(Theo)} %
	S _{rm} (mm)	S _{rm} (mm)	
HSC5	139	120	15
NSC3	203	223	9
NSC4	223	239	7

$S_{rm(Exp)} / S_{rm(Theo)}$ = A direct ratio between theoretical and experimental values.

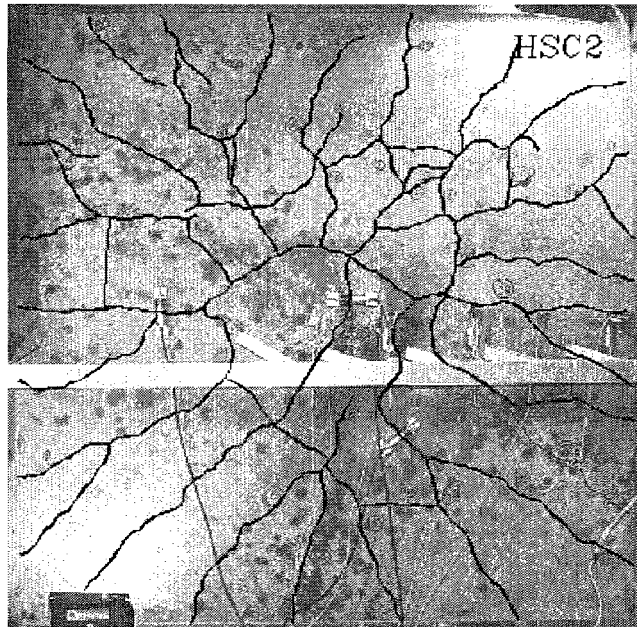


(a) Slab NSC1



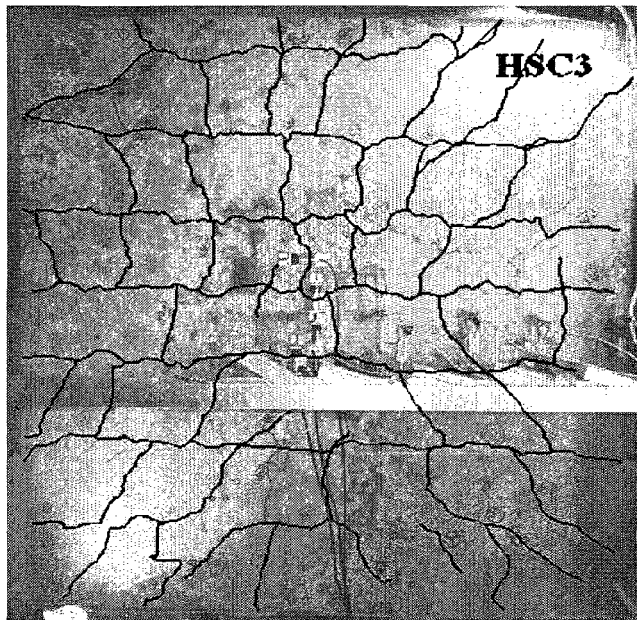
(b) Slab HSC1

Figure 4.19: Crack patterns of Series I



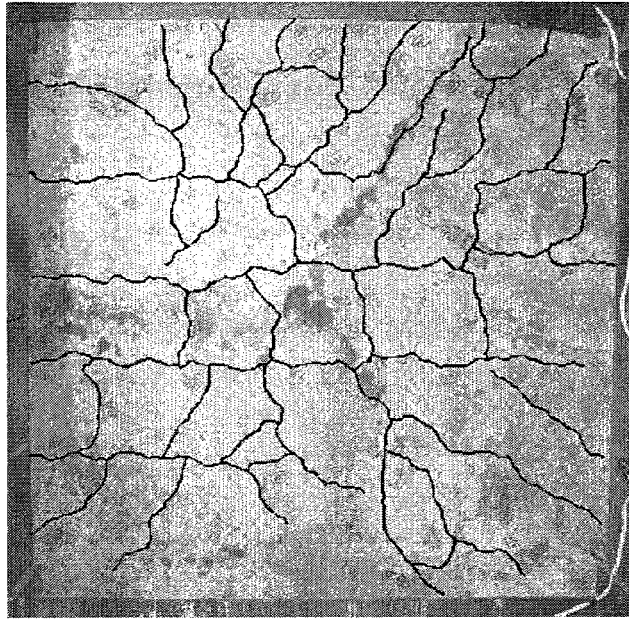
(c) Slab HSC2

Figure 4.19: Crack patterns of Series I (contd)



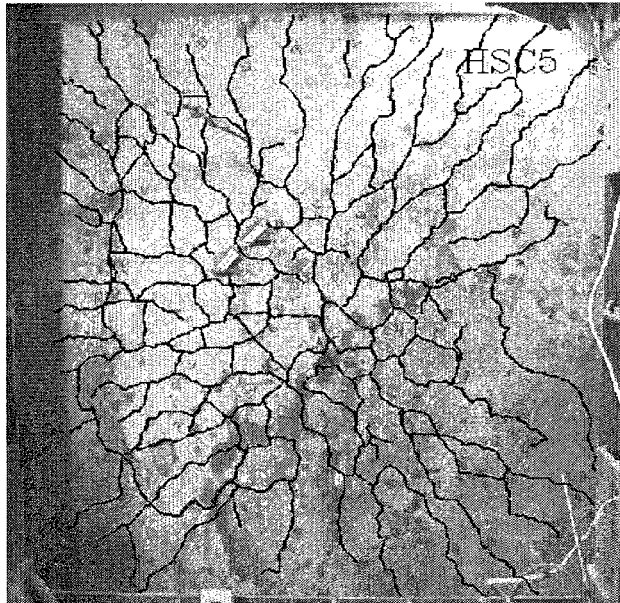
(a) Slab HSC3

Figure 4.20: Crack patterns of Series II



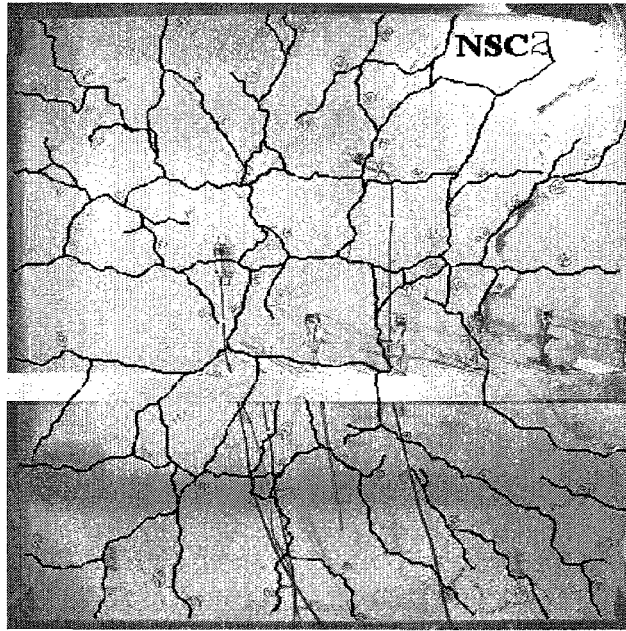
(b) Slab HSC4

Figure 4.20: Crack patterns of Series II (contd)

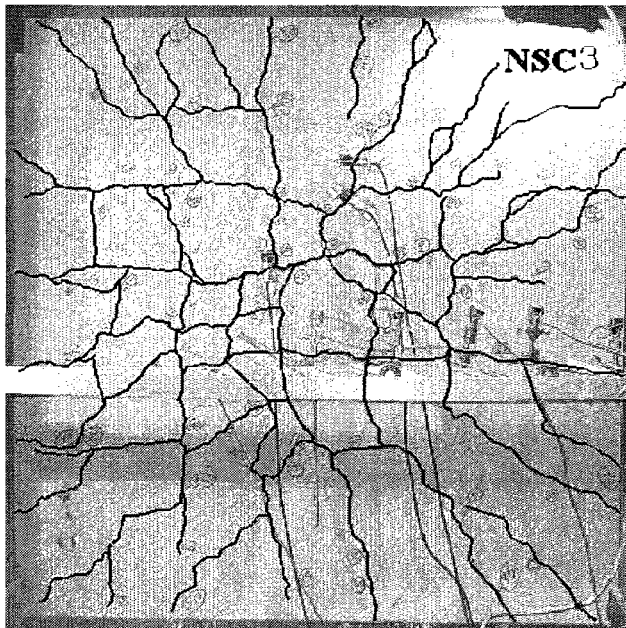


(a) Slab HSC5

Figure 4.21: Crack patterns of Series III



(b) Slab NSC2



(c) Slab NSC3

Figure 4.21: Crack patterns of Series III (contd)

4.7.2 Cracking Width Measurements

Two sets of specimens were designed to investigate the effect of reinforcement spacing and concrete cover on the widths of primary cracks. The crack width was measured at each load stage. In Figures 4.22 through 4.26, the crack width is plotted versus the steel strain. Each of the figures indicates similar trends. The crack width increased as the applied load was increased. However, this increase was not very smooth as concrete is not a homogenous material. It was noticed that the relation of the crack width versus steel strain can be represented by a straight line up to a limiting steel strain of $1000\mu\epsilon$ to $1250\mu\epsilon$ for most of the tested slabs. This strain value corresponds to a steel stress reinforcement stress equals to 200 MPa to 250 MPa. In most of the slabs, the crack width versus steel strain curve tends to behave nonlinearly after the steel strain reaches the value $180\mu\epsilon$. In slab NSC2, the crack width continues to increase after the steel strain reaches the yield point.

To provide a clearer picture of the effect of concrete cover and bar spacing on the widths of cracks, the maximum crack widths of specimens are compared at Table 4.7. All crack width measurements were recorded at the same steel stress level (250 MPa).

The data showed that as the concrete cover increased, crack widths became larger. In the range of concrete cover tested, the maximum crack width could be

influenced by as much as 90% when the concrete cover increased from 30 mm to 50 mm. Also the data showed that increasing the concrete cover by 100% (60 mm) resulted in increasing the maximum crack spacing by 234%.

Table 4.7: Maximum crack width measurements of Series I at 250 MPa steel stress

Slab No.	C (mm)	s (mm)	% C	Experiment	
				W_k (mm)	$W_k / W_{k(NSC1)}$
NSC1	30	150	0	0.406	1.0
HSC1	50	150	67	0.772	1.90
HSC2	60	150	100	0.950-	2.34

W_k = Maximum crack width measured

Of the eight specimens designed for the experimental program, three (NSC1, HSC3, HSC4) were specifically tested to determine the effect of increasing bar spacing on crack width. It can be seen in general that the maximum crack width increased as the bar spacing increased, as shown in Table 4.8. In addition, it appears that the effect of increasing the bar spacing on crack width is less than the effect of increasing the concrete cover. The data showed that for the range of bar spacing tested, the maximum crack width could be influenced by as much as 20% for specimen HSC3. When the bar spacing increased to 250 mm, the influence on crack width were almost the same 19%.

Table 4.8: Maximum crack width measurements of Series II at 250 MPa steel stress

Slab No.	C (mm)	s (mm)	% s increase	Experiment	
				W_k (mm)	$W_k/W_{k(NSC1)}$
NSC1	30	150	0	0.406	1.0
HSC3	30	200	33	0.486	1.20
HSC4	30	250	67	0.483	1.19

W_k = Maximum crack width measured

The crack width measurements for Series III are tabulated in Table 4.9 in order to compare these results with the developed crack width models developed in chapter 5.

Table 4.9: Maximum crack width measurements of Series III at 250 MPa steel stress

Slab No.	s (mm)	C (mm)	h (mm)	Experiment
				W_k (mm)
HSC5	100	30	150	0.327
NSC2	240	30	200	0.248
NSC3	210	40	150	-

W_k = Maximum crack width measured

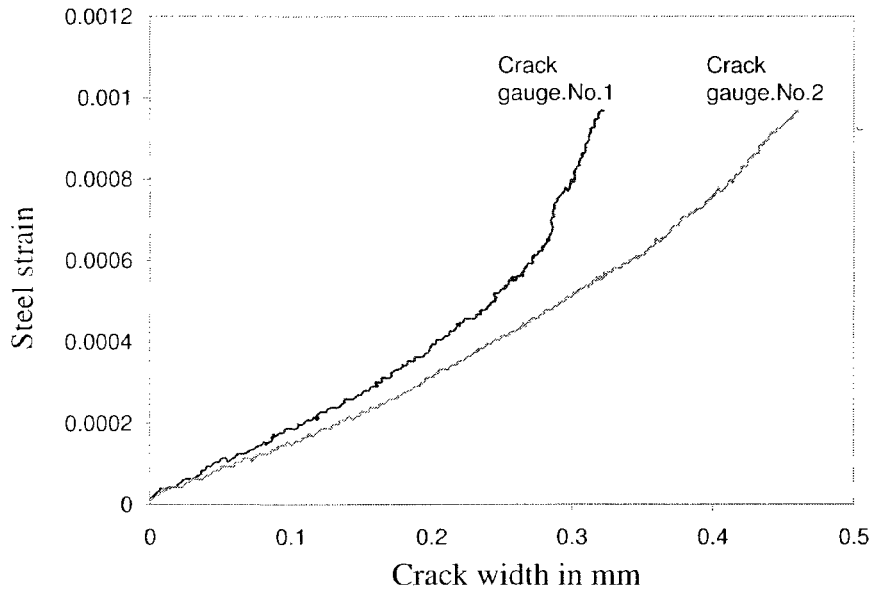


Figure 4.22: Crack width growth versus steel strain for NSC1

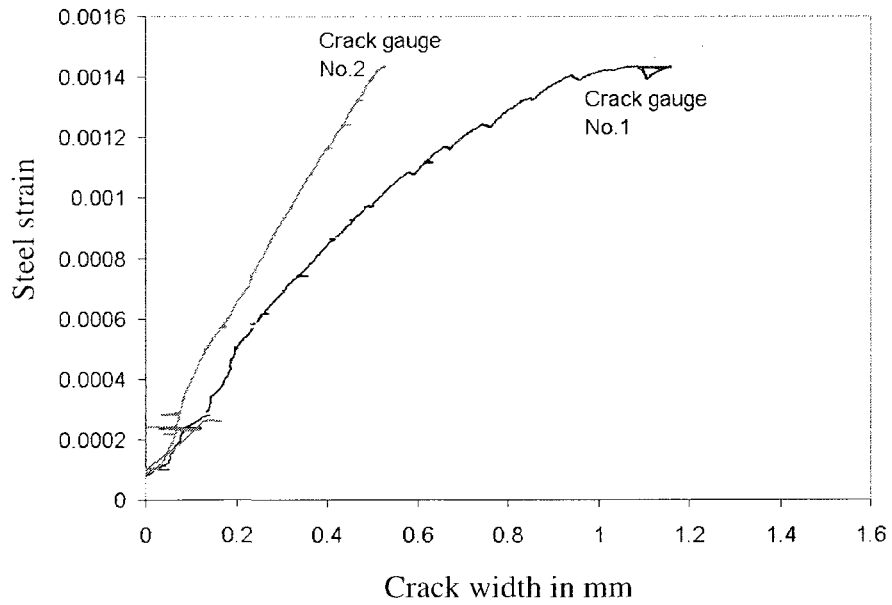


Figure 4.23: Crack width growth versus steel strain for HSC1

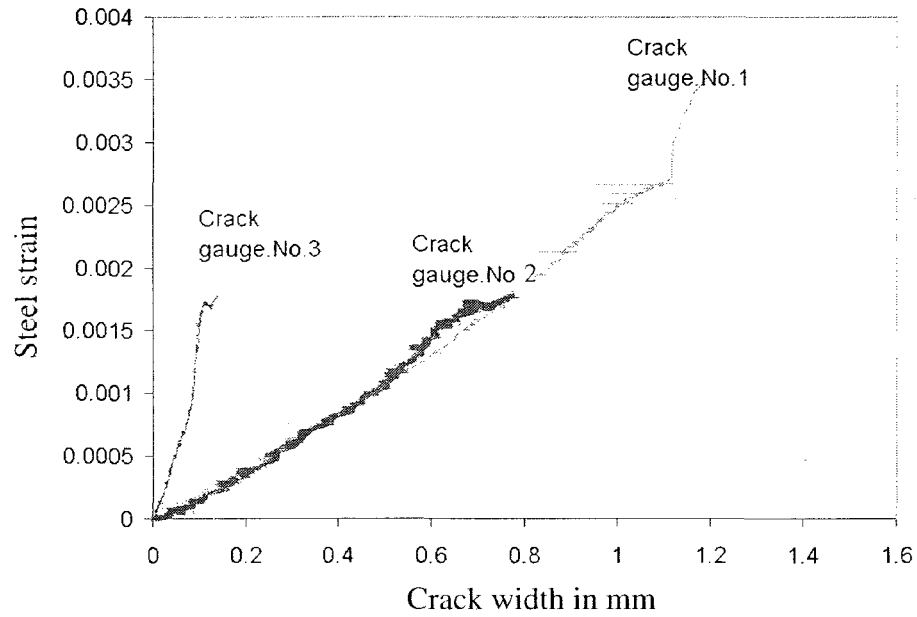


Figure 4.24: Crack width growth versus steel strain HSC3

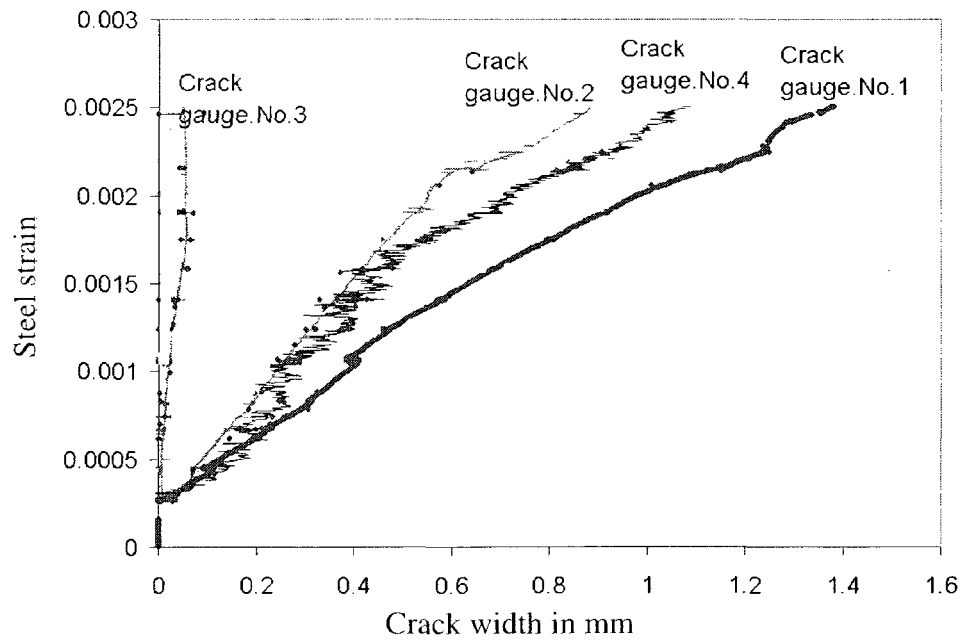


Figure 4.25: Crack width growth versus steel strain for HSC4

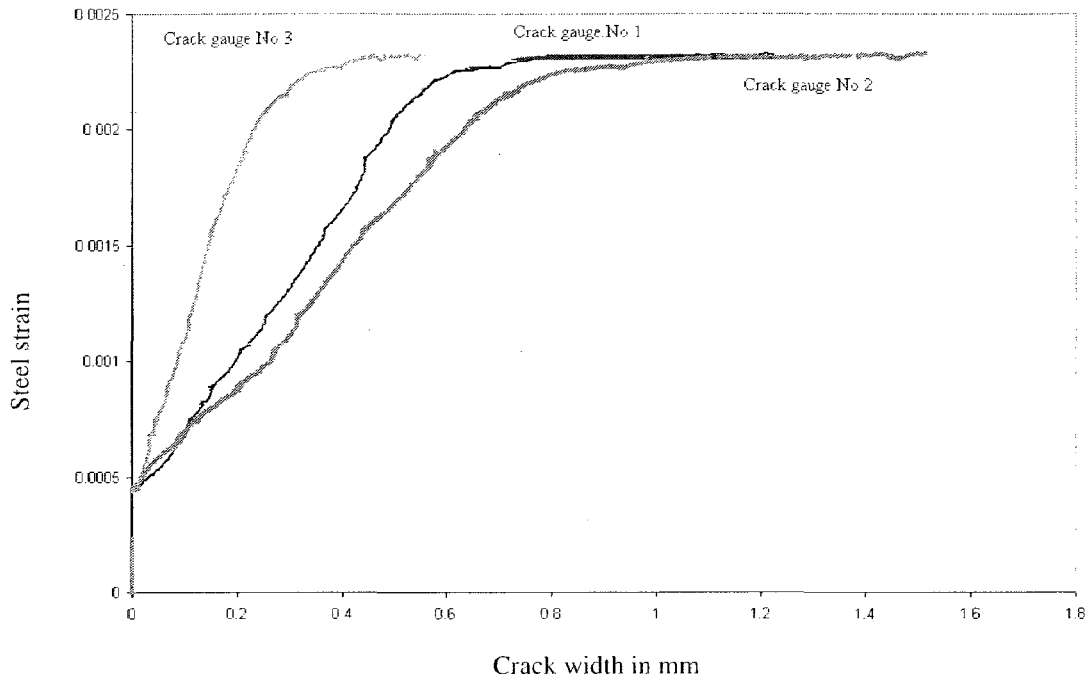


Figure 4.26: Crack width growth versus steel strain for NSC2

Chapter 5

Proposed Crack Analysis

5.1 Introduction

Cracking of reinforced concrete structures is inevitable and it is one of the most common causes of damage in concrete structures that results in huge annual cost to the construction industry. It occurs in a concrete cross-section when the stress in extreme tensile fiber reaches the tensile strength of the concrete. The reinforcing bar undergoes the same strain or deformation before cracking as the surrounding concrete. No slip occurs between the two materials under load with a perfect bond.

Many researchers studied the mechanism of cracking and the influence of different factors such as the bond between concrete and reinforcing steel, reinforcement ratio bar spacing, bar size, concrete cover and concrete properties to develop different expressions for the calculations of crack properties (crack spacing and crack width).

The main focus of this study is directed towards the suitability of available crack width and crack spacing expressions for offshore concrete structural applications. Most of the available expressions for crack width were developed for building structures using normal strength concrete and small concrete cover. However, offshore structures are built using high strength concrete with large concrete cover. Moreover, accurate estimate of the tension stiffening is another important factor for determining the crack width for offshore concrete structures.

5.2 Cracking of Reinforced Concrete Structures

The objective of this chapter is to develop an analytical model for cracking that describes in appropriate details the observed cracking behavior of the reinforced concrete flexural members tested in this study.

When a reinforced concrete member is subjected to a bending moment as shown in Figure 5.1, two types of stresses (longitudinal and lateral stresses) act on the tensile zones of the concrete surrounding the tensile reinforcement. As the longitudinal bending stress acts, the tensile zone undergoes a lateral contraction

before cracking, resulting in a lateral compression between the reinforcing bar and the concrete around it. When a flexural crack starts to develop, this biaxial lateral compression has to disappear at the crack because the longitudinal tension in the concrete is automatically transferred to the reinforcing bar and the tensile stress in the concrete becomes zero at the cracked section. The position of neutral axis rises at the cracked section in order to maintain equilibrium at that section. Although the concrete is assumed to carry no tension at the crack locations, it is still able to develop tensile stresses between the cracks through transfer of bond forces from the reinforcement into the concrete. Tension stiffening arises from this ability of concrete to carry tension between cracks in a reinforced concrete member, and helps control member stiffness deformation, and crack widths related to satisfying serviceability requirement. In the following sections, two methods are developed to calculate the crack width of a flexure member.

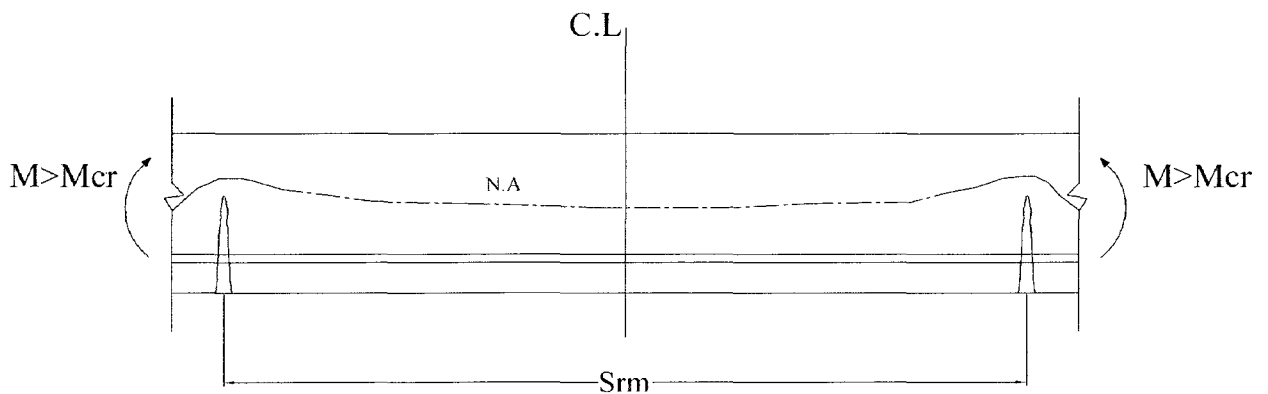


Figure 5.1: Flexural cracking in a singly reinforced concrete member

5.3 Crack Spacing

In 1966 Ferry-Bogres combined the “Classic” bond-slip theory of (Saliger, 1936) and the “No Slip” theory presented by (Base et al, 1966) earlier in the year. The resulting equation was used then by the CEB-FIP code in 1978. However, this concept was abandoned in the new edition of CEB-FIP 1990 code. The same expression, Equation 5.3.1, was adopted later by the Norwegian code (NS 3473E, 1992) and the Canadian code (CSA S474, 2004).

The average crack spacing equation can be divided into two terms. Term A is a function of concrete cover and bar spacing [$A=2.0(c+0.1s)$]. Term B, [$B=k_1k_2d'_{bc}h_{ef}b/A_s$], relates to the type of bar, the diameter, type of stress and the effective area of concrete surrounding the steel. The effective area of concrete was first investigated by (Chi and Kirstein, 1958) and it was defined as the area of concrete around the bar reinforcement that participate in carrying the tensile stresses through the cracked section. For offshore elements, the area of the effective tensile zone is almost equal to the area under the neutral axis. This is due to the use of large bar diameters and thick concrete cover; which is typical for offshore structures. In other words, the variation in tensile strain will be between the maximum value at the extreme fibres and zero at the neutral axis ($\epsilon_2 = \epsilon_{II} = 0$).

$$S_m = 2.0(c + 0.1s) + k_1k_2d'_{bc}h_{ef}b/A_s \quad (5.3.1)$$

$$k_2 = \frac{0.125(\varepsilon_I + \varepsilon_{II})}{\varepsilon_I} \quad (5.3.2)$$

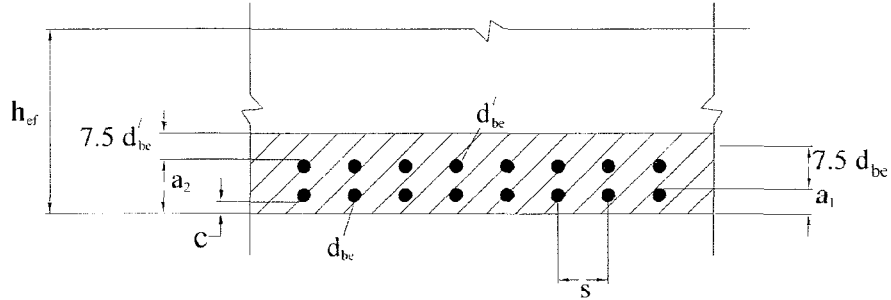


Figure 5.2: Effective embedment thickness

A similar expression for the average crack spacing is recommended by the Eurocode 2 (EC2) as shown in Equation 5.3.3. However, the EC2 uses a constant for Term A equal to 50 mm, indicating that the effect of concrete cover and bar spacing is not variable in the first part of the crack spacing equation. This will lead to an error in estimating the crack spacing, since the CSA and NS estimate Term A equal to 150 mm for a typical offshore concrete section of 400-600 mm thickness and 50-60 mm concrete cover.

$$S_{rm} = 50 + k_1 k_2 \frac{d_b A_{cef}}{4A_s} \quad (5.3.3)$$

$$k_2 = \frac{(\varepsilon_1 + \varepsilon_2)}{2\varepsilon_1} \quad (5.3.4)$$

The crack spacing expression of CEB-FIP is different when compared to other codes (CSA, NS, and EC2). In the mean time, the bond effect of CEB-FIP

(1990) is treated in a different manner. For a cracked reinforced concrete section, an increase in loading will result in an increase in steel strain. This will cause an elongation of the reinforcing bar in which the bar ribs will tend to move towards the nearest crack relative to the surrounding concrete. The stress in the steel caused by steel strain will be reduced due to the bond stress τ_{bk} between the steel and surrounding tensile concrete. Therefore, instead of using the factor k_t to account for bond effect, the CEB-FIP (1990) model code uses the bond stress τ_{bk} directly in the expression as shown in Equation 5.3.5.

$$l_{s,max} = 2 \frac{\sigma_{s2} - \sigma_{sE}}{4\tau_{bk}} \phi_s \quad (5.3.5)$$

$$\text{For stabilized cracking, } l_{s,max} = \frac{\phi_s}{3.6\sigma_{s,ef}} \quad (5.3.6)$$

$$\text{For a single crack formation, } l_{s,max} = \frac{\sigma_{s2}}{2\tau_{bk}} \phi_s \frac{1}{1 + \alpha_e \rho_{s,ef}} \quad (5.3.7)$$

$$\text{For stabilized cracking } S_{rm} = \frac{2}{3} l_{s,max} \quad (5.3.8)$$

where:

$l_{s,max}$ = The length over which slip between steel and concrete occurs, steel and concrete strains, which occur within this length, contribute to the width of the crack (mm), σ_{s2} = Steel stress at crack(MPa),

σ_{sE} = Steel stress at point of zero slip (MPa),

ϕ_s = Bar diameter (mm),

τ_{bk} = The lower fractile value of the average bond stress (MPa),

α_c = The ratio (E_s / E_{ci}),

E_{ci} = The tangent modulus of elasticity of concrete (MPa),

$\rho_{s,ef}$ = The effective reinforcement ratio ($A_s / A_{c,ef}$),

$A_{c,ef}$ = The effective area of concrete in tension limited by slab width and height
equal to the lesser of $2.5(c + \phi / 2)$ or $(h-c)/3$ (mm^2),

S_{rm} = The average width (mm).

The CEB-FIP (1990) expression does not take into account the strain variation coefficient in concrete k_2 . The strain gradient factor k_2 is a very important factor for an offshore concrete section of 400 – 600 mm thick. Therefore, it is evident that the EC2 and CEB-FIP model code expressions are not suitable for offshore concrete structures with a thick cover. These expressions are more suitable for building structures where the concrete cover is relatively constant and small.

The average crack spacing measured at each experiment was considered and presented in Table 5.1 along with numerical estimations of other international codes. For Series I, Figures 5.3 indicate that both EC2 and CEB-FIP (1990) are very

similar in the results for average crack spacing and less by almost 50 % than the experimental results. The crack spacing values estimated by the CSA and NS code were very close to the experiments with only 5% error. For Series II and Series III as shown in Figures 5.4, Figure 5.5, Figure 5.6, the pattern of experiment results were the same compared to the values predicted by other codes with the exception that the crack spacing differences between the experiments and the values estimated by the CSA and NS code were up to 9% higher for Series II and 15 % for Series III.

Table 5.1: Comparison of crack spacing test results with the predictions of other codes

Series No	Slab No.	Experiment	CSA	NS	CEB-FIP	EC2
		S_{rm} (mm)	S_{rm} (mm)	S_{rm} (mm)	S_{rm} (mm)	S_{rm} (mm)
Series I	NSC1	134	127	127	61	83
	HSC1	171	167	167	69	87
	HSC2	185	187	187	70	88
Series II	HSC3	163	148	148	90	99
	HSC4	172	170	170	116	113
Series III	HSC5	120	139	139	95	101
	NSC2	223	203	203	191	153
	NSC3	239	223	223	214	165

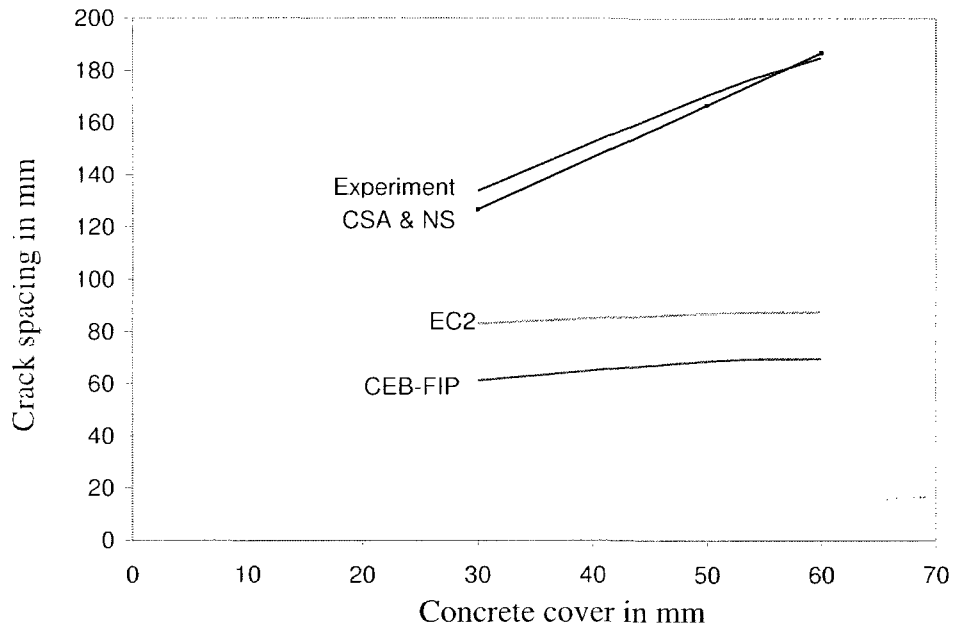


Figure 5.3: Comparison of average crack spacing for Series I

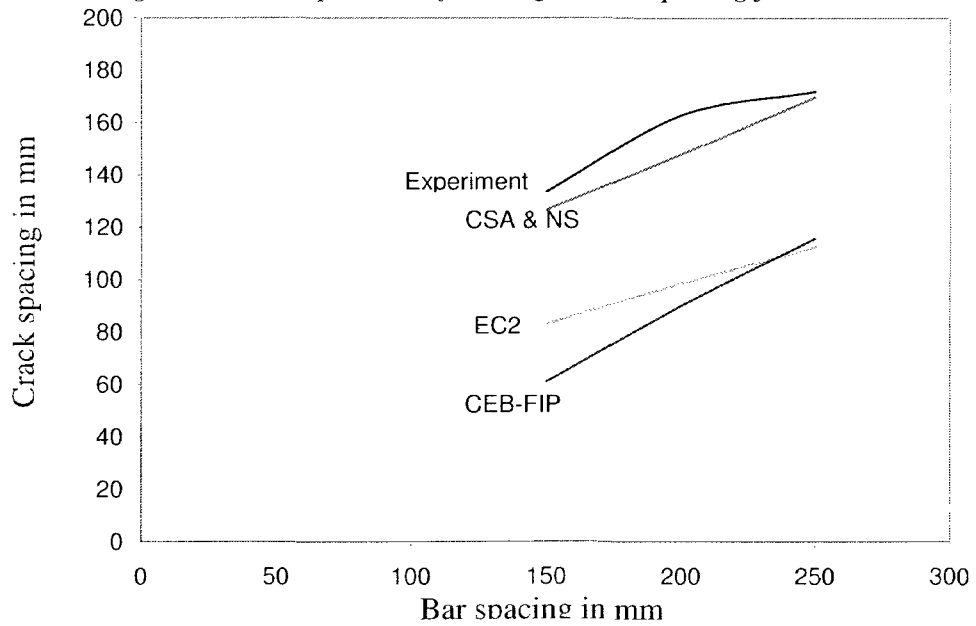


Figure 5.4: Comparison of average crack spacing for Series II

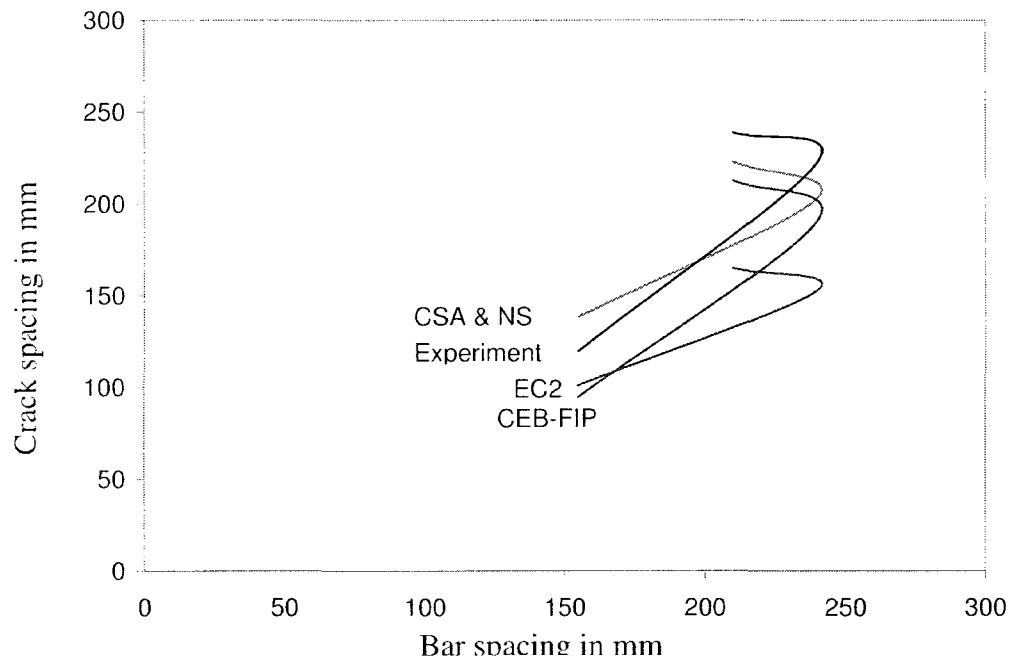


Figure 5.5: Comparison average crack spacing for Series III

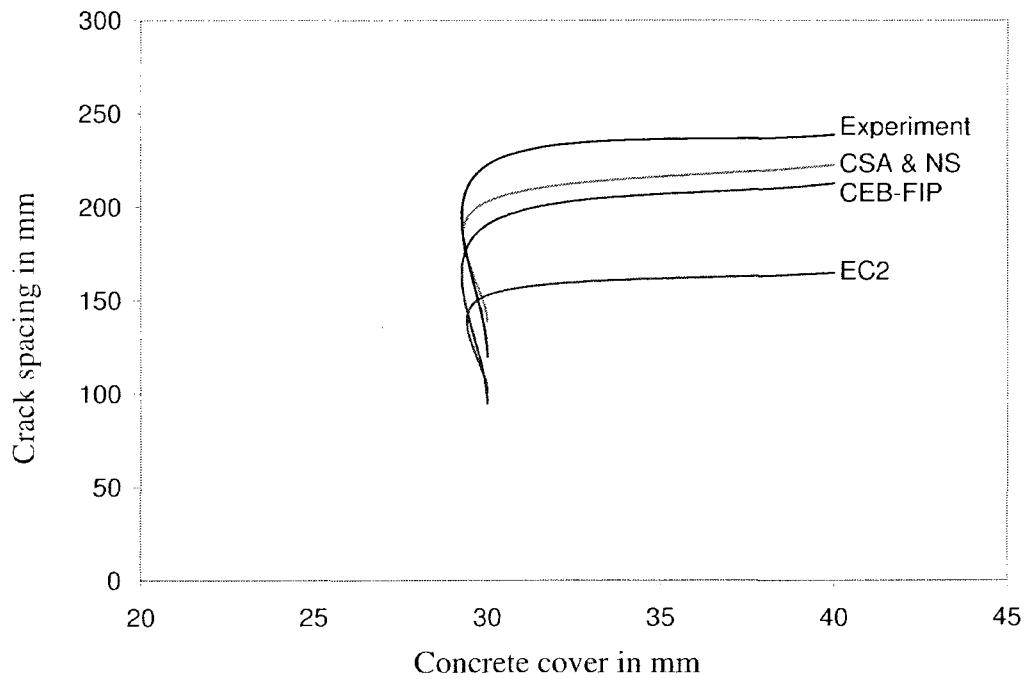


Figure 5.6: Comparison of average crack spacing for Series III

5.4 Cracked Width Calculations Based on Fracture Energy

Once concrete reaches its cracking strength, the concrete reinforcement is assumed to carry all of the tensile loads. In the meantime, with coarse aggregate interlock at narrow widths, energy observed in crack surfaces and the interaction between steel bars and the surrounding concrete means that the concrete continues to carry tensile loads between the cracks. After the formation of the first crack, the average stress in concrete f_c will start to decrease and the area under the curve is known as the fracture energy. This phenomenon is called tension softening for plain unreinforced concrete and tension stiffening for reinforced concrete. This concept is related to the fracture energy of the material.

The average crack width may be calculated as the average crack spacing Equation 5.3.1 times the product of the total average tensile concrete strain after considering the contribution of the tension stiffening. The tension stiffening effect is going to reduce the crack width.

In the CSA offshore code, an expression used in Equation 5.4.2 was originally suggested by (Vecchio and Collins, 1986) to describe the effect of tension stiffening on the concrete strain without consideration for the steel reinforcement ratio, the size of the concrete cover and concrete member thickness. However, this equation provides very approximate values for the tension stiffening effect

$$f_c = f_{cr} / (1 + \sqrt{500\epsilon_1}) \quad (5.4.2)$$

$$f_{cr} = 0.33\lambda\sqrt{f'_c} \quad (5.4.3)$$

The contribution of the concrete in tension between cracks in the European codes was taken as a reduction factor of the total concrete strain. The Norwegian code NS provide the following equation for calculating the crack width. It uses factor r (Equation 5.4.6) to account for tension stiffening effect.

$$w_k = 1.7w_m \quad (5.4.4)$$

$$w_m = r\epsilon_1 S_{rm} \quad (5.4.5)$$

$$r = 1 - \frac{\beta}{2.5k_1} (\sigma_{sr} / \sigma_s)^2 \geq 0.4 \quad (5.4.6)$$

Compared to the CSA code, the NS code calculates the maximum characteristic crack width w_k at the level of steel reinforcement while the CSA code calculates the average crack width w_m at the surface of the concrete. The characteristic crack width, is defined in most of the European codes as the width that only 5% of the cracks will exceed. This characteristic crack width is taken as 70% more than the average crack width (Clark, 1956). The maximum permissible crack width for offshore structures in the CSA code is in the range of 0.25 mm in the splash zone and up to 0.5 mm elsewhere. However, the NS code provides more detailed regulations for crack width limitation depending on the environmental

conditions. Four environment classes were identified in NS; namely, especially aggressive environment, severely aggressive environment, moderately aggressive environment and mildly aggressive environment. Usually, Canadian offshore structures exist in a severely aggressive environment which limits crack width to the range of 0.20 mm and 0.10 mm.

To account for tension stiffening in the CEB-FIP (1990), an empirical shape factor β is used to assess the average strain. The CEB-FIP (1990) code gives the following equation for calculation of the characteristic crack width:

$$w_k = l_{s,max} (\epsilon_{s2} - \beta \epsilon_{sr2} - \epsilon_{cs}) \quad (5.4.7)$$

where:

w_k = Characteristic maximum crack width (mm),

w_m = Average crack width (mm),

ϵ_{s2} = Steel strain of transformed section in which the concrete in tension is ignored,

ϵ_{cs} = The free shrinkage of concrete, generally a negative value,

ϵ_{sr2} = The steel strain at crack, under a force causing stress equal to f_{ctm} ; within A_{cef} ,

β = An empirical factor to assess average strain within $l_{s,max}$.

For tension stiffening, the (EC2-91) uses the factor ξ which is a dimensionless coefficient. Moreover, the (EC2-91) limits the maximum crack width

to 0.30 mm for sustained load under normal environmental conditions which will not impair the proper functioning of the structure. The characteristic crack width is estimated by the next expression.

$$w_k = \beta S_{rm} \xi \varepsilon_{sm} \quad (5.4.8)$$

where:

w_k = Design crack width,

S_{rm} = Average stabilized crack spacing,

ξ = A dimensionless coefficient between 0 and 1, representing the effect of the participation of concrete in the tension zone to stiffen the member,

ε_{sm} = Mean strain under relevant combination of loads and allowing for the effect such as tension stiffening or shrinkage,

β = Coefficient relating the average crack width to the design value and equals to 1.7 and 1.3, respectively, for section whose minimum dimension exceed 800 mm or is smaller than 300 mm .

In the past 30 years, many researchers have proposed other analytical models, using fracture energy approach, to predict the cracking response and tension stiffening effect in reinforced concrete members. The tension stiffening values can be recommended based on the actual measured tension softening values and appropriate experimentally fitted constants. The tension softening values for

normal strength concrete can be calculated from the fracture energy tests as recommended by (Gopalarantnam and Shah, 1985) where, a unique relationship between stress-crack width exists as shown in Equation. 5.4.9.

$$\beta = \frac{f_c}{f_{cr}} = \exp(kw^\lambda) \quad (5.4.9)$$

where:

w =crack width (mm).

k and λ =constants depends on concrete mix properties.

The fracture energy and tension properties of high-strength concrete was tested by (Marzouk and Chen, 1995) as shown in Figure 5.7 and a similar model for tension softening was developed. A tension-stiffening model was developed for high strength concrete based on the experimental results from over 20 concrete slabs using finite element analysis (Marzouk and Chen 1993). The proposed model is given in Equation 5.4.10 to represent the descending portion of the normalized average tension stress vs. normalized crack

$$\beta = \frac{f_t}{f'_t} = \frac{\epsilon_t / \epsilon_{t0}}{1.3863(\epsilon_t / \epsilon_{t0} - 1)^{1.6655} + \epsilon_t / \epsilon_{t0}} \quad (5.4.10)$$

For descending portion $\epsilon_t / \epsilon_{t0} \geq 1.0$

where:

ϵ_1 = Concrete tensile strain,

ϵ_{10} = Concrete cracking strain.

Based on the experimental results of four high-strength concrete specimens (Marzouk and Chen, 1993), the average concrete cracking strain ϵ_{10} is equal to $118\mu\epsilon$ and the ultimate averaged concrete tensile strain f'_t is equal to 3.284 MPa . For normal-strength concrete, the results of three specimens reported by (Guo and Zhang, 1987) are selected to calculate the averaged cracking strain ϵ_{10} , equal to $106.35\mu\epsilon$, and the ultimate averaged concrete tensile strain f'_t , equal to 2.384 MPa .

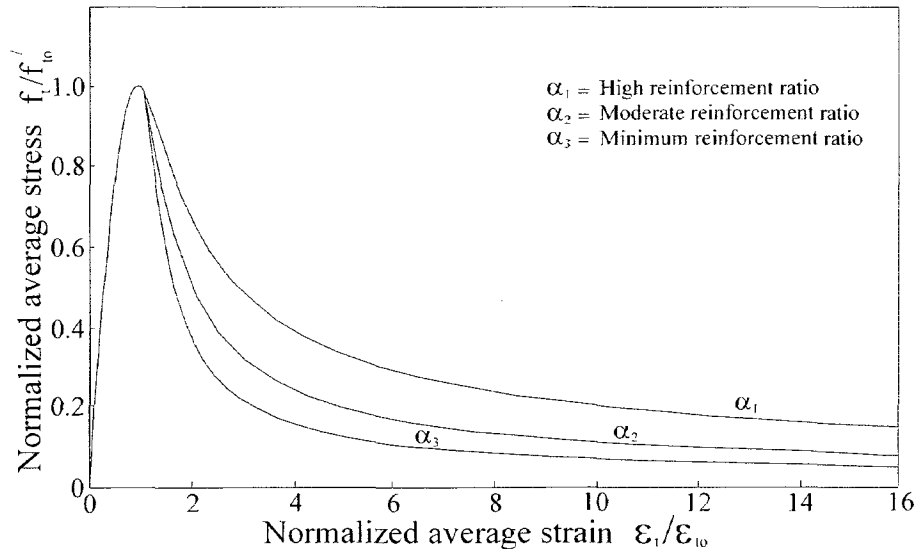


Figure 5.7: Complete tension stiffening model for high strength concrete

(Marzouk and Chen 1995)

5.4.1 Comparison of Crack Width Test Results with the Predictions of Other International Codes

Various code equations presented in Section 5.4 for predicting crack width for reinforced concrete slab were used to compare the test results to the predictions of these equations. For most of the specimens, the crack width measuring gauges (CDT) were mounted on the concrete tension surface around the centre of the specimens due to the fact that the largest stresses will exist within that area. Both the CSA and NS codes provide slightly different values for crack width estimates. This difference is due to the fact that the NS acknowledges the difference between the stress in steel at the crack and the stress in steel when the crack starts to happen. In contrast, the CSA code ignores the steel stress variation and provides the crack width at the concrete surface. Moreover, the CSA recommends the use of the modulus of rupture (Equation 5.4.3) to define the cracking strength of concrete. On the other hand, the NS uses the European approach of defining a function of nominal tensile strength and a factor that accounts for the type of forces applied on the section (Equation 5.4.1.1).

$$\text{Concrete tensile strength} = 1.3k_w f_{tn} \quad (5.4.1.1)$$

where:

k_w = Coefficient accounts for type of forces applied on the section,

f_m = Nominal tensile strength of the concrete in the structure (*MPa*).

For Series I and Series II, Figures 5.8 to 5.9 indicate that both EC2 and CEB-FIP are very similar in results for maximum crack width and less by 75 % than the experimental results. The CSA and NS gave closer results than the EC2 and CEB-FIP but less by 50% than the experiment results. In other words the European and the CSA codes underestimate the maximum crack width by a large percentage. For Series III as shown in Table 5.2, the European codes can provide a good prediction for maximum crack width for normal strength concrete specimen with small concrete cover but they fail to provide an accurate prediction for high strength concrete specimens. For detailed crack width calculations, see Appendix A1

Table 5.2: Comparison of the test results with the predictions of other international codes

Series No	Slab No.	Experiment	CSA	NS	CEB-FIP	EC2
		W_k (mm)	W_m (mm)	W_k (mm)	W_k (mm)	W_k (mm)
Series I	NSC1	0.406	0.227	0.269	0.107	0.135
	HSC1	0.772	0.351	0.354	0.114	0.142
	HSC2	0.950-	0.438	0.397	0.115	0.143
Series II	HSC3	0.486	0.252	0.314	0.143	0.160
	HSC4	0.483	0.287	0.361	0.174	0.183
Series III	HSC5	0.327	0.248	0.294	0.133	0.165
	NSC2	0.248	0.324	0.430	0.236	0.249
	NSC3	-	0.425	0.473	0.185	0.268

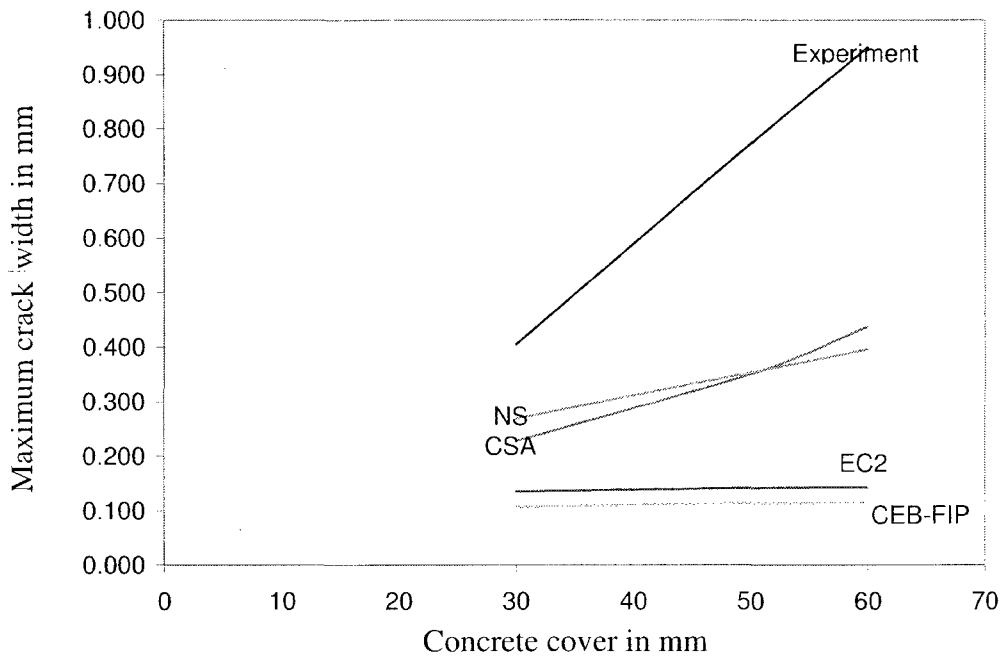


Figure 5.8: Comparison of maximum crack width for Series I

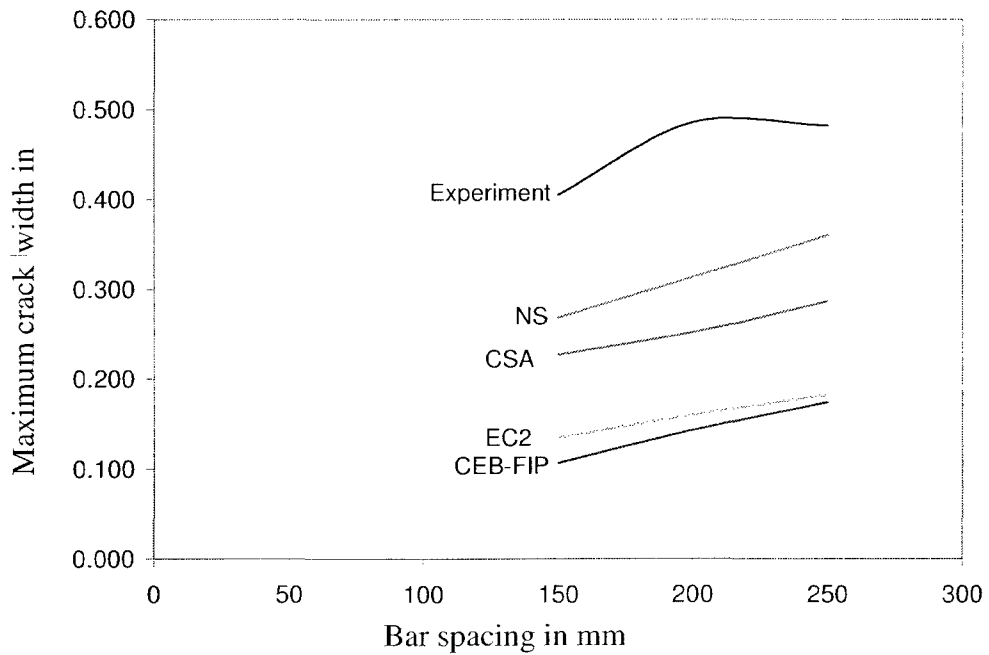


Figure 5.9: Comparison of maximum crack width for Series II

5.5 Calculating Crack Width Using Modified Tension Chord

Assumptions (MTCA)

When a reinforced concrete member starts to crack due to flexural tensile load, as shown in Figure 5.10, the crack results from the difference in elongations between the steel, Δe_s , and the concrete, Δe_c over half of the crack spacing and the maximum slip of steel relative to the concrete will be equal to :

$$\Delta_{\text{slip}} = \Delta e_s - \Delta e_c \quad (5.5.1)$$

The crack width is the sum of the slip in two adjacent half segments.

$$w = 2\Delta_{\text{slip}} \quad (5.5.2)$$

For both steel and concrete, the total elongation over one half of crack spacing as shown in Figure 5.6 may be calculated from the following equations:

$$\Delta e_s = \epsilon_{sm} \left(\frac{S_{rm}}{2} \right) \quad (5.5.3)$$

$$\Delta e_c = \epsilon_{cm} \left(\frac{S_{rm}}{2} \right) \quad (5.5.4)$$

where:

ϵ_{cm} = Average concrete strain,

ϵ_{sm} = Average steel strain,

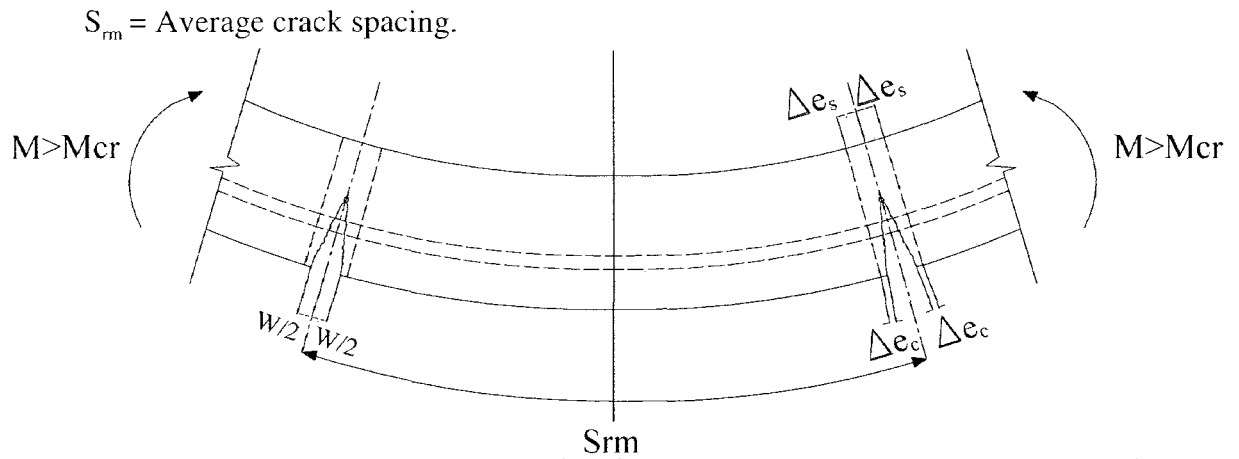


Figure 5.10: Elongations of the steel and concrete between two consecutive cracks

5.5.1 Average Concrete Tensile Strain (ϵ_{cm}) in Tension Chord

The tension chord model (Marti et al, 1998) is used to calculate ϵ_{cm} since it simplifies the analysis of the reinforced concrete members under a flexural loading. Besides, the tension chord model gives a better understanding of the cracking mechanism in reinforced concrete members.

At $M > M_{cr}$, cracking occurs and the steel stress along the reinforcement varies from a maximum value at the crack to a minimum value midway between the cracks as shown in Figure 5.11.

Consider a segment of a singly reinforced concrete member subjected to a bending moment M , greater than the cracking moment M_{cr} , as illustrated in Figure 5.12.a. The idealized cracked section consists of two longitudinal reinforced

concrete chords, one representing the compressive zone of depth kd and width b and the other representing the tensile zone consisting of the effective tensile area of the concrete A_{ct} at the steel level, and the reinforcing steel area A_{st} .

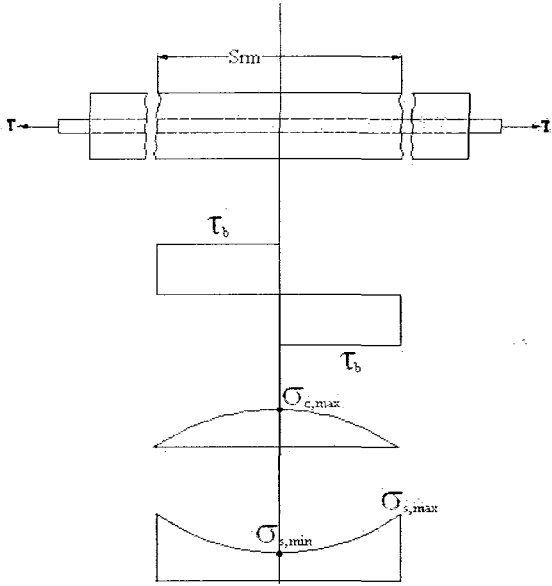


Figure 5.11: Elongations Bond shear stress, concrete and steel stress

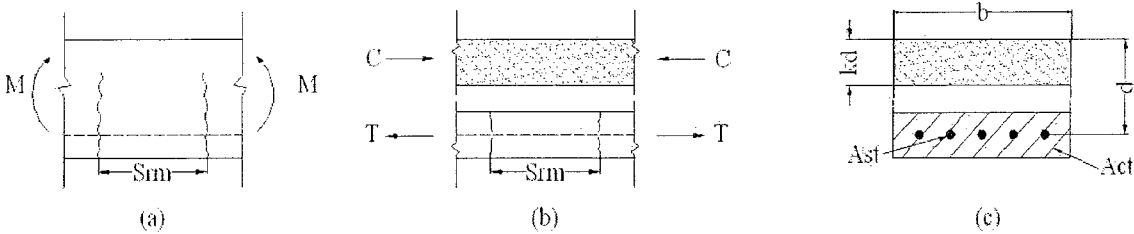


Figure 5.12: Tension Chord in a singly reinforced concrete member

The concrete section under flexural loading is composed to compression cord subjected to compressive force C and tension cord subjected to tensile force T . The

tensile longitudinal zone between consecutive cracks is subjected to an axial tensile force T , and shown in Figure 5.12. The length of the segment represented by S_m , is equal to crack spacing. The origin of the axial coordinate x is taken midway between the two cracks at point "O". The free body diagram of the right side of the section at distance x is shown in Figure 5.12.b. An infinitesimal element of length dx is taken out from the segment. The free body diagrams of the steel and concrete elements are shown in Figures 5.12. c and 5. 12. d respectively

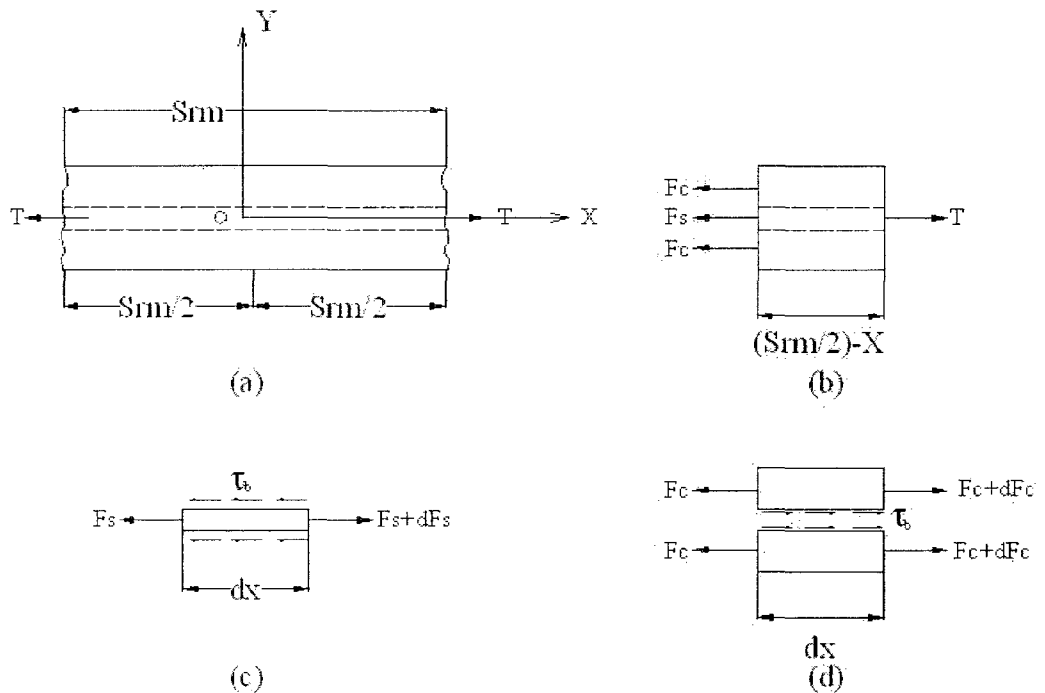


Figure 5.13: Free body diagram in a tension Chord

The equilibrium for the free body of differential concrete element of length dx shown in Figure 5.13.d yields

$$F_c = F_c + dF_c + (\pi d_b dx) \tau_b \quad (5.5.1.1)$$

$$\frac{dF_c}{dx} = -\pi d_b \tau_b \quad (5.5.1.2)$$

Integrating the differential Equation 5.5.1.2 for concrete element and considering the appropriate boundary conditions, $F_c=0$ at the crack ($x = s_{rm} / 2$), results in

$$\int dF_c = - \int \pi d_b \tau_b dx \quad (5.5.1.3)$$

$$F_c = \pi d_b \tau_b \left(\frac{s_{rm}}{2} - x \right) \quad (5.5.1.4)$$

and the concrete stress may be expressed as

$$\sigma_c = \frac{F_c}{A_c} = \frac{4 \tau_b \rho_{ef}}{d_b} \left(\frac{s_{rm}}{2} - x \right) \quad (5.5.1.5)$$

where:

τ_b = The bond stress at the steel-concrete interface,

d_{be} = The nominal diameter of the tensile reinforcing bar,

$\rho_{ef} = A_{st} / A_{ct}$ = The effective reinforcement ratio, (ratio of tensile reinforcement area to the area of the effective concrete in tension),

$$A_{ct} = h_{ef} b ,$$

h_{ef} = Effective embedment thickness, mm, taken as the greater of $a_2 + 7.5d_{be}$ but not greater than the tension zone or half the shell thickness.

At the crack ($x = s_{rm} / 2$), the concrete stress is minimum, thus;

$$\sigma_{c(\min)} = 0 \quad (5.5.1.6)$$

and at the center of the segment ($x = 0$), the concrete stress is maximum

$$\sigma_{c(\max)} = \frac{2\tau_b s_{rm} \rho_{ef}}{d_b} \quad (5.5.1.7)$$

The average concrete stress is

$$\sigma_{cm} = \frac{1}{2} [\sigma_{c,\max} + \sigma_{c,\min}] = \frac{1}{2} \left[\frac{2\tau_b s_{rm} \rho_{ef}}{d_b} + 0 \right] = \frac{\tau_b s_{rm} \rho_{ef}}{d_b} \quad (5.5.1.8)$$

Thus, the average concrete strain is

$$\epsilon_{cm} = \frac{\sigma_{cm}}{E_c} = \frac{\tau_b s_{rm} \rho_{ef}}{E_c d_b} \quad (5.5.1.9)$$

5.5.2 Bond Shear Stress (τ_b)

Bond strength between concrete and reinforcement is an important factor in calculating the crack width. The force in the bar is transmitted to the surrounding concrete by bond shear stress, τ_b .

Bond shear stress depends on several factors, including the concrete tensile strength and cover, steel stress, bar size and spacing, confining effects and load history. Several experimental and theoretical investigations were conducted on the behavior of bond for normal and high reinforced concrete. Marti et al. (1998) presented the bond stress τ_b as twice the concrete tensile strength f'_c for the service load less than yield load. Gilbert (2005) indicated that bond stress τ_b reduces as the stress in the reinforcement increases and proposed the following equation.

$$\tau_b = \alpha_1 \alpha_2 f_{ct} \quad (5.5.2.1)$$

where:

α_1 = Depends on the steel stress at crack,

α_2 = For short or long term calculations,

f_{ct} = The direct tensile strength of concrete.

Another study (Alavi-Fard and Marzouk, 2004) indicated that the square root of the compressive strength approach adopted by the Canadian Standard in the bond strength equation does not provide a good prediction of the bond strength for the high-strength concrete specimens tested in their study. The bond strength of high-strength concrete, from 50 to 90 MPa is more appropriately proportional to the cubic root. In the British Code (BS 8110, 1985) the bond strength of concrete is

proportional to the power of 1/3 and to the power of 2/3 in both the European code (CEB-FIP, 1990) and the Norwegian Code (NS 3474E, 1992).

5.5.3 Average Steel Tensile Strain (ϵ_{sm}) in Tension Chord

Due to the low tensile strength of concrete, cracking of concrete in offshore structures starts at early stage of loading. For crack width analysis, the serviceability limit state shall govern the crack width calculations and the stress in steel reinforcement f_s has been selected as the serviceability limit. This value considered as the end of serviceability limit after which both materials will behave nonlinearly as shown in Figure 5.14.

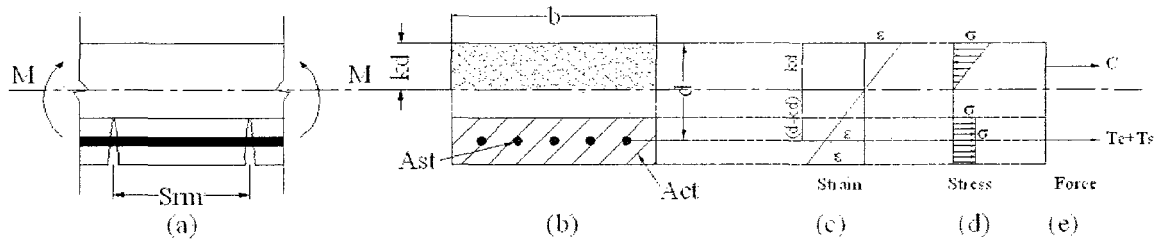


Figure 5.14: Analytical model for flexural cracking in a singly reinforced flexural member

The strain at the tension surface where the crack width has been measured is calculated using:

$$\epsilon_{sm} = \left(\frac{f_s}{E_s} \cdot \frac{h - kd}{d - kd} \right) \quad (5.5.3.1)$$

The average crack width at the extreme tension fiber will be

$$w_m = S_{rm} \left[\left(\frac{f_s}{E_s} \cdot \frac{h - kd}{d - kd} \right) - \frac{\tau_b S_{rm} \rho_{ef}}{E_c d_b} \right] \quad (5.5.3.2)$$

where:

h = The total member thickness,

f_s = Stress in the steel reinforcement at the end of the serviceability limit.

5.6 Numerical Example

Sample calculations using modified tension chord assumptions (MTCA) and fracture energy principles for crack width estimation are presented for Slab HS1.

For more details of the numerical example calculations see Appendix A2.

The following input data were obtained from Marzouk and Chen (1995) was measured in the laboratory and has been assumed in the calculations:

$$E_c = 51400 \text{ MPa}, E_s = 200000 \text{ MPa}, f'_t = 3.294 \text{ MPa}, \epsilon_{t0} = 118.6 \mu\epsilon$$

The averaged bond stress (τ_b) of high-strength concrete at the serviceability limit were obtained from (Alavi-Fard and Marzouk, 2004) experimental results:

$$\tau_b = 5.399 \text{ MPa}$$

5.6.1 Cracked Width Calculations Using the Modified Tension Chord

Assumptions

-Crack spacing calculation:

The average crack spacing S_{rm} can be calculated from the following Equation 5.16

$$S_{rm} = 2.0(c + 0.1s) + k_1 k_2 d_{be} h_{ef} b / A_s$$

$$S_{rm} = 167 \text{ mm}$$

-Crack width calculation:

$$w_m = S_{rm} \left[\left(\frac{f_s}{E_s} \cdot \frac{h - kd}{d - kd} \right) - \frac{\tau_b S_{rm} \rho_{ef}}{E_c d_b} \right]$$

Crack width calculated at $f_s = 250 \text{ MPa}$

$$w_m = 0.351 \text{ mm}$$

$$w_k = 1.7 w_m = 0.596 \text{ mm}$$

5.6.2 Cracked Width Calculations Based on Fracture Energy

Values obtained from the experiment HSC1:

$$f_s = 250 \text{ MPa} , S_{rm} = 171 \text{ mm}$$

-Crack width calculation neglecting tension stiffening effect

$$w_{m1} = S_{rm} \left[\left(\frac{f_s}{E_s} \cdot \frac{h - kd}{d - kd} \right) \right] = 0.364 \text{ mm}$$

The tension stiffening is going to reduce the crack width by

$$w_{m2} = \frac{f_t}{E_c} S_{rm}$$

$$f_t = \frac{f'_t(\epsilon_1 / \epsilon_{10})}{1.3863(\epsilon_1 / \epsilon_{10} - 1)^{1.6655} + \epsilon_1 / \epsilon_{10}} = 0.495 \text{ MPa}$$

Crack width calculated at $f_s = 250 \text{ MPa}$

$$w_m = w_{m1} - w_{m2} = 0.362 \text{ mm}$$

$$w_k = 1.7 w_m = 0.618 \text{ mm}$$

5.7 Comparison of Test Results with the Developed an Analytical Model and Different Code Predictions

The maximum crack width measured during each experiment was considered and presented in Table 5.4 along with the numerical predictions of the modified tension chord assumptions (MTCA) and fracture energy method.

The difference in the assumptions between the MTCA and fracture energy method comes from their definitions of the cracking phenomena. The MTCA defines the cracking in a reinforced concrete member due to flexural tensile load as the difference in elongations between the steel, $\Delta\epsilon_s$, and the concrete, $\Delta\epsilon_c$ over half of the crack spacing. The contribution of tension stiffening after cracking stage in the MTCA is represented by subtracting the concrete strain ϵ_{cm} from the steel

strain ϵ_{sm} of the member. The fracture energy method follow the same procedure for calculating the crack width with the exception that the tension stiffening values is recommended based on the actual measured tension softening values and appropriate experimentally fitted constants.

Table 5.3: Comparison of the test results of crack width with the modified tension chord assumptions and fracture energy

Series No	Slab No.	f'_c (MPa)	Bar spacing (mm)	Concrete cover (mm)	Experiment	MTCA	Fracture energy
					W_k (mm)	W_k (mm)	W_k (mm)
Series I	NSC1	35	150	30	0.406	0.388	0.416
	HSC1	68.5	150	50	0.772	0.596	0.618
	HSC2	70	150	60	0.950	0.743	0.743
Series II	HSC3	66.7	200	30	0.486	0.431	0.481
	HSC4	61.2	250	30	0.483	0.490	0.502
Series III	HSC5	70	100	30	0.327	0.424	0.369
	NSC2	33	240	30	0.248	0.557	0.618
	NSC3	34	210	40	-	-	-

From Figures 5.16 and 5.17, both the MTCA and fracture energy method predictions for maximum crack width were closer to the experiment results than code predictions, about 4% different, for a maximum crack width of 30 mm concrete cover and 150 mm bar spacing. This percentage increases up to 22 % when the concrete cover increase up to 60 mm. In Figure 5.17, it is clear that the

MTCA and fracture energy method predictions for maximum crack width, about 11%, is much closer to the experiments for 30 mm concrete cover and bar spacing that ranges from 150 mm to 250 mm as shown in Figure 5.17.

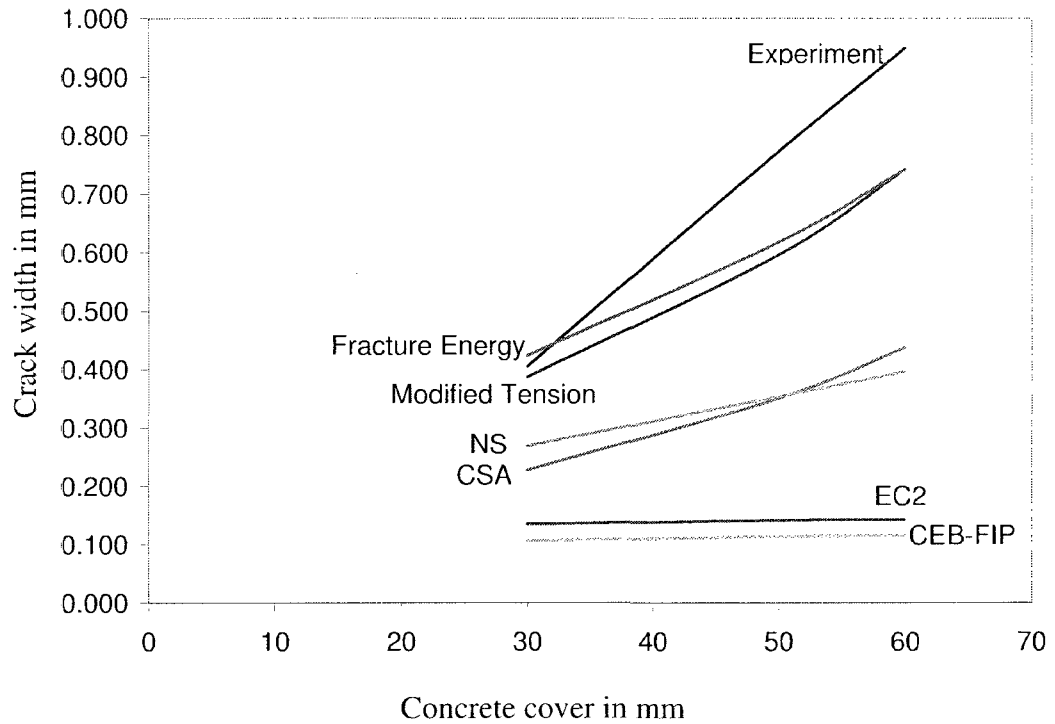


Figure 5.15: Comparison of crack width for Series I

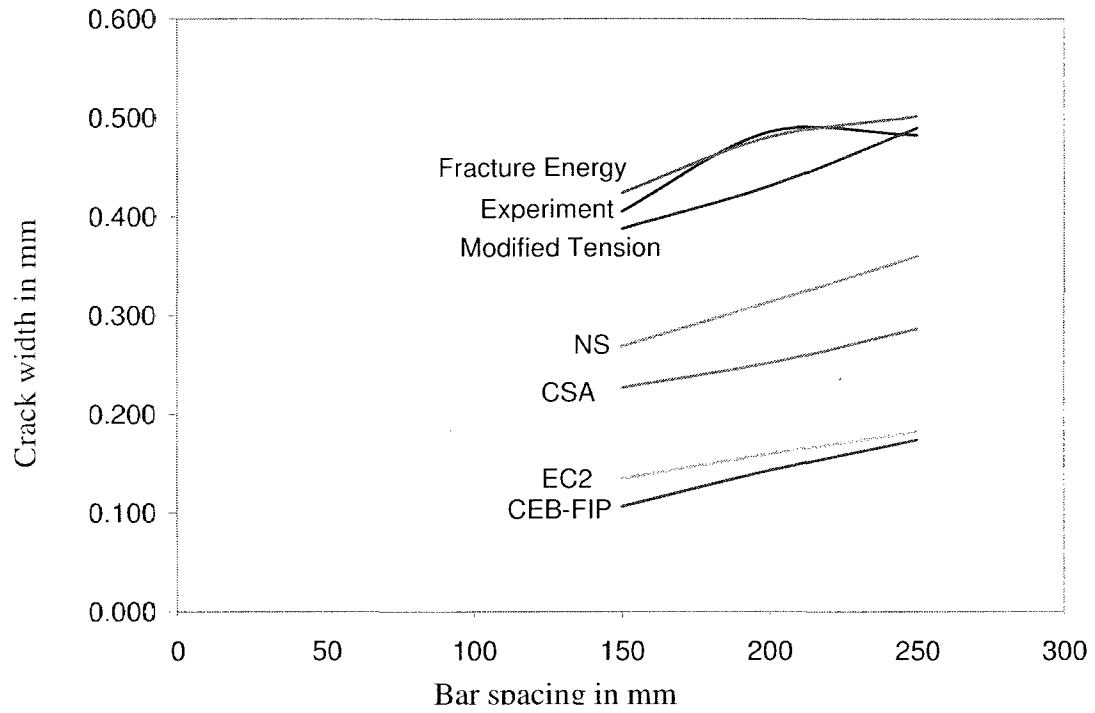


Figure 5.16: Comparison of crack width for Series II

Chapter 6

Conclusions and Recommendations

6.1 Summary

The overall objective of this study was focused directly toward examining the suitability of the different approaches for calculating the crack width and crack spacing of concrete structures for offshore concrete structural applications. The design of offshore structures is controlled by mandatory design codes to ensure structural safety and integrity. Most of the available expressions for crack width were developed for building structures using normal strength concrete and normal

concrete cover. However, offshore structures are built using high strength concrete with thick concrete cover.

A comprehensive experimental and theoretical investigation is presented in this thesis. The main focus in this study was to develop an analytical model for cracking that describes, in appropriate detail, the observed cracking behavior of the reinforced concrete flexural members tested in this thesis. The research work was divided into two main phases: experimental and theoretical. The experimental work included investigating the effectiveness of increasing concrete cover and bar spacing on crack properties.

The theoretical study included two parts. The first part investigated the suitability of available crack width and crack spacing code expressions for offshore concrete structure applications. The second part included the development of a numerical crack analysis model based on tension chord method and a second model based on the fracture energy principles. Either model is suitable for offshore applications since it takes in account the use of high strength concrete and large concrete cover.

6.1.1 Experimental Investigation

Eight reinforced concrete slabs were tested at the structural lab of Memorial University. The tests results are divided into three groups. The first group (Series I)

was designed to investigate the effect of concrete cover on the crack width and crack spacing. The group was made of three slabs designated as NSC1, HSC1, and HSC2. All the slabs had the same depth of 200 mm, same bar spacing 150 mm and bar diameter 25 mm with different concrete covers 30mm-60mm. The second group (Series II), HSC3 and HSC4, was designed to investigate the effect of bar spacing on the crack width and crack spacing. Specimen NSC1 from the first group (Series I) was considered for the comparison as a part of this series. The slabs of this group have the same slab depth of 200 mm, the same concrete cover of 30 mm, the same bar diameter of 25 mm and different bar spacing. The recommended values of the concrete cover and bar spacing are typical for the ones used in Canadian offshore applications. The first and the second group were designed to represent heavily reinforced concrete walls that normally fail under punching failure mode as the case for most offshore structures. However, the third group (Series III) was designed to investigate the effect of pure flexure failure and ductile shear failure. The third group includes HSC5, NSC2, and NSC3.

A large test data was recorded and the related graphs were prepared. The behavior of the slabs were presented in terms of the load-deflection relationship at different load stages including service and ultimate load, as well as crack width-

steel strain relationship. Failure mode, crack patterns and crack spacing were also depicted by means of photographs.

Once the concrete cover increased from 30 mm to 60 mm in Series I, the crack pattern changed from radial cracks to tangential cracks that extended outside the circumference of the column. Moreover, the average developed crack spacing increased every time the concrete cover increased for each specimen.

Most of the reinforced concrete slabs In Series II the crack pattern that dominates is the tangential crack which formed along the direction of the reinforcement. The average crack spacing was less than the bar spacing.

An increase of 67% in the concrete cover resulted in an increase in crack spacing by 27% experimentally and 32% theoretically according to the recommended expression. Once the concrete cover increased by 100%, the average crack spacing increased by 38% experimentally and 47% theoretically. These measurements were taken at steel stress level of 250 MPa ($0.625 f_y$). The bar spacing in Series II had more effect on the crack spacing compared to the concrete cover as shown in Table 4.5. Once the bar spacing increased by 67%, the crack spacing increased experimentally by 28% and theoretically by 34%.

With the third group (Series III), a comparison of the experimental results of the average crack spacing measurements and theoretical estimations of the

Canadian code CSA (Equation 2.8.1) were made. The data showed a good agreement between the CSA average crack spacing equation and the experimental results as shown in Table 4.6.

The widths of the primary cracks were examined in the two sets to determine the effect of reinforcement spacing and concrete cover. It was noticed that the relation of the crack width versus steel strain can be represented by a straight line up to a limiting steel strain of $1000\ \mu\epsilon$ to $1500\ \mu\epsilon$ for most of the tested slabs. This strain value corresponds to a steel stress reinforcement stress equals to 200 MPa to 250 MPa ($0.50-0.625 f_y$).

The data showed that as the concrete cover increased in Series I, the crack widths became larger. The maximum crack width could be influenced by as much as 90% when the concrete cover increased from 30 mm to 50 mm. Also the data showed that increasing the concrete cover by 100% (60 mm) resulted in increasing the maximum crack spacing by 234%.

Of the eight specimens designed for the experimental program, three (NSC1, HSC3, HSC4) were specifically tested to determine the effect of increasing bar spacing on crack width. It can be seen, in general, that the maximum crack width increased as the bar spacing increased. In addition, it appeared that the effect of increasing the bar spacing on crack width was less than the effect of increasing

the concrete cover. The data of Series III showed that for the range of bar spacing tested, the maximum crack width could be influenced by as much as 20% for specimen HSC3. When the bar spacing increased to 250 mm, the influence on crack width was almost the same 19%.

The crack width measurements for all of the three series were tabulated in order to compare these results with the developed crack width models developed in chapter 5.

6.1.2 Theoretical Investigation

The theoretical investigation included two parts. The first part investigated the suitability of available crack width and crack spacing code expressions for offshore concrete structure applications. The second part included the development of a numerical crack analysis model based on tension chord method and fracture energy principles.

The experimental test results of crack spacing in all the tested slabs showed that the proposed crack spacing equation of the Canadian Standard 2004 offshore code (Equation 6.1.2.1) is a suitable equation.

$$S_{rm} = 2.0(c + 0.1S) + k_1 k_2 d_{be} h_{ef} b / A_s \quad (6.1.2.1)$$

The average crack spacing equation of the CSA code can be divided into two terms. Term A is a function of concrete cover and bar spacing

[$A=2.0(c + 0.1S)$]. Term B, [$B=k_1k_2d'_{bc}h_{ef}b/A_s$], relates to the type of bar, the diameter, type of stress and the effective area of concrete surrounding the steel. The effective area of concrete is defined as the area of concrete around the bar reinforcement that participate in carrying the tensile stresses through the cracked section. For offshore elements, the area of the effective tensile zone is almost equal to the area under the neutral axis. This is due to the use of large bar diameters and thick concrete cover; which is typical for offshore structures. In other words, the variation in tensile strain will be between the maximum value at the surface and zero at the neutral axis ($\epsilon_2 = \epsilon_{II} = 0$). Second, due to the low tensile strength of concrete, cracking of concrete in offshore structures starts at early stage of loading. For crack width analysis, the serviceability limit state shall govern the crack width calculations and the stress in steel reinforcement f_s has been selected as the serviceability limit. This value considered as the end of serviceability limit after which both materials will behave in a non-linear manner.

For Series I, the average crack spacing values estimated by Equation 6.1.2.1 were very close to the experiments with only 5% error. For Series II and Series III, the average crack spacing difference between the experiments and the values estimated by the CSA code were up to 9% higher for Series II and 15 % for Series III.

Crack width calculation based on fracture energy principles can be estimated as the average crack spacing (Equation 6.1.2.1) times the product of the total average tensile concrete strain after considering the contribution of the tension stiffening. The tension stiffening effect is going to reduce the crack width.

The fracture energy and tension properties of high-strength concrete were tested by Marzouk and Chen (1995) and a tension-stiffening model was developed for high-strength concrete based on the experimental results from over 20 concrete slabs using finite element analysis (Marzouk and Chen, 1993). The proposed model given in Equation 5.4.10 represents the descending portion of the normalized average tension stress vs. normalized crack. This model is very realistic since it takes into account the concrete mix properties and the reinforcement ratio.

Another numerical model (MTCA) based on the tension chord method to calculate the maximum crack width is proposed. In this model, three assumptions were made based on the experimental evidence and the theoretical investigations. The first assumption, the serviceability limit state shall govern the crack width calculations and the stress in steel reinforcement f_s has been selected as the serviceability limit. This value of steel stress for most of the tested slabs is equal to 200 MPa to 250 MPa after which both materials will behave nonlinearly. Since the

crack width measurements were taken at the tension surface of the elements, the steel strain should be shifted to the concrete surface as shown in Equation 5.5.3.1.

Second, the bond strength of high-strength concrete, 50 to 90 MPa, is more appropriately proportional to the cubic root. Third, due to the use of large bar diameters and thick concrete cover elements in offshore structures, the area of the effective tensile zone is almost equal to the area under the neutral axis.

The new model (MTCA), Equation 5.5.3.2, allows designers to specify concrete cover and reinforcement ratio during the design process to control flexural crack width to an acceptable limit.

In other words, the difference in the assumptions between the MTCA and fracture energy method comes from their definitions to the cracking phenomena. The MTCA defines the cracking in a reinforced concrete member due to flexural tensile load as the difference in elongations between the steel, Δe_s , and the concrete, Δe_c over half of the crack spacing. The contribution of tension stiffening after cracking stage in the MTCA is represented by subtracting the concrete strain ϵ_{cm} from the steel strain ϵ_{sm} of the member. The fracture energy method follow the same procedure for calculating the crack width with exception that the tension stiffening values is recommended based on the actual testing of the concrete mix

under tensile load and measuring tension softening values and appropriate experimentally fitted constants.

Both methods MTCA and fracture energy method predictions for maximum crack width were closer to the experiment results than code predictions, about 4% different, for a maximum crack width of 30 mm concrete cover and 150 mm bar spacing. This percentage will increase up to 22 % when the concrete cover increase up to 60 mm. For Series II, the MTCA and fracture energy method predictions for maximum crack width, about 11%, is much closer to the experiments for 30 mm concrete cover and bar spacing that ranges from 150 mm to 250 mm.

The findings of this study, including the proposed equation, were based on an analysis of high strength reinforced concrete two-way slabs under short-term flexural loading. The effect of long-term loading such as creep and shrinkage that increase the crack widths over time were outside the scope of this study.

6.2 Conclusions

The experimental results and the theoretical study discussion in the previous chapters support the following:

- The experiments proved that the relationship between steel strain and crack width on the tension face is approximately linear up to values that range from $1000\mu\epsilon$ to $1800\mu\epsilon$ steel strains.

- Increasing the concrete cover in Series I can affect the pattern of the crack spacing. The tangential cracks in slab NSC1 were much more pronounced along lines parallel to the reinforcement crossing through the column stub. This pattern changed to radial cracks once the concrete cover increased.
- The test results showed that as the concrete cover increased by 67%, the average crack spacing became larger by 27% experimentally and 32% theoretically. Once the concrete cover increased by 100%, the average crack spacing increased by 38% experimentally and 47% theoretically. These measurements were taken at 250 MPa steel stresses.
- All the reinforced concrete slabs of Series II as shown in exhibited a tangential crack pattern which forms along the direction of the reinforcement. The tangential cracks were function of the bar spacing as it was evident for Series II. Once the bar spacing is increased the average tangential crack spacing is also increased.
- The test results indicated that once the bar spacing increased by 67%, the crack spacing increased experimentally by 28% and theoretically by 34%.
- In general, the calculated average crack spacing were lower than test results and as both the concrete cover and bar spacing increased, the crack spacing increased theoretically and experimentally.

- The Canadian offshore code expression (Equation 6.1.2.1) shows that it can give a good prediction of crack spacing for offshore concrete structure members.
- In the range of concrete cover tested, the maximum crack width could be influenced by as much as 90% when the concrete cover increased from 30 to 50 mm. Also the data showed that increasing the concrete cover by 100% (60 mm) resulted in increasing the maximum crack spacing by 234%.
- The effect of increasing the bar spacing on crack width is less profound than the effect of increasing the concrete cover. The data showed that for the range of bar spacing tested, the maximum crack width could be influenced by as much as 20% for specimen HSC3 (200 mm bar spacing). When the bar spacing increased to 250 mm, the influence on crack width were almost the same 19%.
- The analytical investigation revealed that the crack width and crack spacing calculated using CSA and NS are relatively close. In the mean time, the results of evaluating the crack width and crack spacing provided by EC2 and CEB-FIP are reasonably close.
- However, the values of the crack width and crack spacing calculated based on the EC2 and CEB-FIP are less by 75% than the experiment results while the values estimated by the CSA and NS is less by 50 %. The difference is due to

the effect of ignoring the contribution of the concrete cover in estimating the crack width.

- The EC2 recommends a constant of 50 mm for the effect of the concrete cover and crack spacing; while the CSA and NS estimate the effect of the concrete cover and bar spacing to be about 150 mm for a typical offshore concrete section of 400 mm-600 mm thickness and 50 mm-60 mm concrete cover. However, the CEP-FIP ignores the effect of concrete cover thickness and strain gradient on the thick offshore member.
- Ignoring the concrete cover effect can be acceptable for building structures and for standard concrete members with a small cover; however, it is not acceptable to be used for offshore members.
- A fracture energy model that it takes into account the concrete mix properties and the reinforcement ration was proposed. Another numerical model (MTCA) based on tension chord method to calculate the maximum crack width was developed. Both methods the fracture energy method and the MTCA method provided good estimates for the crack width compared to test results.

6.3 Recommendations for Future Research

The following recommendations are suggested for future work in the area of flexural crack behaviour:

1. Further investigations should include the effect of bar diameter for high strength reinforced concrete slabs.
2. The effect of the increase of the slab thickness over 200 mm needs further investigation.
3. The analytical model can be extended to include the effect of long term flexural cracking of creep and shrinkage.
4. Flexural cracking of high strength concrete slabs can be investigated under other type of loading such as; dynamic and cyclic loading.

References

- ACI (2001). "Control of Cracking in Concrete- Committee 224", ACI Bibliography No. 9, *American Concrete Institute*, Michigan, USA.
- ACI-318 (2005). "Building Code requirement of Structure Concrete". Detroit, USA.
- Alavi, M.F. and Marzouk, H. (2004). "Bond of High strength Concrete under Monotonic Pull- Out Loading". *Magazine of Concrete research*, 56(6):545-557.
- Base, G.D.; Read, J.B.; Beeby, A.W., and Taylor, H.P.J. (1966). "An Investigation of the Crack Control Characteristics of Various Types of Bar in Reinforced Concrete Beams". Cement and Concrete Association, Research Report 41.018, Parts I and II and Supplement, London.
- Broms, B.B. (1963). "Mechanism of Tension Cracking in Reinforced Concrete Members – Phase II". Cornell University.
- Broms, B.B. (1965). "Crack Width and Crack Spacing in reinforced Concrete Members". *ACI Journal*, 62(10):1237-1255.
- Broms, B.B. and Lutz, L.A. (1965). "Effects of Arrangement of Reinforcement on Crack Width and Spacing of Reinforced Concrete Members". *ACI Journal, Proceedings*, 62(11): 1395-1410.
- CEB-FIP (1990). "Model Code for Concrete Structures". In *comité' Euro-Internationale de Beton/Federation Internationale de la Procontrainte*. Lausanne, Switzerland.

- CEB-FIP (1978). "Model Code for Concrete Structures". In *comité' Euro-Internationale de Beton/Federation Internationale de la Procontrainte*. Paris, France.
- Chi, M. and Kirstein, A.F. (1958), "Flexural Cracks in Reinforced Concrete Beams". *ACI Journal*, 54(10):865-878.
- Clark, A. P. (1956). "Cracking of reinforced Concrete flexural Members". *ACI Journal*, 52(8):851-862.
- Crisfield *mm*, M.A. (1986). "Snap-Through and Snap Back Response in Concrete Structures and the Danger of Under Integration". *International journal for Numerical Methods in Engineering*, 22:751-767.
- CSA Standard (2004). "Concrete Structures, S474". Canadian Standard Associations, Mississauga, Ontario, Canada.
- Hallgren, M. (1996). "Punching Shear Capacity of Reinforced High Strength Concrete Slabs". Doctoral Thesis, Department of Structural Engineering, Royal Institute of Technology, Stockholm, Sweden, 206p.
- Hillerborg, A.; Modèer, M, and Petersson, P.E. (1976). "Analysis of Crack Formation and Crack Growth in Concrete by Means of Fracture Mechanics and Finite Elements". *Cement and Concrete Research*, 6(6):773-782.
- Hognestad, E. (1962). "High strength Bar as Concrete, Part 2- Control of Flexural Cracking, Part:2- Control of Flexural Cracking". *PCA Research and Development Laboratories*, 4(1):46-63.
- Hussein, A. (1990). "Behaviour of Reinforced Concrete Slabs Made with High-Strength Concrete". Master's thesis, Faculty of Engineering and Applied Science, Memorial University of Newfoundland, St. John's, Newfoundland and Labrador, Canada, August, 145p.

- Faver, R. et al. (1983). "Fissuration et Deformations". *International du Beton (CEB)*, Lausanne, Switzerland, 249.
- Ferry-Borges, J. (1966). "Cracking and Deformability of Reinforced Concrete Beams". Publications, IABSE (Zurich), (26): 75-95.
- Frosch, R.J. (1999). "Another Look at Cracking and Crack Control in Reinforced Concrete". *American Concrete Institute Structural Journal*, 96(3):437-442.
- Gergely, P. and Lutz, L.A. (1968). "Maximum Crack Width in Reinforced Concrete Flexural Members". *American Concrete Institute*, 87-117.
- Gilbert, R.I (2005). "Time-Dependent Cracking and Crack Control in Reinforced Concrete Structure". Serviceability of Concrete: A Symposium Honoring Dr. Edward G. Nawy, Ed. Barth, F., Co-Ed. Froch, R, Nassif, H. and Scanlon, 15(225):223-240.
- Gopalaratnam, V.S., and Shah, S.P. (1985). "Softening Response of Plain Concrete in Direct Tension". *ACI Journal*, 82(3):310-323.
- Goto, Y. (1971). "Cracks Formed in Concrete around Deformed Tension Bars". *ACI Journal*, 68: 244-251.
- Guo, Z.H., and Zhang, X.Q. (1987). "Investigation of Complete Stress-Deformation Curves for Concrete in Tension". *ACI Material Journal*, 84(4):278-285.
- Gustafsson, P.J. and Hillerborg. (1988), A. "Sensitivity in Shear Strength of Longitudinally Reinforced Concrete Beams to Fracture Energy of Concrete". *ACI Structural Journal*, 85(30):286-294.
- Kaar, P.H. and Hognestad, E. (1965). "High Strength Bars as Concrete Reinforcement Part:7- Control of Cracking in T-Beam". *PCA Research and Development Laboratories*, 7(1):42-53.

- Kaar, P.H. and Mattock, A.H. (1963). "High Strength Bars as Concrete Reinforcement Part:4- Control of Cracking". PCA Research and Development Laboratories, 5(1):15-38.
- Lenohardt, F. (1977). "Crack Control in Concrete Structures". International association for bridge and structural engineering. IBASE Surveys, S-4/77, IABE Periodical 3/77.
- Makhlou H. and Malhas, F. (1996), "The Effect of Thick Concrete Cover on the Maximum Flexural Crack Width Under Service Load". ACI Structural Journal, 93(3):257-265.
- Marti, P., Alvarez, M., Kaufmann, W. and Sigrist, V. (1998). "Tension Chord Model for Structural Concrete". *Structural Engineering International*, 287-298.
- Marzouk, H. and Chen, Z.W. (1993). "Finite Element Analysis of High-Strength Concrete Slabs". *ACI Structural Journal*, 90(5):505-513.
- Marzouk, H. and Chen, Z.W. (1995). "Fracture Energy and Tension Properties of High-Strength Concrete". *Journal of Material in Civil Engineering*, 7(2):108-116.
- Narayanan, R.S. (1994). "Concrete structures: Euro-code EC2 & BS8110 compare". Longman group, England.
- Nawy, E. (1968). "Crack Control in Reinforced Concrete Structures". ACI Journal, 65(10):825-836.
- Nawy, E and Blair, K.W. (1972). "Crack control, serviceability, and limit design of two-way action slabs and plates". Engineering Research Bulletin No. 53, College of Engineering, Rutgers University, 131p.
- NS (1992), "Concretes Structures Design rules, 3473E". Norwegian Council for Building Standardization [NBR], Norway, 4th Edition.

- Oh, B.H. and Kang, Y.J. (1987). "New Formulas for Maximum Crack Width and Crack Spacing in Reinforced Concrete Flexural Members". *ACI Structural Journal*, 84(2): 103-112.
- Phillips, D.V. and Zhang, B. (1993). "Direct Tension Tests on Notched and Un-notched Plain Concrete Specimens". *Magazine of Concrete Research*, 45(162):pp.25-35.
- Rashid, M.I. (2004). "Concrete slabs Reinforced with GFRP Bars". Master's thesis, Faculty of Engineering and Applied Science, Memorial University of Newfoundland, St. John's, Newfoundland and Labrador, Canada, June, 220p.
- Rizkalla, S.H., Hwang, L.S. and EL Shahawi, M. (1983). "Transverse Reinforcement Effect on Cracking Behavior of Reinforced Concrete members". *Canadian Journal of Civil Engineering*, 10: 566-581.
- Saliger, R. (1936). "High-Grade Steel in Reinforced Concrete", Proceedings, Second Congress of the International Association for Bridge and Structural Engineering, merlin-Munich.
- Sozen, M.A. and Seiss, C.P. (1963). "Investigation of Multiple Panel Reinforced Concrete Floor Slabs: Design Methods- Their Evaluation and Comparison". *ACI Journal, Proceeding*, 60(8):999-1027.
- Watstein, D. and Parsons, D.E. (1943). "Width and Spacing of Tensile Cracks in Axially Reinforced Concrete Cylinders". *Journal of Research, National Bureau of Standards*, 31: (RP 1545).
- Watstein, D. and Mathey, R.G. (1959). "Width of Cracks in Concrete at the Surface of Reinforcing Steel Evaluated by Means of Tensile Bond Specimens". *ACI Journal*, 56(1): 47-56.

Vecchio, F.J. And Collins, M.P. (1986). “ The Modified Compression Field Theory for Reinforced Concrete Elements Subjected to Shear”. *ACI Journal*, 83(2):219-231.

Appendix A1

Table A1.1: Reinforced concrete cracked section properties

Series No	Slab No.	E_c (MPa)	n	kd (mm)	d (mm)	$d - kd$ (mm)	I_{cr} (mm ⁴)	Distance from neutral axis to tension fiber y_t (mm)
Series I	NSC1	30000	6.667	64.94	157.4	92.4585	5.4E+08	135.058
	HSC1	51400	3.891	48.62	137.4	88.7826	2.7E+08	151.383
	HSC2	51400	3.891	46.43	127.4	80.9707	2.3E+08	153.571
Series II	HSC3	51400	3.891	47.45	157.4	109.948	3E+08	152.548
	HSC4	51400	3.891	43.25	157.4	114.154	2.5E+08	156.754
Series III	HSC5	51400	3.891	28.63	112	83.3722	8E+07	121.372
	NSC2	30000	6.667	37.40	162	124.597	2E+08	162.597
	NSC3	30000	6.667	21.56	104.35	82.791	4.3E+07	128.441

Steel rebars modulus of elasticity $E_s = 200000$ MPa

Table A1.2: Crack properties calculation using (CSA S474, 2004)

Series No	Slab No.	f_s (MPa)	f'_c (MPa)	ϵ_1	h_{ef} (mm)	S_{mm} (mm)	f_{cr} (MPa)	w_m (mm)
Series I	NSC1	250	35	0.00183	100	127	1.952	0.227
	HSC1	250	68.5	0.00213	100	167	2.731	0.351
	HSC2	250	70	0.00237	100	187	2.761	0.438
Series II	HSC3	250	66.7	0.00173	100	148	2.695	0.252
	HSC4	250	61.2	0.00172	100	170	2.582	0.287
Series III	HSC5	250	70	0.00182	75	139	2.761	0.248
	NSC2	250	33	0.00163	100	203	1.896	0.324
	NSC3	250	34	0.00194	75	223	1.924	0.425

$k_1 = 0.40$, $k_2 = 0.125$

Table A1.3: Crack properties calculation using (NS 3473E, 1992)

Series No	Slab No.	σ_s (MPa)	σ_{sr} (MPa)	h_{ef} (mm)	S_{rm} (mm)	k_w	f_{ct} (MPa)	w_k (mm)
Series I	NSC1	250	10.56	100	127	1.30	2.873	0.269
	HSC1	250	5.96	100	167	1.30	4.225	0.354
	HSC2	250	4.52	100	187	1.30	4.394	0.397
Series II	HSC3	250	9.29	100	148	1.30	4.225	0.314
	HSC4	250	9.69	100	170	1.30	4.394	0.360
Series III	HSC5	250	8.65	75	139	1.35	4.563	0.294
	NSC2	250	11.77	100	203	1.30	2.873	0.430
	NSC3	250	7.71	75	223	1.35	2.9835	0.473

$$k_1 = 0.40, k_2 = 0.125, \beta = 0.5$$

Table A1.4: Crack properties calculation using (EC2, 1991)

Series No	Slab No.	σ_s (MPa)	h_{ef} (mm)	ρ_r	S_{rm} (mm)	w_k (mm)
Series I	NSC1	250	45.019	0.0760	83	0.135
	HSC1	250	50.461	0.0678	87	0.142
	HSC2	250	51.190	0.0668	88	0.143
Series II	HSC3	250	50.849	0.0518	99	0.160
	HSC4	250	52.251	0.0403	113	0.183
Series III	HSC5	250	40.457	0.0312	101	0.165
	NSC2	250	54.199	0.0155	153	0.249
	NSC3	250	42.814	0.0098	165	0.268

$$k_1 = 0.80, k_2 = 0.50, \beta = 1.30$$

Table A1.5: Crack properties calculation using (CEB-FIP, 1990)

Series No	Slab No.	σ_s (MPa)	$\rho_{s,ef}$	$l_{s,max}$ (mm)	S_{rm} (mm)	ϵ_{s2}	$f_{ctm}(t)$ (MPa)	ϵ_{sr2}	w_k (mm)
Series I	NSC1	250	0.0760	92.117	61	0.00125	2.2	0.0001	0.107
	HSC1	250	0.0678	103.251	69	0.00125	3.3	0.0002	0.114
	HSC2	250	0.0668	104.743	70	0.00125	3.3	0.0002	0.115
Series II	HSC3	250	0.0518	135.260	90	0.00125	3.3	0.0003	0.143
	HSC4	250	0.0403	173.736	116	0.00125	3.3	0.0004	0.174
Series III	HSC5	250	0.0312	142.350	95	0.00125	3.3	0.0005	0.133
	NSC2	250	0.0155	286.050	191	0.00125	2.2	0.0007	0.236
	NSC3	250	0.0098	319.170	213	0.00125	2.2	0.0011	0.185

Appendix A2

A2.1 Numerical Example

Sample calculations using modified tension chord assumptions (MTCA) and fracture energy principals for crack width estimation are presented for Slab HS1. Slab HS1 is a simply supported slab along all four edges with a side dimension of 1900 mm in both directions. Central load was applied on the slab through a 250 × 250 mm column stub. The dimensions and reinforcement details of a typical test slab are shown in Figure A2.1 and Table A2.1.

Table A2.1: HSC1 properties

Slab No.	c (mm)	h (mm)	b (mm)	No. of bars	s (mm)	d _{bc} (mm)	A _s (mm ²)	f' _c (MPa)	ρ %
HSC1	50	200	1900	13	150	25.2	6500	68.5	2.48

The following input data were obtained from Marzouk and Chen (1995) that measured in the laboratory and has been assumed in the calculations:

$$E_c = 51400 \text{ MPa}, E_s = 200000 \text{ MPa}, f'_c = 3.294 \text{ MPa}, \epsilon_{to} = 118.6 \mu\epsilon.$$

The averaged bond stress (τ_b) of high-strength concrete were obtained from Alavi-Fard and Marzouk (2004).

$$\tau_b = 5.399 \text{ MPa}$$

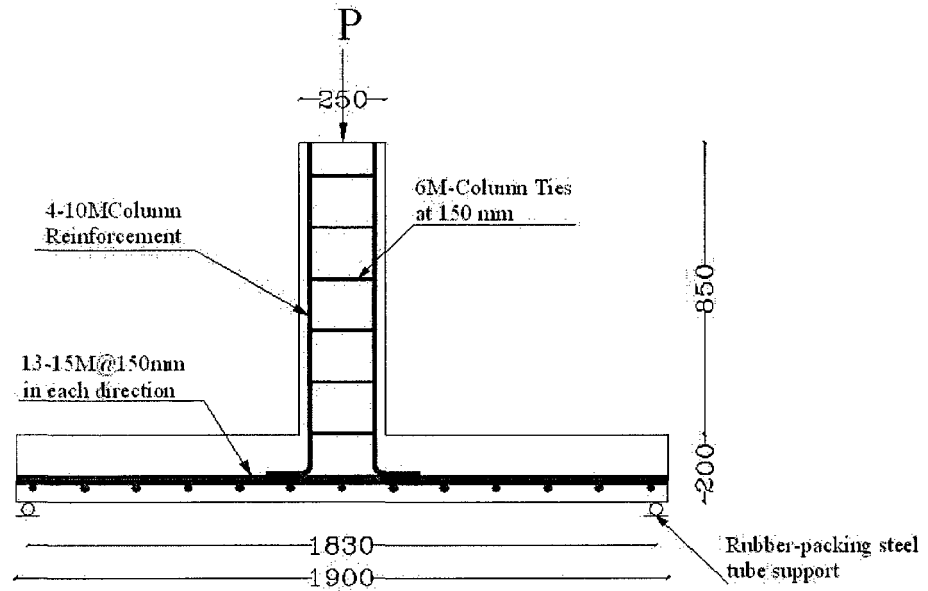


Figure A2.1: Slab HS1 details

A2.1.1 Cracked width calculations using the modified tension chord assumptions

A2.1.1.1 Cracked section analysis

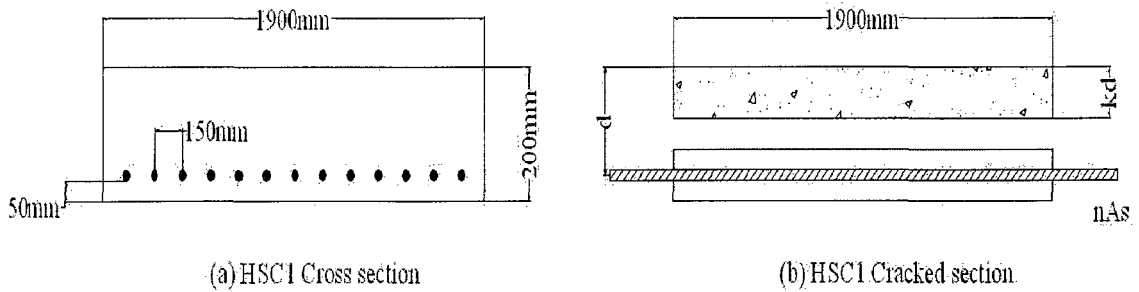


Figure A.2.2: Crack section analysis of HSC1

-Depth of compressive zone kd

$$n = \frac{E_s}{E_c} = \frac{200000}{51400} = 3.891$$

$$nA_s = 25291.5 \text{ mm}^2$$

$$kd = 48.617 \text{ mm}$$

$$I_{cr} = 2.7 \times 10^8 \text{ mm}^4$$

-Effective tension area

$$A_{ct} = h_{ef} \cdot b$$

$$1. \quad h_{ef} = a_2 + 7.5d_{be} = \left(50 + \frac{25.2}{2}\right) + 7.5 \times 25.2 = 251.6 \text{ mm}.$$

$$2. \quad h_{ef} = (h - kd) = 200 - 48.617 = 151.383 \text{ mm}.$$

$$3. \quad h_{ef} = \frac{1}{2} \cdot \text{Slab thickness} = 100 \text{ mm}.$$

$$h_{ef} = 100 \text{ mm}$$

$$A_{ct} = h_{ef} \times b = 100 \times 1900 = 190000 \text{ mm}^2$$

Therefore, the effective reinforcement ratio is:

$$\rho_{ef} = \frac{A_s}{A_{ct}} = \frac{6500}{190000} = 0.0342$$

-Crack spacing calculation:

The average crack spacing S_m can be calculated from the following Equation 5.16

$$S_m = 2.0(c + 0.1s) + k_1 k_2 d_{be} h_{ef} b / A_s$$

$$S_m = 2.0(50 + 0.1 \times 150) + 0.4 \times 0.125 \times 25.2 \times 100 \times 1900 / 6500 = 167 \text{ mm}$$

-Crack width calculation:

$$w_m = S_m \left[\left(\frac{f_s}{E_s} \cdot \frac{h - kd}{d - kd} \right) - \frac{\tau_b S_m \rho_{ef}}{E_c d_b} \right]$$

Crack width calculated at $f_s = 250 \text{ MPa}$

$$w_m = 167 \left[\left(\frac{250}{200000} \cdot \frac{200 - 48.617}{137.4 - 48.617} \right) - \frac{5.399 \times 167 \times 0.0342}{51400 \times 25.2} \right] = 0.351 \text{ mm}$$

$$w_k = 1.7 w_m = 0.596 \text{ mm}$$

A2.1.2 Cracked width calculations based on fracture energy

Values obtained from the experiment HSC1:

$$f_s = 250 \text{ MPa} , S_m = 171 \text{ mm}$$

-Crack width calculation neglecting tension stiffening effect

$$w_{mt} = S_m \left[\left(\frac{f_s}{E_s} \cdot \frac{h - kd}{d - kd} \right) \right] = 0.364 \text{ mm}$$

The tension stiffening is going to reduce the crack width by

$$w_{m2} = \frac{f_t}{E_c} \cdot S_{rm}$$

$$f_t = \frac{f'_t(\epsilon_t / \epsilon_{t0})}{1.3863(\epsilon_t / \epsilon_{t0} - 1)^{1.6655} + \epsilon_t / \epsilon_{t0}} = 0.495 \text{ MPa}$$

Crack width calculated at $f_s = 250 \text{ MPa}$

$$w_m = w_{m1} - w_{m2} = 0.362 \text{ mm}$$

$$w_k = 1.7 w_m = 0.618 \text{ mm}$$



